UNIVERSITY OF OKLAHOMA

GRADUATE COLLEGE

UNDERSTANDING THE ALKYL DONOR SPECIFICITY OF AROMATIC PRENYLTRANSFERASES

A DISSERTATION

SUBMITTED TO THE GRADUATE FACULTY

in partial fulfillment of the requirements for the

Degree of

DOCTOR OF PHILOSOPHY

By

ERIN MICHELLE SCULL
Norman, Oklahoma
2019

Downloaded from SHAREOK. Persistent Handle URL: https://hdl.handle.net/11244/320363

UNDERSTANDING THE ALKYL DONOR SPECIFICITY OF AROMATIC PRENYLTRANSFERASES

A DISSERTATION APPROVED FOR THE
DEPARTMENT OF CHEMISTRY AND BIOCHEMISTRY

BY

Dr. Shanteri Singh, Chair

Dr. Wai Tak Yip

Dr. Christina Bourne

Dr. Chuanbin Mao

Dr. Lloyd Bumm

© Copyright by ERIN MICHELLE SCULL 2019
All Rights Reserved.

Acknowledgements

I would like to thank my mentor Dr. Shanteri Singh for her continuous mentorship, encouragement, and guidance, which was invaluable to my success research, completion of this PhD program, and writing this dissertation.

I would also like to thank my colleagues in the Singh lab, both past and present, for their help, support, and joyful collaborations. Specifically, I would like to thank Dr. Chandrasekar Bandari, Tejaswi Bavineni, Eric Gardner, Miranda Schene and Andrea Batchev for their incredible contributions to this work.

A special thanks to the facility managers in the Chemistry and Biochemistry department at the University of Oklahoma. I would like to thank Dr. Susan Nimmo for her continued help with NMR spectroscopy and her appreciated friendship as well as Dr. Leonard Thomas for his valuable guidance and patience in x-ray crystallography.

In addition, I would like to thank my parents, Carla and David, as well as my sister Lyndsey for always taking my calls and lending a sympathetic ear. I could not have done this without you.

Table of Contents

Acknowledgements iv

List of Tables ix

List of Figures x

Abstract xii

Chapter 1: Introduction to Aromatic Prenyltransferases 1

Important Natural Products 1

Prenyltransferases 4

Aromatic Prenyltransferase 5

Global fold and Overall Structure 8

Global fold 8

Structure 9

Prenyl Binding Site 10

Aromatic Binding Site 12

Reactions mechanism 15

Chapter 2: Determination of Alkyl-Donor Specificity of Tyrosine-*O* Prenyltransferase SirD from *Leptosphaeria maculans* [a] 18

Introduction 18

Research Objectives 20

Contribution 22

Results and Discussion 22

RP-HPLC and HRMS Studies 24

Kinetic Studies 25

SirD Structural Model....28
NMR Studies....29
Conclusions....30
Experimental....30
General methods....31
Overexpression and purification of SirD....32
In-vitro SirD assay....32
SirD structural model....33
Chapter 3. Determination of Alkyl-Donor Specificity of a Tryptophan-*C4*-Prenyltransferase FgaPT2 from *Aspergillus fumigatus*.[b]....35
Introduction....35
Research Objectives....40
Contribution....41
Results and Discussion....41
RP-HPLC and HRMS Studies....42
Kinetic studies....46
NMR Studies....50
Conclusions....53
Experimental....54
General materials....54
General methods....54
In-vitro FgaPT2 assay....55
Chapter 4. Alkyl donor specificity of a Naptherpin prenyltransferase, NphB....57

Introduction.....57
Research Objective.....59
Contributions.....60
Results61
Description of the alkyl pyrophosphate library.....61
Chemoenzymatic syntheses of alkylated 1,6 dihydroxy naphthalene.....64
Chemoenzymatic syntheses of alkylated sulfabenzamide.....70
NphB mutational studies.....75
Structure characterization of sulfabenzamide products.....77
Discussion.....83
Experimental.....86
Protein Expression and Purification.....86
In vitro Activity Assays.....87
Chapter 5. Biocatalytic applications of prenyltransferases in drug diversification: A proof-of-concept study using FDA approved antibiotic, daptomycin.....90
Introduction.....90
Research Objectives.....92
Contributions.....92
Results and discussion.....93
Assaying the alkyl pyrophosphate substrate tolerance of CdpNPT to construct daptomycin analogues.....93
Derivatization and determination of bioactivity of daptomycin.....99
Experimental.....113

Appendix 118

Copy-right permission 118

References 126

List of Tables

Table 1. Summary of HRMS data of alkyl-*O*-Tyr analogues from SirD catalyzed alkylation reaction with L-Tyr and synthetic alkyl-PP analogues.....25

Table 2. Kinetic parameters for SirD with 1 mM L-Tyr and 0.025 - 6 mM alkyl-PP analog in 25 mM Tris, 5 mM $MgCl_2$, 50 mM KCl, pH 7.5 at 35 °C. 26

Table 3. Summary of HRMS data of alkyl-Trp analogues. 44

Table 4. Kinetic parameters for FgaPT2 with L-Trp. 47

Table 5. Summary of HRMS data of 1,6-DHN analogues from NphB catalyzed alkylation reaction with 1,6-DHN and synthetic alkyl-PP analogues. 64

Table 6. Summary of HRMS data of sulfabenzamide analogues from NphB catalyzed alkylation reaction with sulfabenzamide and synthetic alkyl-PP analogues. 72

Table 7. NMR data of alkylated sulfabenzamide 80

Table 8 HRMS analytical scale daptomycin analogues.....98

Table 9. HRMS data of purified alkyl daptomycin analogues 101

Table 10. In-vitro MIC ($\mu g\ mL^{-1}$) values for Daptomycin and daptomycin derivatives. 104

List of Figures

Figure 1. Prenylated compounds 3

Figure 2 . Aromatic prenyltransferase substrates. 7

Figure 3. Ribbon structure of FgaPT2 (PDB ID 314X) 9

Figure 4. Sirodesmin biosynthetic pathway. 18

Figure 5. Products of SirD 20

Figure 6. Library of synthetic alkyl-PP 22

Figure 7. RP-HPLC chromatograms of SirD catalyzed reactions. 23

Figure 8. Percent conversion 24

Figure 9. Michaelis-Menten kinetic plots for SirD reactions 27

Figure 10: Structural model of SirD. 28

Figure 11. NMR confirmed structures. 30

Figure 12. The role of FgaPT2 in fumigaclavine C biosynthesis 35

Figure 13. Active site of FgaPT2 37

Figure 14. Accepted aromatic substrates by FgaPT2. 38

Figure 15. FgaPT2 mutants reactions 40

Figure 16. Synthetic alkyl-PP analogues used in this study. 42

Figure 17. RP-HPLC chromatograms of FgaPT2 catalyzed reactions. 43

Figure 18: The percent conversion of alkyl-PP analogues. 45

Figure 19. Michaelis-Menten inetic plots for FgaPT2 reactions 48

Figure 20. NMR characterized structures 51

Figure 21: UV absorption spectra of L-Trp and C3-A17-Trp. 52

Figure 22: The active site of FgaPT2 structure (PDB:3I4X) 53

Figure 23. NphB catalyzed step in the biosynthesis of naptherpin[36] 58

Figure 24. Library of synthetic alkyl-PP analogues. 63

Figure 25. Percent conversion. 63

Figure 26 RP- HPLC chromatograms. 69

Figure 27. RP- HPLC chromatograms. 74

Figure 28. NphB mutation analysis. 76

Figure 29. Sulfabenzamide derivatives. 79

Figure 30. Daptomycin structure 92

Figure 31. Synthetic alkyl pyrophosphate library 94

Figure 32. Percent Conversion Daptomycin analogues using CdpNPT 95

Figure 33. HPLC chromatograms 97

Figure 34. CdpNPT catalyzed reaction producing daptomycin derivatives 99

Figure 35. Daptomycin derivatives and placement on the indole ring. 100

Figure 36. MIC improvement of Daptomycin analogues compared to daptomycin. 106

Figure 37. LogP vs MIC improvement plots for daptomycin and daptomycin analogues. 111

Abstract

Chemoenzymatic synthesis is a leading technique in the diversification and late stage modification of complex molecules, due to the high regio and stereo specificities of the enzymes. Over the last decade, the broad aromatic substrate scope for a class of prenyltransferases known as aromatic prenyltransferases has been extensively studied. Aromatic prenyltransferase catalyzed prenylation reactions are highly prevalent in nature and contribute to the amazing structural and functional diversity of natural products. Given their natural function and broad aromatic substrate promiscuity, aromatic prenyltransferases have been investigated as biocatalytic tool essential to facilitate chemoenzymatic natural product diversification. Although many studies have accomplished highlighting the acceptor substrate scope of this class of enzyme none have explored the enzyme's potential to transfer unnatural alkyl groups. Herein, we investigate the alkyl donor specificity of four aromatic prenyltransferases, SirD, FgaPT2, NphB and CdpNPT, in combination with our extensive library of synthetic alkyl pyrophosphates. To further highlight the feasibility of aromatic prenyltransferases as a powerful biocatalyst, we successfully diversified FDA approved drug compounds, subsequently resulting in the improved *in vitro* activity of the modified compound.

Chapter 1: Introduction to Aromatic Prenyltransferases

Important Natural Products

Prenylation is ubiquitous across all biological systems and has been known to enhance lipophilicity of compounds giving the compounds a stronger affinity to biological membranes, as well as altering binding specificity and providing isoprenoid chains to be incorporated into the carbon scaffold. As a result, prenylated natural products display different pharmacological activities distinct from their non prenylated precursors attracting attention amongst the medical and scientific community (Figure 1)[1]. Indole diketopiperazines, derived from L-tryptophan and a second amino acid, typically and L-proline, L-tryptophan, L-histidine, L-phenylalanine or L-leucine, are a unique class of prenylated natural products with a wide spectrum of biological and pharmacological activities.[2] This class includes the tryprostatins A and B, nocardioazines, fumitremorgin C and Echinulin. Tryprostatin A and B, originally cultured from the fungus *Aspergillus fumigatus* and *A. tamari,* are found to inhibit cell cycle progression of various cancer cell lines.[3] It has been determined that tryprostatin A is active against tubulin polymerization, disrupting the interaction between microtuble associated proteins (MAP) and the C-terminal domain of tubulin. Although tryprostatin B also arrest cell cycle progression at lower concentrations than tryprostatin A it has a different mechanism of action as compared to tryprostatin A.[3] Echinulin and cyclomarazine A and B posses biological and pharmacological activites.. Specifically, echinulin and its analogues show antiviral, anticancer, and neuroprotective activity.[5][6] Cyclomarazine A and B, a reverse N-prenylated compound, has moderate antibacterial activity against

vancomycin-resistant *Entrococcus faecium* and methicillin-resistant *Staphylococcus areus.*[7]

Aurachins, a unique family of natural products featuring a quinoline chromophore with a C-3 or C-4 farnesyl or geranyl substitution, display multiple biologically active properties.[8] Due to their structural similarities to ubiquinol and vitamin K, aurachins act as inhibitors of the electron transport chain, specifically by inhibiting various cytochrome complexes. They have been reported to possess strong antimicrobial, antifungal and antiplasmodial characteristics. Napyradiomycins, a group of natural products isolated from *Actinomycetes*, were previously identified as antibacterial antibiotics; however, they have recently been identified to exhibit cytotoxicity against human cancer cell lines. It has been speculated that the inhibitory effect against mitochondrial electron transport thus decreasing ATP production explains their mechanism of again against cancer cells.[9, 10] Diazepinomycin, an unusual metabolite found in bacterium *Micromonospora* sp. RV115, features a benzodiazepine derivative with a farnesyl side chain and underwent phase II clinical trials for the treatment of glioblastoma multiforme. Diazepinomicin inhibits the Ras-MAPK signaling pathway, crosses the blood-brain barrier and accumulates in gliomas possibly binding to the peripheral benzodiazepine receptor, a component of the mitochondrial permeability transition pore which is involved in the regulation and initialization of apoptosis.[11-13] Cudraflavone B, a prenylated flavone produced in *C. tricuspidata* with a long list of pharmacological activities such as anti-proliferative, monoamine oxidase (MAO) inhibitory effects, apoptotic activity in gastric carcinoma and melanoma cells as well as

hepatoprotective activity, neuroprotective effects and reactive oxygen species inhibition against glutamate-induced neurotoxicity.[14] Therefore, this natural product has the potential to treat neurodegenerative diseases such as Alzheimer's, Parkinson's disease, ischemia and may prove useful in treating variety of cancers.[15] These compounds illustrate the vast structural and pharmacological diversity of prenylated natural products.

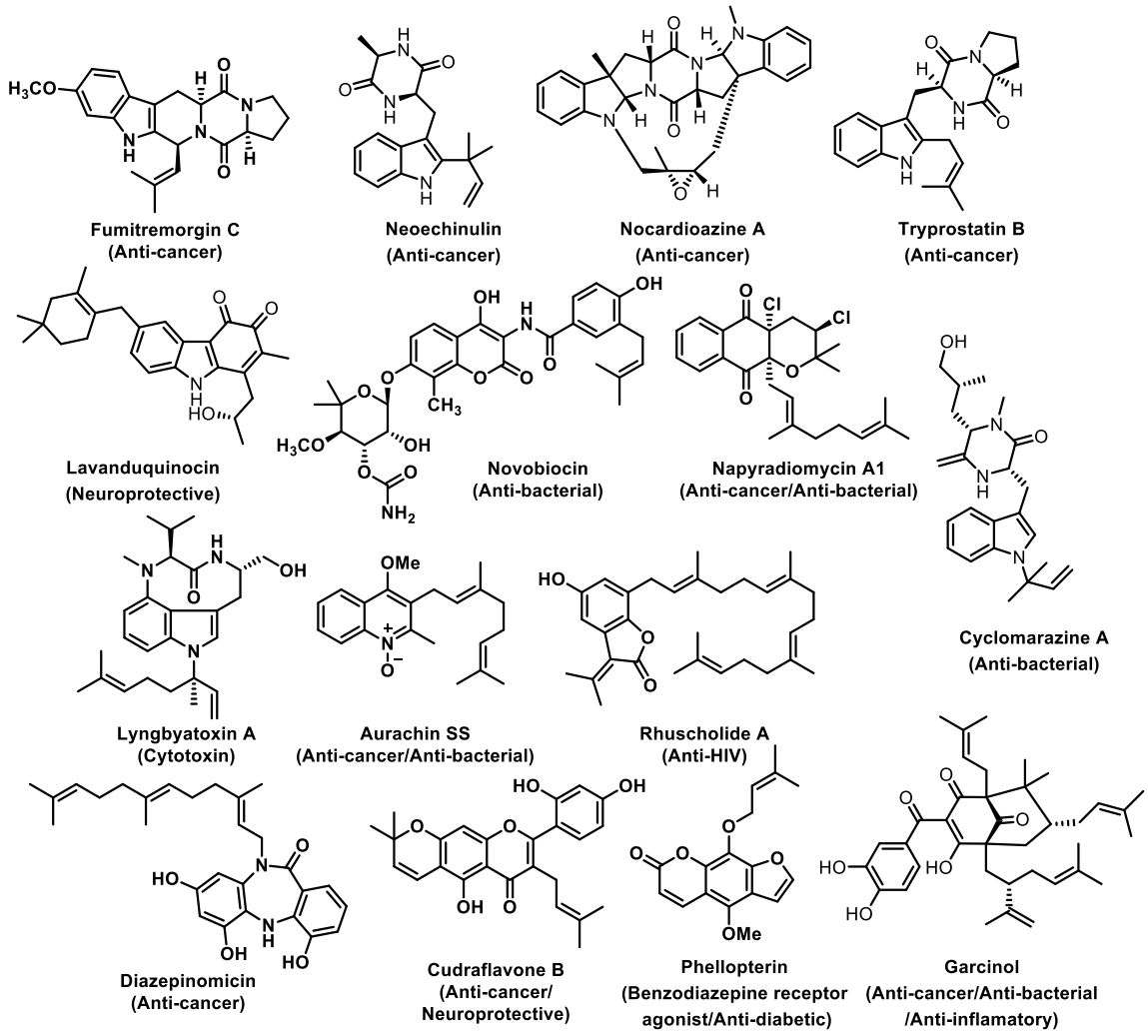


Figure 1. Prenylated compounds
Examples of prenylated compounds displaying biological and pharmacological activities.

Prenyltransferases

Prenyltransferases are a large and diverse family of enzymes responsible for catalyzing the transfer of prenyl groups onto an assortment of acceptor compounds.[16] Based on their biochemical and structural characteristics, as well as their primary amino acid sequences, this large family of enzymes is organized into smaller subcategories. Isopentenyl pyrophosphate (IPP) and dimethylallyl pyrophosphate (DMAPP) are products from the mevalonate pathway that can serve as the initial precursors for the prenyl pyrophosphate biosynthesis as well as prenyl donors for protein, peptide, tRNA and aromatic prenyltransferase enzymes.[17] In the biosynthesis of linear isoprenoids, prenyl diphosphate synthases catalyze the transfer of prenyl groups onto alkene carbons through sequential condensation reactions of IPP with other prenyl diphosphates[18]. Protein prenyltransferases are capable of transferring C_{15} and C_{20} carbon chains to nucleophilic cysteine residues near the C-terminus of the protein, while peptide prenyltransferases of the TruF family catalyze the posttranslational side chain prenylation of peptides.[19, 20] Prenyltransferases are also capable of modifying nucleic acids found in tRNA by attaching prenyl and geranyl groups onto the amino group of adenosine and sulfur atom in 5-methylaminomethyl-2-thiourdine nucleotides.[21, 22] Further, a large and well-studied family of aromatic prenyltransferase (PT) enzymes catalyze the transfer of prenyl moieties from prenyl donors such as dimethylallyl pyrophosphate (DMAPP, C_5), geranyl pyrophosphate (GPP, C_{10}), farnesyl pyrophosphate (FPP, C_{15}) onto a large variety of aromatic acceptors.

Aromatic Prenyltransferase

In nature, aromatic PTs perform prenylation reactions on naphthalene, flavonoid, xanthone, coumarin, polyphenol and indole alkaloid aromatic compounds to generate multiple secondary metabolites in plants, fungi and bacteria.[23-25] Prenylation can occur late or early in the biosynthetic pathway, wherein the prenylated products can be further tailored by cyclization, hydroxylation, oxidation or further functionalization. Therefore, aromatic PTs contribute to the bioavailability and structural diversity of secondary metabolites by increasing the lipophilicity or contributing to the overall carbon scaffold. Prenylated secondary metabolites exhibit remarkable biological activities, e.g., anti-microbial activity, anti-cancer activity, anti-virus activity, and anti-oxidant activity[26-28]. Aromatic PTs are capable of performing C-C, C-O, C-N bond formation, and in certain conditions C-S prenylation.[12, 29-32] The reactions can take place in a forward or "normal" prenylation, where the C1 position of the prenyl donor connects directly to the aromatic moiety of the acceptor compound; alternately the reactions can take place in a "reverse" manner, where the C3 or tertiary carbon of the prenyl donor connects to the aromatic acceptor.[33] This class of enzymes all shares a common ααββ structural motif, known as the PT barrel.[34-41]

Within the large group of soluble aromatic PT enzymes, two main classes exist, the super family dimethylallyl tryptophan synthases (DMATS) and the CloQ/NphB group.[28, 36, 42-44] The DMATS superfamily is mostly responsible for prenylating nitrogen containing compounds such as indole alkaloids and indole alkaloid derivatives and are found primarily in fungi although some can be found in bacteria. Aromatic PTs belonging to the CloQ/NphB group utilize aromatic compounds such as phenols,

naphthalenes, phenazines, and flavonoids as aromatic substrates and are found in both bacteria and fungi.[45] Many of these soluble aromatic PTs exhibit considerable substrate promiscuity towards both donor and acceptor compounds accepting unnatural and synthetic analogues, a property critical to the development of synthetically useful biocatalysts (Figure 2). These enzymes are tools capable of regio-specifically functionalizing complex compounds in ways not currently achievable *via* synthetic means. Aromatic PTS are becoming a valuable tool for the late stage modification of complex natural and unnatural products, which is useful for the development of novel pharmaceutical candidates.

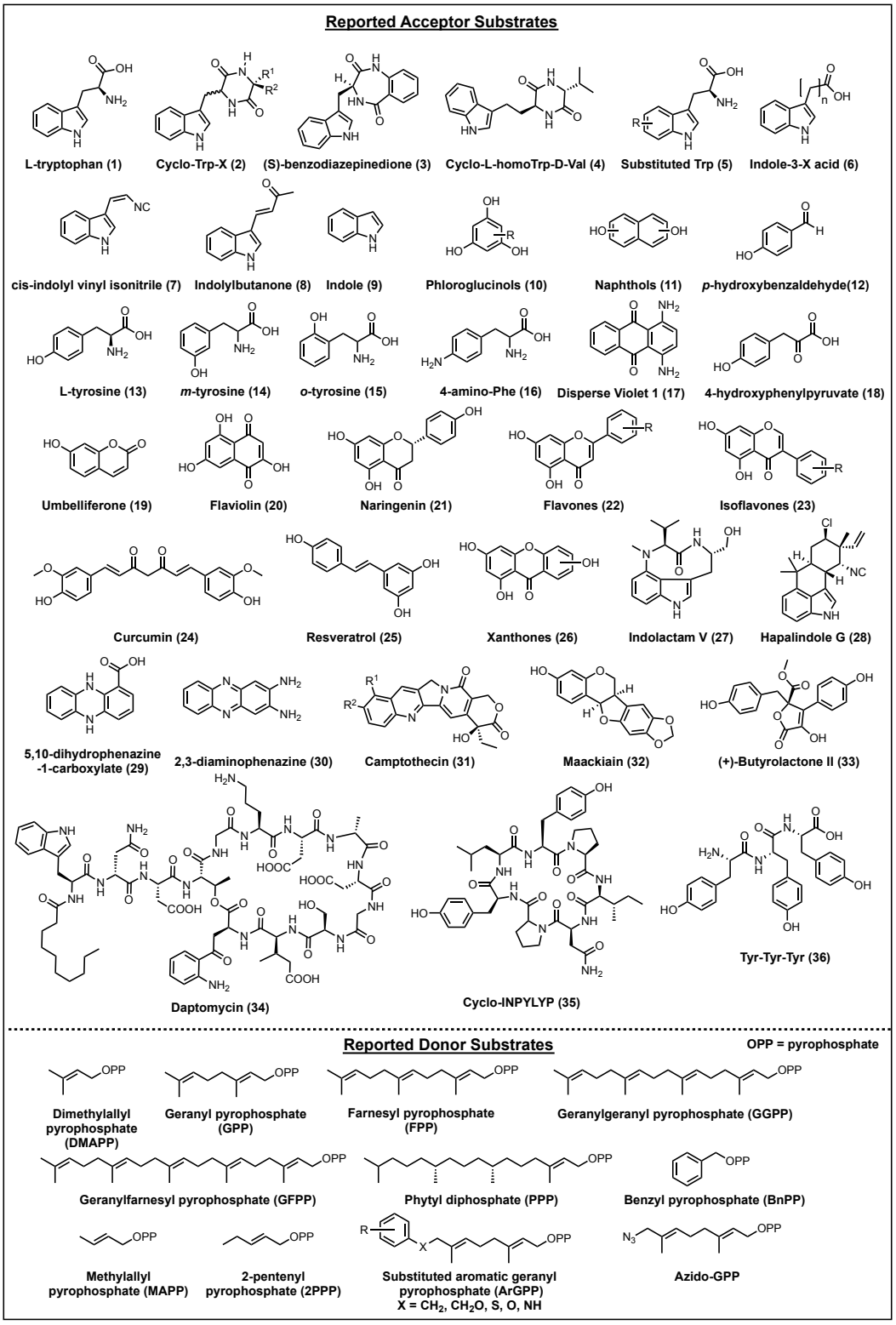


Figure 2 . Aromatic prenyltransferase substrates.
Known aromatic acceptor substrates and pyrophosphate donor substrates accepted by aromatic prenyltransferases.

Global fold and Overall Structure

Global fold

To date, all enzymes belonging to the super family of soluble aromatic prenyltransferases adopt a similar β-barrel fold found exclusively within this class.[34, 36, 38, 40, 46-49] This fold was originally observed in the enzyme NphB, a prenyltranserase involved in the biosynthesis of the prenylated polyketide naphterpin in *Streptomyces* sp. Strain CL190.[36] This novel fold, which was termed a PT-barrel, is reminiscent of the better-known TIM barrel, which is a $(\beta\alpha)_8$-barrel fold, but differing in the connectivity of the secondary structure elements.[50] The PT-barrel is comprised of a cylindrical β-sheet of ten anti-parallel β-strands surrounded by a secondary ring of solvent exposed α-helices. The secondary connectivity forms an AABB repeating motif; however, variability exists within known structures of soluble aromatic prenyltransferase due to helical kinks, additional helices and β-strands. The ten β-strands are arranged centrally, in a sequential antiparallel configuration generating a generous solvent accessible active site (Figure 3)[51].

As stated, most variations of the overall fold can be found within helices and loops surrounding the cylindrical β-sheet. For example, in the structure of EpzP, a phenazine prenyltransferase found in *Streptomyces cinnamonensis* DSM 1042, three additional 3_{10}-helices were found, one of which is located on the resolved C-terminus, owing responsibility for sealing up one end of the barrel.[46] Similarly, C-terminal helixes can be found on several other PT especially those belonging to the CloQ/NphB family (EpzP, FamD1/AmbP3, NphB, CloQ). In the case of CloQ, two α-helixes can be found following the final repeating unit; however, from the crystal structure only α11 is

covering the opening of the barrel and participating in substrate interactions.[37] Moreover, much of the variance in the global fold can be attributed to the overall size differences between aromatic PTs. Aromatic PTs range in size from 302 to 464 residues. The additional residues of the larger enzymes are found in the extended loop regions located on either side of the barrel opening. These regions are typically seen in the DMATS superfamily of enzymes such as FgaPT2 and CdpNPT and have been shown to exclude the barrel opening and participate in substrate binding.[49] [35]

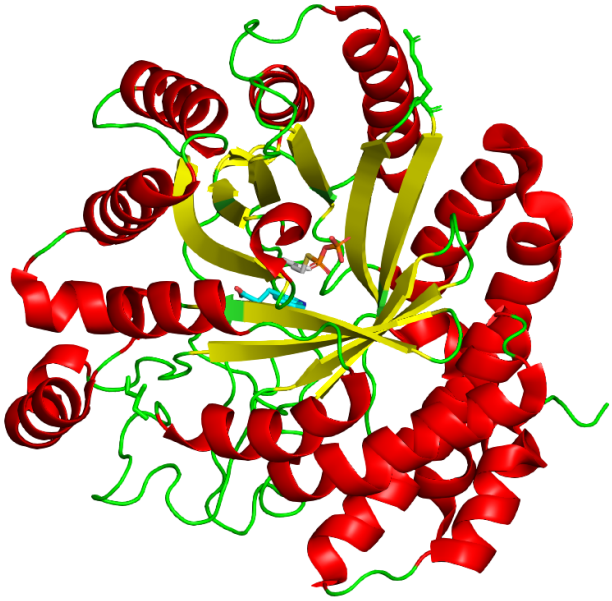


Figure 3. Ribbon structure of FgaPT2 (PDB ID 314X)
Ribbon structure of FgaPT2 showing 10 β–strands (yellow) α- helices (red) of the PT-fold. The ligands tryptophan and DMSPP are seen bound in the central cavity of the barrel.

Structure

The overall interior architecture of the β-barrel's catalytic chamber is shared among the enzymes of this class.[35, 47, 52] The central cavity can be separated into three distinct

regions. Located at the top of the barrel is the prenyl donor binding pocket, lined with basic, positively charged residues, and non-charged polar residues which participate in ionic and hydrogen bonding interactions between the sidechains of the residues and the negatively charged phosphate moiety of the prenyl donor. The middle region of the cavity possess a conserved cluster of aromatic residues, mainly tyrosine. The hydroxyl group of the tyrosine form a "tyrosine shield", protecting the allylic cation generated by the cleavage of the phosphate group from unwanted nucleophilic attack by solvent molecules. The third and bottom region of the cavity is composed mainly of hydrophobic residues responsible for the interaction and stability of the aromatic acceptor substrate and necessary intermediates. In many structures, the base of the barrel is occluded by structural elements such as rigid helices, α-helix or 3_{10}-helix, or extended loops.[36, 49, 53] The bottom region of the cavity offers the greatest amount variability, dictating substrate specificities and well as regio-specificities of the prenylated product.

Prenyl Binding Site

Due to the ubiquitous nature of the pyrophosphate moiety of the donor substrates in prenyltransferase reactions, it is not surprising that the residues found in this region are highly conserved. The α- and β-phosphates are anchored by hydrogen bonds with water molecules and polar residues as well as ionic interactions with positively charged basic residues lowering the ionization energy for the phosphate moiety.[19] Among the most structurally conserved residues surrounding the pyrophosphate binding site include arginine, lysine, asparagine and glutamine. The basic residues interact with the

pyrophosphate group and neutralize the negative charge while the polar residues and water mediated interactions fix the substrate into the active site via hydrogen bonding. The positively-charged pyrophosphate binding site does differ slightly between the magnesium-independent and magnesium-dependent PTs. It can be seen in the structure of NphB, a magnesium-dependent PTs, that two structurally conserved basic residues in the magnesium-dependent PT are missing, the loss of the positive charge is compensated by a magnesium ion that is coordinately via the aspartate side chain of Asp62.[36] Although the majority of the residues participating in the binding of the α- and β-phosphate groups are conserved, some variability is found. Similarly, water mediated hydrogen bonding between polar residues and the electronegative oxygen atoms is seen in many structures of aromatic PTs but is not strictly conserved throughout. [36, 49] A highly structurally and functionally conserved cluster of tyrosine and other aromatic residues reside in this location of the active site surrounding the bridging oxygen to the prenyl group. Believed to be responsible for shielding the carbocation intermediate of the activated prenyl group, the ring of tyrosine and aromatic residues are a catalytic characteristic of all aromatic PTs. [23, 40, 47, 49, 54]Although the prenyl donors for aromatic PTs are variable in chain length, upon comparison of the structures it is clear that neither the pyrophosphate binding domain nor the "tyrosine shield" region is dependent on the chain length of the pyrophosphate donor nor aromatic acceptor.

Aromatic Binding Site

Aromatic prenyltransferases are well known for their relaxed substrate specificities. [44, 54, 55] Tolerance is attributed to the spacious hydrophobic binding pocket, accommodating both the aromatic acceptor substrate and the carbon chain tail of the prenyl donor. The pocket is formed by nonpolar and hydrophobic residues of different sizes with varied numbers of interactions to the substrate. Structural similarities and differences of residues in contact with the substrate are of particular interest, as even small changes in the binding pocket have been known to alter the catalytic function. [56] Despite obvious differences in substrate specificity and regio-selectivity, residues found in the active site of aromatic PTs are relatively similar.

In many cases, the binding site residues remain functionally conserved but differ in the size of the amino acid side chain, changing the dimensions of the catalytic chamber. This is seen when comparing the acceptor binding site residues of aromatic PTs found in the DMATS family members, AtaPT, AnaPT, CdpNPT, FgaPT2 and FtmPT1. [47] The residues found in the aromatic acceptor binding pocket of AtaPT have relatively short side chains, lending the enzyme one of the largest solvent accessible surface area as well as greatest overall volume of the structurally characterized aromatic PTs . For example, residues Leu83, Gln172, Ser192 and G251 are found lining the active site of AtaPT, whereas the residues in equivalent positions of AnaPT are Phe103, Gln192, Phe212 and Phe265. Other spatial differences in the aromatic binding site can be seen in CdpNPT upon comparison to FgaPT2. Residue Thr102 and Arg244 in FgaPT2 are replaced with Ala271 and Ala313 in CdpNPT, enlarging the binding site relative to the

first. Additionally, positions Phe103, Gly126, Ile266, and Val340 on AnaPT are replaced with larger amino acids in CdpNPT corresponding to Leu109, Ala313, Phe272, and Met349. Variation in size of the active site is not limited to indole PT, size difference can be seen in the CloQ/NphB family of aromatic PTs as well. The binding site of EpzP was found to be larger than that of CloQ when comparing the larger amino acids Phe68, Phe161, Tyr233 and Trp295 to those smaller residues Thr64, Thr161, Ser236, Leu298 in EpzP. The various sizes of the aromatic binding site can explain the catalytic specificities of each PTs towards different aromatic substrates, prenyl donors as well as the orientation of the substrate.

Because the aromatic binding site accommodates both the prenyl chain of the donor and the aromatic substrate, and is the most variabile amongst aromatic PTs, the majority of mutational studies have focused attention on this region. Mechanistic mutational studies have been conducted to better understand the essential residues required for catalysis. For example, a conserved glutamate residue, found within most indole prenyltransferases, was proven to be necessary for catalysis through selective mutations.[56] In the case of FtmPT1, single mutant E102Q was generated and incubated with its native substrates. This enzyme variantwas unable to catalyze the conversion to tryprostatin B, to the limits of detection, in the presence of the precursor compound, brevianamide F. Interestingly, while both glutamate and glutamine are capable of forming hydrogen bonds with the N-1 atom of brevianamide F, only glutamate contains a negative charge at that position that can serve as a catalytic base, an apparent requirement for catalysis. As a follow up to these results, a similar more recent mutational study was performed in bacterial indole PT, AmbP1 which catalysis

the magnesium dependent selective C-3 geranylation of 3-((Z)-2'-isocyanoethenyl) indole. To study the importance of glutamate at position 209, mutations E209A and E209L were generated, thus replacing the carboxyl group with one that lacks hydrogen-bonding capabilities, and for Leu also or presents a bulkier isopropyl group. Both AmbP1 variants were inactive, further supporting the previous studies results, implicating the importance of the conserved glutamate in catalysis. In addition to a better understanding of the catalytic mechanism, the mutation of key residues has resulted in altered donor and acceptor selectively, increased catalytic abilities, and new regio-specificities of enzyme.[38, 39] Recently, a structure-based engineering study was conducted on the endophenazine prenyltransferase, EpzP, wherein the active site was modeled after a more efficient endophenazine enzyme, PpzP.[47] The resulting single residue mutation, A285Q, yielded a 14-fold increase in catalytic activity when compared to the wild-type enzyme and a two-fold increase in catalytic activity compared to PpzP[46]. Similarly, indolactam prenyltransferases, TleC and MpnD which perform the reverse prenylation and geranylation of indolactam V respectively, a underwent single, double, and triple mutations switching the preference for either geranyl pyrophosphate (GPP) or DMAPP and changing the regio- and stereo-selectivity of the enzymes.[53] Mutant K174A of tryptophan prenyltransferase FgaPT2, generated through site-directed mutagenesis, was able to switch prenylation positions and prenyl attachment from its native C-4 normal prenylation capabilities to C-3 reverse reaction [57]. Aromatic PTs are becoming a well-studied biosynthetic enzyme family with strong potential for rational design and engineering to further advance the field of chemoenzymatic synthesis.

Reactions mechanism

Despite a diverse substrate scope of aromatic PTs, the catalytic mechanism is expected to proceed in a similar manner . Specifically, the mechanism of the alkylation reaction has been characterized to proceed via a dissociative S_N1- like mechanism involving a carbocation-mediated electrophilic aromatic substitution[56, 58, 59]. To discern between the dissociative and associative mechanism, positional isotope exchange (PIX) experiments were performed using FgaPT2, a magnesium dependent prentyltransferase from *Aspergillus fumigatus.*[58] In this experiment, DMAPP was synthesized with an ^{18}O –label on the bridging oxygen between the C1 dimethylally and pyrophosphate group [56]. The isotopically label DMAPP was enzymatically reacted with tryptophan and partially converted into product. The unreacted starting material was analyzed for isotopic scrambling via ^{31}P NMR spectroscopy revealing that 15% of the isotopically labelled DMAPP contained the ^{18}O-label in a non-bridging position. These results could possibly indicate a carbocation formation stable enough to allow for a P-O bond rotation in the active site by which the C-O bond cleavage is a reversible step. This would support a S_N1-like dissociative mechanism by which a partially stabilized carbocation could proceed forward to form the arenium ion with the aromatic substrate, or the reaction could proceed backwards, re-associating with the pyrophosphate group to re-form the starting material, DMAPP. To further test the mechanism, a known unreactive tryptophan analog, 6-flurotryptophan, was used in the identical PIX experiment and revealed a similar ratio of non-bridging to bridging isotopic label in the

unreacted starting material. This is believed to further support the existence of a carbocation intermediate mediating the stepwise dissociative mechanism.

Solving the crystal structure of aromatic PTs provided further insight into the enzymatic mechanism. Structures were solved in the presence of the bound substrates providing a snap-shot of the active sight immediately before catalysis. Generally, the pyrophosphate prenyl donors, DMAPP or GPP, bind to a highly conserved binding site, comprised primarily of positively charged and nonpolar residues, neutralizing the negative charge of the pyrophosphate moiety. Most soluble aromatic PTs are metal ion independent, excluding NphB who's prenyl binding site is dependent on the presence of a Mg^{2+} metal ion. Activation of the prenyl moiety involves the release of the pyrophosphate group, generating an allylic carbocation intermediate capable of multiple resonance forms leading to either a forward (C-2) or a reverse (C-3) addition of the alkyl group. Studies have indicated the double bond at the β-position of the prenyl donor is crucial for the stability of the carbocation, loss or change location did not yield any product[60]. As seen in the crystal structure of both NphB/CloQ and DMATS family of aromatic prenyltransferase, the carbon chain moiety of the prenyl donor is sandwiched between a conserved tyrosine residue and the aromatic substrate, facilitating the carbocation intermediate *via* stabilizing π-cation interactions and protecting its reaction with unwanted nucleophiles including solvents. Key charged residues, such as glutamate and lysine, are believed to assist during catalysis participating in deprotonation as the substrate undergoes an electrophilic aromatic substitution. Once the arenium ion is formed, the last deprotonation step is thought to be performed either directly by a key

residue or via water mediated interactions, restoring aromaticity and yielding the final product.

Conclusions and future directions.

Over the last decade, many advances have been made towards the structural and biochemical characterization of aromatic PTs, resulting in over 50 biochemically characterized and 14 known structures for the enzymes of this class. This family of aromatic PTs has a diverse and vast acceptor substrate scope while also possessing the ability to accept multiple non-native substrates as well. Since aromatic PTs have the capability to functionally diversify biologically relevant scaffolds, thus producing natural and unnatural products they have the potential to chemoenzymatically synthesize a rich and untapped source of biologically and pharmacologically interesting compounds. High structural complexity and limited late stage functionalization methods prevent cost effective total synthesis of many natural products, limiting their usefulness as pharmaceuticals. Consequently, the high demand for chemo- and regio-selective catalysts is driving the development of biomimetic chemoenzymatic synthetic methodology. Although much of the proposed utility of aromatic PTs has been directed at their promiscuous aromatic substrate scope, we aim to showcase their ability to diversity natural products and pharmaceutical compounds through non-native alkylation. The successful utilization of unnatural acceptor and donor substrates with aromatic PTs will dramatically enhance the accessibility to a large unexplored chemical space.

Chapter 2: Determination of Alkyl-Donor Specificity of Tyrosine-*O* Prenyltransferase SirD from *Leptosphaeria maculans* [a]

Introduction

Sirodesmin PL is a non-host specific phytotoxin produced by the pathogenic fungus *Leptosphaeria maculans*, known for causing the devastating blackleg disease in canola. Sirodesmin PL is a member of the epipolythiodioxopiperazine (ETP) class of secondary metabolites found in fungi. Like other ETPs, sirodesmin PL features a disulphide bridge across a diketopiperazine ring and exhibits antifungal, antibacterial, antiviral activities[61-63]. Interest in the properties of this secondary metabolite sparked a drive to investigate into the biosynthetic gene cluster and biosynthetic pathway for sirodesmin PL, leading to the discovery of a putative prenyltransferase gene *sirD*[64]. SirD was found to be responsible for the *O*-prenylation of L-Tyrosine in the first pathway specific step for the biosynthesis of sirodesminPL (Figure 4)[65]

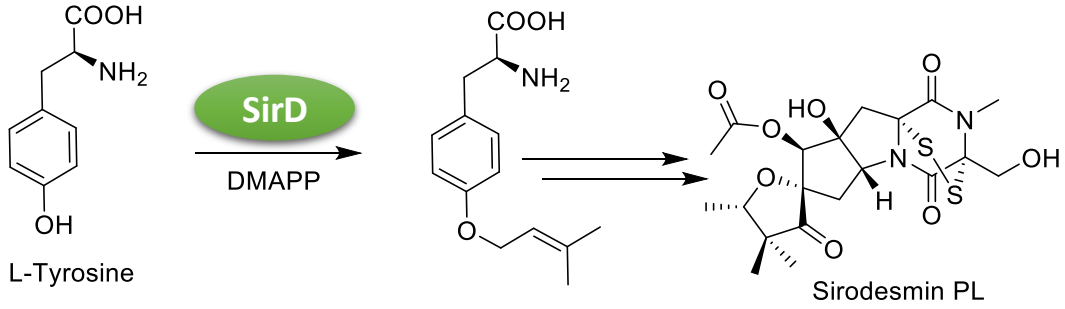


Figure 4. Sirodesmin biosynthetic pathway.
Biosynthetic pathway for sirodesmin PL involving SirD in the first committed step of the pathway.

[a] Reprinted with permission from: John Wiley and Sons and ChemBioChem, Authors Chandrasekhar Bandari, Erin M. Scull, Johanna M. Masterson, Rachel H. Q. Tran, Steven B. Foster, Kenneth M. Nicholas, and Shanteri Singh. "Determination of Alkyl-Donor Promiscuity of Tyronside Prenyltransferase SirD from *Leptosphaeria maculans" ChemBioChem* ***2017,*** *18 (23), 2323-2327* DOI 10.1002/cbic.201700469. Copyright 2017 ChemBioChem. Copy-right permission has been included in the appendix.

Due to its high sequence similarity to known DMATS enzymes, prenyltransferase SirD is presumed to have the characteristic PT-fold, although the structure remains unknown. The functionally of SirD is independent of metal cations alike with other indole PTs. In addition to its native function in the synthesis of dimethylallyltyrosinde, SirD has been shown to accept tryptophan, tryptophan derivatives, tyrosine and tyrosine derivatives such as 4-aminophenylalanine, 4-methoxytryptophan, 7-methyltryptophan, 4-mecraptophenylalanine, and L-3, 4- dihydroxyphenylalanine (Figure 5).[66, 67] Through the structural elucidation of the enzymatic products, SirD is capable of catalyzing O-, C-, N- and S-, prenylation[30, 66]. Specifically, SirD catalyzes normal S-prenylation of the sulfhydryl group of mecraptophenylalanine as well as the normal N-prenylation of the amino group of 4-aminophenylalanine. SirD also catalyzes the N- and C- prenylations of tryptophan and tryptophan derivatives with the ability of transferring the prenyl group onto three different sites of the indole ring (N1, C6, C7), performing a normal prenylation at C6 and a reverse prenylation at C7 and N1. Through these studies, it was concluded that the electronic properties of the substituents on the indole ring played a role in determining the regio-specificity of the prenylation. Incubation with 4-methyltryptophan yielded a normal prenylation at C7 and a reverse prenylation at N1, while 4-methoxytrptophan gave a normal and reverse prenylation only a C7. Similar to other DMATs[60, 68, 69], SirD catalyzed reactions when incubated with unnatural pyrophosphate donors methylallyl pyrophosphate (MAPP), 2-pentenyl pyrophosphate (2-pen-PP), and benzyl pyrophosphate[32]. Further, it is believed that these studies provide evidence that SirD follows the dissociative electrophilic alkylation mechanism proposed for the prenylation by other DMATSs where the orientation of the

substrate in the enzymatic active site and electronic effects play a pivotal role in determining position and prenylation type.

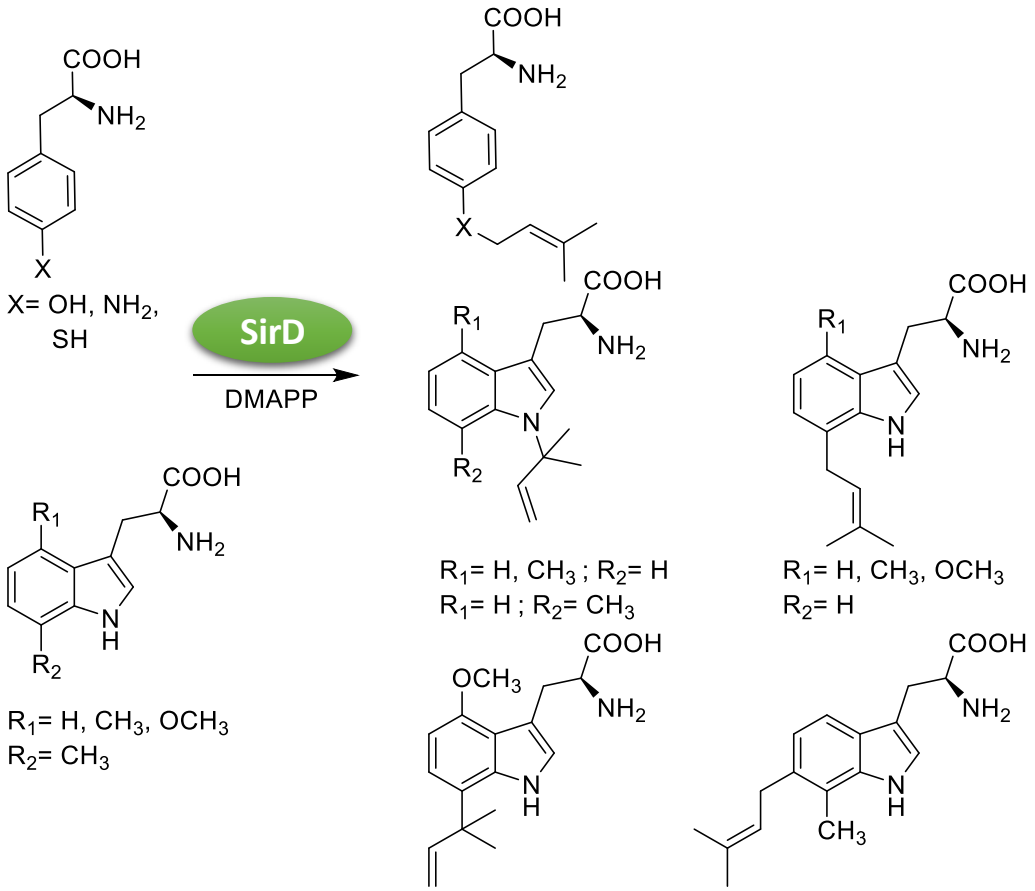


Figure 5. Products of SirD
SirD enzymatic products after incubation with tyrosine or tryptophan derivatives with DMAPP

Research Objectives

Studies thus far by different groups were focused on investigation of acceptor substrate specificity of SirD. These studies have demonstrated that SirD accepts derivatives of L-Tyr and L-Trp, catalyzing normal (attachment via C1′ of DMAPP) or reverse (attachment via C3′ of DMAPP) prenylation of *O*-, *N*-, *S*- and *C*- nucleophilic centers (Figure 5).[30, 66] However, apart from a couple of unnatural alkyl donor (2-pentenyl-

and benzyl- groups[70]) studies, not much is known about the unnatural alkyl-donor specificity of SirD. The goal of this study is to understand the alkyl donor specificity of SirD. To do this, we assessed the alkyl donor specificity of SirD using 21 synthetic alkyl pyrophosphate (alkyl-PP) analogues, performed the kinetic studies and identified the regio-specificity of the alkylated products using NMR spectroscopy.

Contribution

In this study, the library of alkyl-donors (Figure 6) was synthesized by Dr. Chandrashekar Bandari, Johanna Masterson, and Rachel Tran. The large-scale tyrosine alkylation reaction, HRMS analysis and NMR characterization was done by Dr. Chandrashekar Bandari. My contributions involve expression and purification of SirD, reverse phases high-performance liquid chromatography (RP-HPLC) assessment of alkyl-donor specificity of SirD and determination of kinetic parameters for SirD catalyzed reaction with diverse alkyl-donors. Most of the contents including text, tables and figures for this chapter were directly taken from the publication .[71]

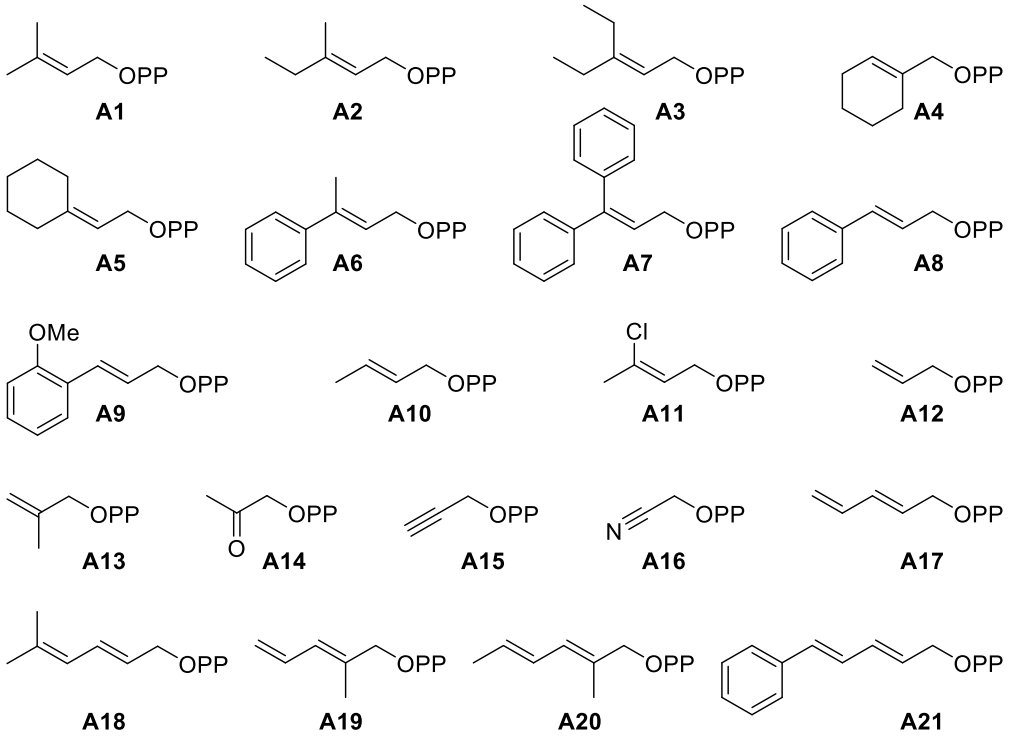


Figure 6. Library of synthetic alkyl-PP
Pyrophosphate analogues assessed with SirD catalyzed reaction with L-Tyr.

Results and Discussion

The recombinant SirD was overexpressed in *Escherichia coli* BL21(DE3) cells transformed with a codon optimized synthetic *sirD* gene in pET28a vector. The

resulting SirD with *N*-terminal His_6-fusion protein was purified to homogeneity via Ni-NTA affinity chromatography. Standard uniform assay conditions (1.2 mM alkyl-PP analog, 1 mM L-Tyr, 5 µM SirD, 25 mM Tris, 5 mM $MgCl_2$, 50 mM KCl, pH 7.5, 16 h at 35 °C) were adopted to facilitate the assessment of donor substrate specificity of the SirD with synthetic alkyl-PP analogues (Figure 6). Production of alkyl-L-Tyr derivatives was determined by a RP-HPLC end point assay (Figure 7) with subsequent confirmation by HRMS coupled with liquid chromatography (LC) analysis for all positive reactions to afford complete analysis of the desired product (Table 1).

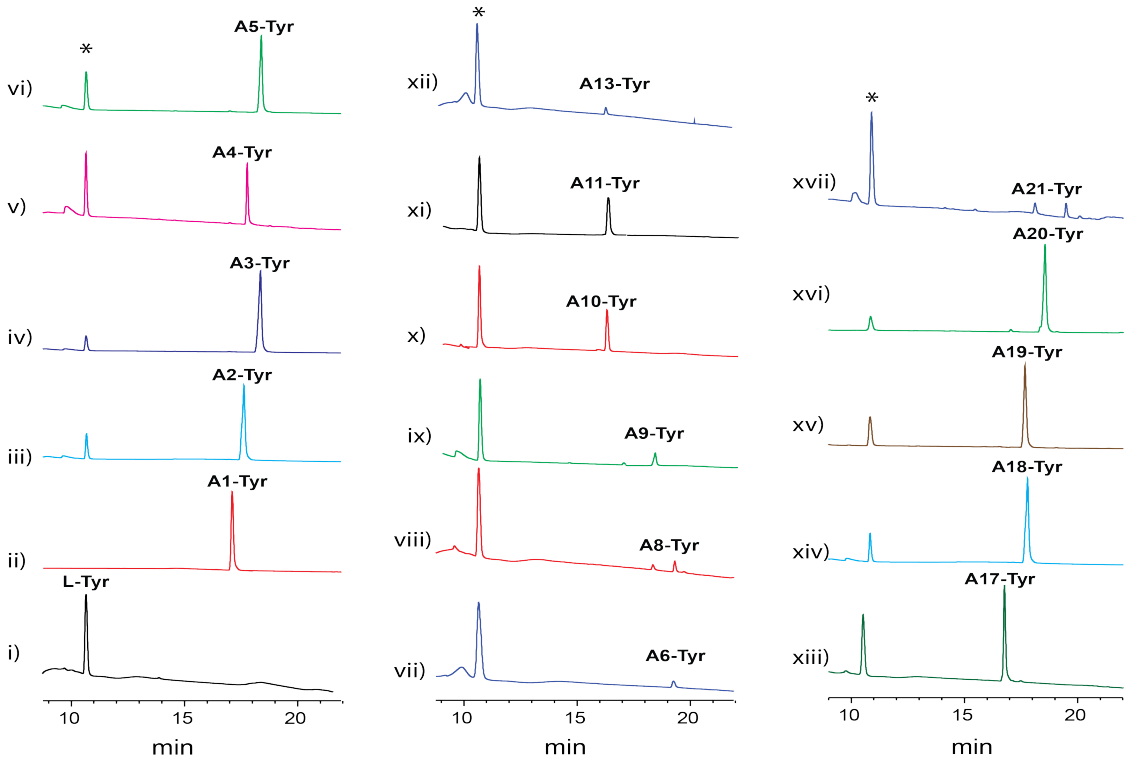


Figure 7. RP-HPLC chromatograms of SirD catalyzed reactions.
*Reactions were incubated with L-Tyr and alkyl-PP analogues that led to the formation of corresponding alkyl- L-Tyr analogues. The remaining L-Tyr and product of the reaction are labeled with * symbol and compound number respectively.*

RP-HPLC and HRMS Studies

An initial assessment of the SirD catalyzed alkylation of L-Tyr with 21 synthetic alkyl-PPs based upon RP-HPLC of analytical scale reaction is illustrated in Figure 7, wherein 16 of 21 synthetic analogues in SirD catalyzed reactions resulted in corresponding alkylated L-Tyr products. Fourteen of the 16 positive SirD reactions produced a single corresponding mono-alkylated L-Tyr products, whereas, two analogues (**A8** and **A21**) resulted in two mono-alkylated L-Tyr products each as confirmed by HRMS analysis (Table 1). Of the 21 putative substrates tested with SirD, 9 led to appreciable (>50%) production of the corresponding *O*-alkyl- L-Tyr, an additional 2 led to moderate (25-50%) conversion, and 5 offered detectable product (<25%) under the conditions described (Figures 9 and 10). Except for **A7**, **A12** and **A14**, all analogues with a double bond at the β-position served as substrates.

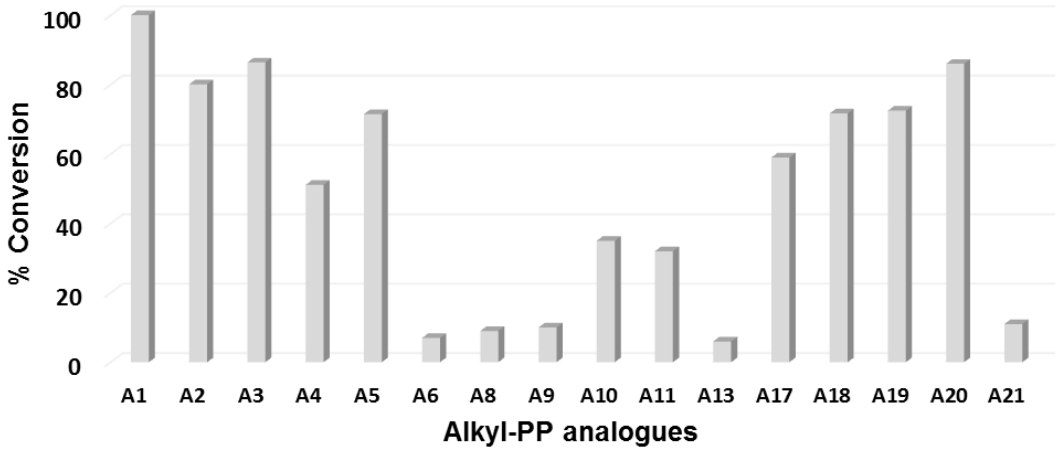


Figure 8. Percent conversion
Percent conversion of alkyl-PP analogues to the corresponding alkyl-L-Tyr catalyzed by SirD based upon RP-HPLC. No product formation was observed in the absence of SirD or alkyl-PP analog.

Table 1. Summary of HRMS data of alkyl-*O*-Tyr analogues from SirD catalyzed alkylation reaction with L-Tyr and synthetic alkyl-PP analogues

Enzyme Product	Chemical Formula	Calculated Mass	Observed Mass
A1-Tyr	$C_{14}H_{20}NO_3$ $[M+H]^+$	250.1443	250.1446
A2-Tyr	$C_{15}H_{22}NO_3$ $[M+H]^+$	264.1600	264.1599
A3-Tyr	$C_{16}H_{24}NO_3$ $[M+H]^+$	278.1756	278.1756
A4-Tyr	$C_{16}H_{22}NO_3$ $[M+H]^+$	276.1600	276.1585
A5-Tyr	$C_{17}H_{24}NO_3$ $[M+H]^+$	290.1756	290.1757
A6-Tyr	$C_{19}H_{22}NO_3$ $[M+H]^+$	312.1600	312.1599
A8-Tyr	$C_{18}H_{20}NO_3$ $[M+H]^+$	298.1443	298.1444
A9-Tyr	$C_{19}H_{22}NO_4$ $[M+H]^+$	328.1549	328.1553
A10-Tyr	$C_{13}H_{18}NO_3$ $[M+H]^+$	236.1287	236.1274
A11-Tyr	$C_{13}H_{17}ClNO_3$ $[M+H]^+$	270.0897	270.0895
A13-Tyr	$C_{13}H_{18}NO_3[M+H]^+$	236.1282	236.1274
A17-Tyr	$C_{14}H_{18}NO_3[M+H]^+$	248.1287	248.1283
A18-Tyr	$C_{16}H_{22}NO_3$ $[M+H]^+$	276.1600	276.1605
A19-Tyr	$C_{15}H_{20}NO_3$ $[M+H]^+$	262.1443	262.1443
A20-Tyr	$C_{16}H_{22}NO_3$ $[M+H]^+$	276.1600	276.1604
A21-Tyr	$C_{20}H_{22}NO_3$ $[M+H]^+$	324.1600	324.1597

Kinetic Studies

The SirD steady-state kinetic parameters for reactions with alkyl-L-Tyr yield > 25% were determined based on product formation monitored by HPLC (Table 2, Figure 9). Importantly, the K_M values for most of the analogues remained similar except for **A18**, where a 5 - 6-fold increase in the K_M compared to **A20** is observed, likely caused by the steric factors in the active site of the enzyme due to the presence of extra terminal methyl group. Surprisingly, **A11**, where an electron withdrawing chloro group replaced one of the methyl groups of DMAPP, and **A10**, which lacks a methyl group of DMAPP, were equally efficient (Table 2). However, both **A10** and **A11** were ~200 fold worse compared to the natural alkyl donor, **A1**, even though their K_M was 3 – 4 times lower than **A1**. Interestingly, where direct comparisons could be made, the analogues that contained groups to enhance the stability of carbocation[72] via increased conjugation

or resonance stabilization correlated with the increased catalytic efficiency. For example, the k_{cat} values of the reaction correlated with conjugation by methyl group in the order, **A1** > **A2** > **A3** > **A10** > **A17** (Table 2). Even among the analogues containing conjugated double bonds (**A17- A20**), the increase in the k_{cat} values of the reaction correlated with the presence of methyl group in the order, **A20** > **A19** > **A18** > **A17** (Table 2). While the literature precedence suggests cinnamyl carbocations to be highly stable,[73] cinnamyl analogues did not serve as good alkyl donors for the SirD reaction with L-Tyr. This is likely attributed to the steric hindrance in the active site of the enzyme due to the aromatic group in the analog (Table 2). Similar results were obtained for other analogues containing aromatic groups. However, the analogues that contained a triple bond at the β-carbon (**A15** and **A16**) did not serve as donors, likely due to the reduced stability of the carbocation[72] by the attached sp-hybridized alkynyl group in addition to the steric requirement of the enzyme. Similarly, the analogues with electron withdrawing groups at the β-carbon (**A14**) did not serve as donors.

Table 2. Kinetic parameters for SirD with 1 mM L-Tyr and 0.025 - 6 mM alkyl-PP analog in 25 mM Tris, 5 mM $MgCl_2$, 50 mM KCl, pH 7.5 at 35 °C.

Alkyl-PP analog	k_{cat} (min^{-1})	K_M (mM)	k_{cat} / K_M ($mM^{-1}min^{-1}$)
A1	41 ± 3	0.23 ± 0.06	178 ± 15
A2	18 ± 2	0.20 ± 0.11	90 ± 31
A3	3.3 ± 0.2	0.24 ± 0.08	14 ± 3
A4	0.33 ± 0.02	0.13 ± 0.03	2.5 ± 0.6
A5	3.5 ± 0.3	0.21 ± 0.05	16 ± 2
A10	0.060 ± 0.003	0.07 ± 0.06	0.9 ± 0.2

A11	0.04 ± 0.02	0.05 ± 0.04	1.0 ± 0.3
A17	0.05 ± 0.01	0.26 ± 0.07	0.20 ± 0.06
A18	0.10 ± 0.06	0.73 ± 0.19	0.14 ± 0.02
A19	0.22 ± 0.08	0.17 ± 0.04	1.3 ± 0.3
A20	0.74 ± 0.02	0.12 ± 0.05	6.1 ± 0.8

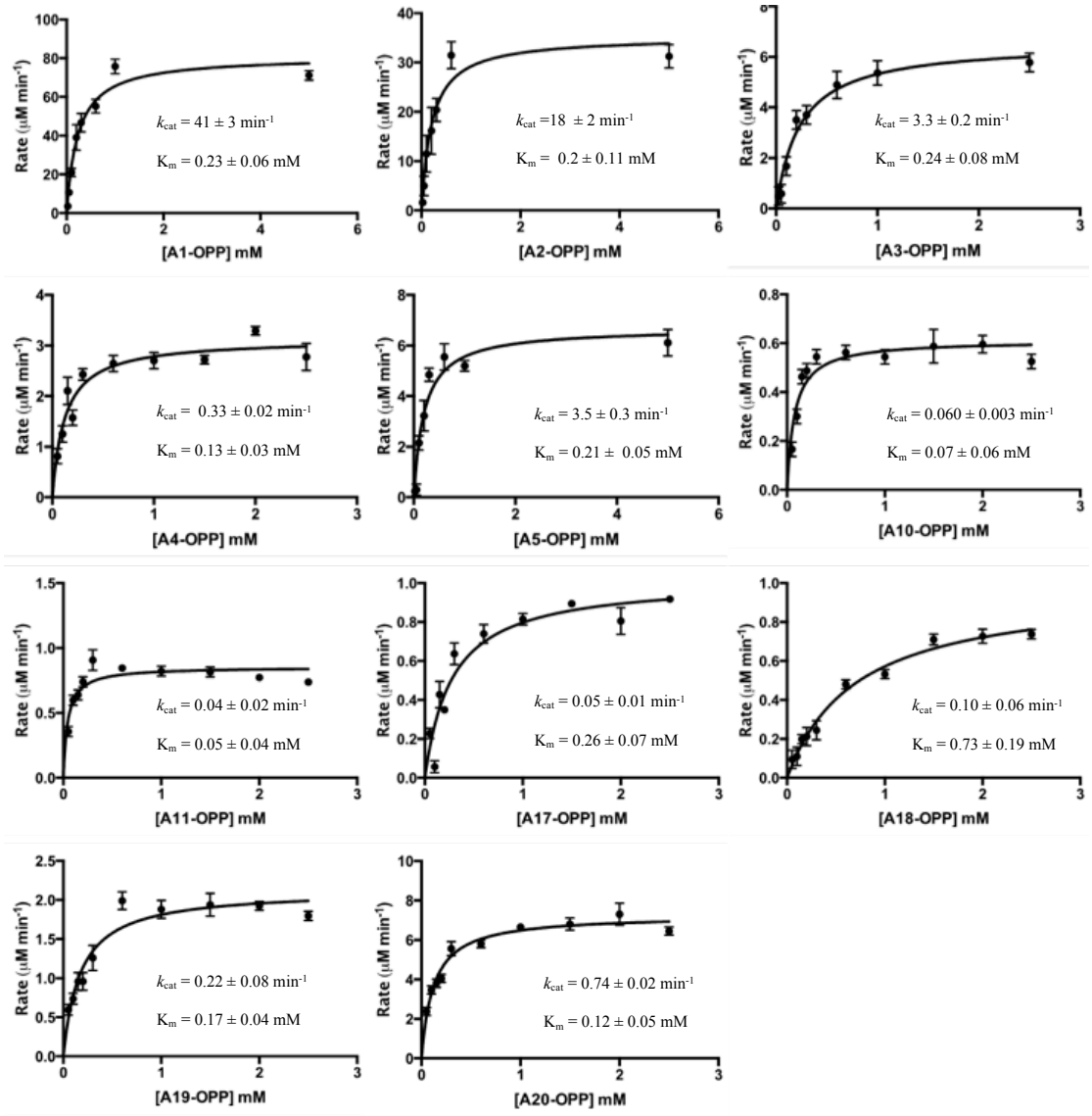


Figure 9. Michaelis-Menten kinetic plots for SirD reactions
Kinetic parameters detemered by Michaelis-Menten plots with 1mM Tyrosine and varying concentrations of pyrophosphate analogues

SirD Structural Model

In order to understand the alkyl-PP chain-length selectivity by SirD, we generated a homology model of SirD based on the template structure of FgaPT2 (PDB accession number 3I4X) that covered 92% sequence length of SirD (a.a. 27-440), and shared 30% sequence identity and 65% sequence similarity with SirD using SWISS-MODE.[74] In the SirD structural model, the L-Tyr and the non-hydrolyzable form of DMAPP (DMSPP) were docked posed for catalysis in a similar manner as in other ABBA PT structures (Figure 10).[24, 36, 40, 41, 47, 49]

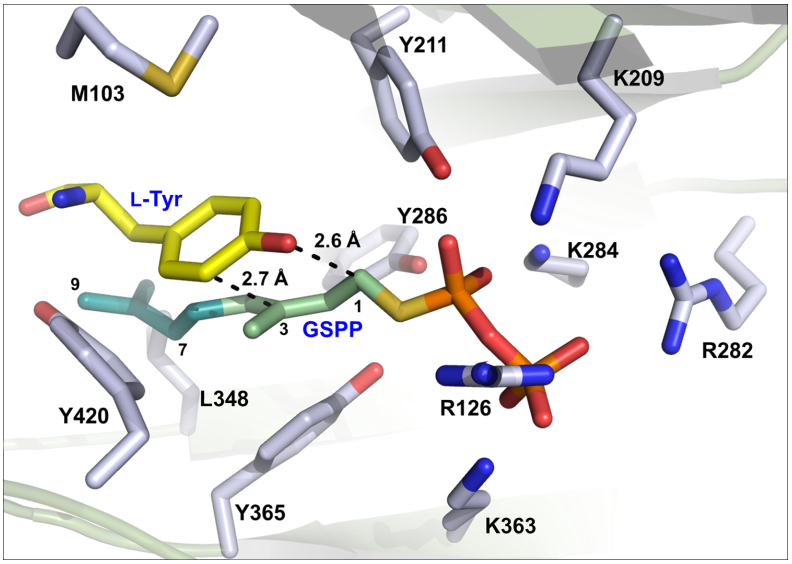


Figure 10: Structural model of SirD.
Structure is based on the template structure of FgaPT2 (PDB 3I4X) with docked L-Tyr (colored in yellow) and dimethylallyl thiopyrophosphate (DMSPP, colored in green). Colored in ligh-blue stick models are the active site residues of SirD interacting with DMSPP and L-Tyr.

Briefly, the docking of the DMSPP and L-Tyr in the active site of SirD was performed to be consistent with the conserved interactions found among the class of ABBA PTs.[24, 36, 40, 41, 47, 49] These include hydrogen bonding interactions of the amine side chain of conserved basic residues (R126, K209, R282, K284, and K363; Figure 10)

and the conserved aromatic residues (Y211, Y 286, Y365 and Y420) positioned to shield and stabilize the alkyl carbocation via π-cation interactions (Figure 10). Interestingly, according to the SirD model displayed in Figure 10, the distance between -OH of L-Tyr and -C1' of DMSPP; as well as C-3 of L-Tyr and -C3' of DMSPP are ~2.6 Å. While the distance may facilitate either C1′- normal *O*-prenylation or C3′-reverse prenylation, the nucleophilicity of the -OH group seems to drive the observed normal *O*-alkylation of L-Tyr by SirD. In the SirD model, the alkyl chain of the natural donor, **A1** seem to stack on the aromatic ring of the Y365. The current SirD model suggests steric clash to be a potential contributing factor to the low or no turn-over of alkyl donors containing long carbon chain or bulky aromatic groups.

NMR Studies

The SirD alkylation reactions with product yield > 25% were scaled up and purified via RP-HPLC to understand the regio-chemistry of alkyl group transfer. Based on the NMR characterization of the regiospecificity of SirD catalyzed alkyl-transfer performed by Dr. Bandari, all alkyl-L-Tyr (Figure 6, **A1**, **A2**, **A3**, **A4**, **A5**, **A10**, **A11**, **A17**, **A18**, **A19**, **A20**) were confirmed as *O*-alkylation of L-Tyr analogues (Figure 11). Additionally, SirD produced two mono-alkylated L-Tyr products in the presence of **A8** and **A21**. This suggests possibility of alkylation of L-Tyr at other nucleophilic center apart from –OH of L-Tyr. Based on the proximity of -C3 of L-Tyr to -C3' of DMSPP in the current SirD model (Figure 10), the reverse alkylation at –C3 of L-Tyr seems more likely, in addition to the normal *O*-alkylation. However, a better understanding of the relationship between substrate and SirD regioselectivity requires more studies including the crystal structures of SirD bound to different substrates.

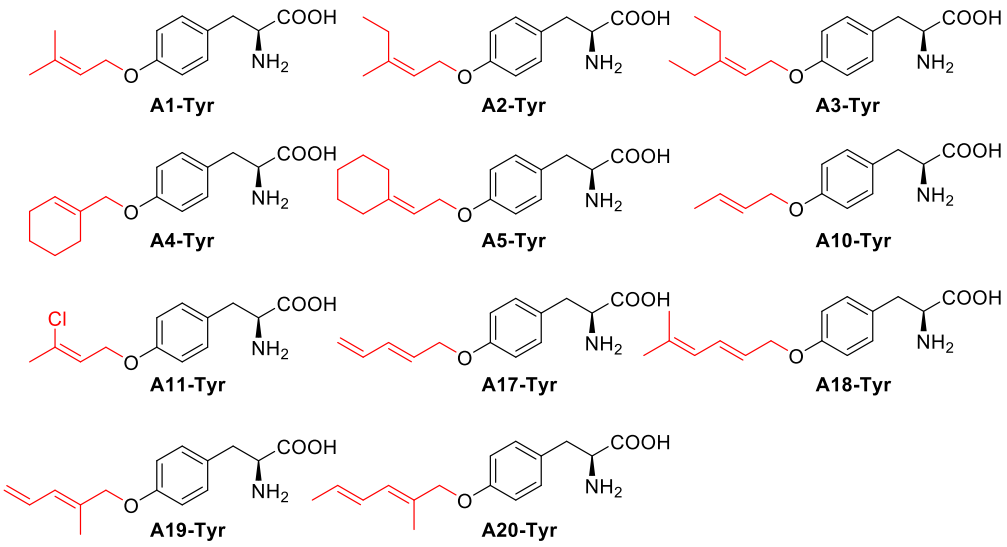


Figure 11. NMR confirmed structures.
Structures of alkyl-tyrosine products of SirD reaction with alkyl-PP analogues determined by NMR.

Conclusions

In summary, the presented work demonstrates the pliable nature of SirD towards a wide range of allylic alkyl donors, which is expected to be further expanded via enzyme engineering. In addition, our work also demonstrates SirD to catalyse mostly regiospecific, normal *O*-alkylation of L-Tyr. Thus, these studies highlight the potential utility of SirD for chemoenzymatic differential alkylation of natural products and open the door for interrogation of the alkyl donor specificity of other prenyltransferases.

Experimental

Unless otherwise stated, all chemicals and reagents were purchased from Sigma-Aldrich (St. Louis, MO, USA), Acros (New Jersey, USA), Alfa-Aesar (Ward Hill, MA, USA) or TCI (Portland, OR, USA) and were reagent grade or better. PD-10 column and Ni-NTA superflow columns were purchased from GE Healthcare (Piscataway, NJ).

General methods

All reactions were conducted in oven- or flame-dried glassware under a nitrogen atmosphere with anhydrous solvents, unless otherwise noted. Reactions were monitored by thin-layer chromatography (TLC) (EMD Millipore Corp, Billerica, MA, USA) and visualization was accomplished with UV light (254 nm) followed by staining with phosphomolybdic acid solution or anisaldehyde solution and heating. Flash column chromatography was performed using ACS grade solvents and silica gel (SiliCycle Inc, P60, particle size 40-63 μm). HPLC was accomplished using Agilent 1220 system equipped with a DAD detector. **Method A (HPLC):** To monitor SirD reactions, analytical reverse-phase (RP) HPLC employed a Gemini-NX, C-18 (5 μm, 4.6 mm × 250 mm) column (Phenomenex, Torrance, California, USA) [gradient of 1% B to 10% B over 10 min, 10% B to 50% B over 5 min, 50% B to 100% B for 12 min, 100% B to 1% B over 1 min, 1% B for 7 min (A = ddH_2O with 0.1% TFA; B = acetonitrile) flow rate = 1 mL min^{-1}; A_{220}]. The reaction was monitored by the retention time difference between starting material and product. **Method B (HPLC):** Semi-preparative RP HPLC was conducted on a Gemini-NX, C-18 (5 μm, 10 mm × 250 mm) column (Phenomenex, Torrance, California, USA) to purify the L-Tyr analogues [gradient of 1% B to 10% B over 10 min, 10% B to 50% B over 5 min, 50% B to 100% B for 12 min, 100% B to 1% B over 1 min, 1% B for 7 min (A = ddH_2O with 0.1% TFA; B = acetonitrile) flow rate = 2 mL min^{-1}; A_{220}]. High-resolution mass spectrometric (HRMS) data and liquid chromatography mass spectrometric (LCMS) were obtained on Agilent 6545-QTOF W/1290 HPLC mass spectrometer at the University of Oklahoma, Department of Chemistry and Biochemistry.

Overexpression and purification of SirD

The *Leptosphaeria maculans* SirD in pET28a vector bearing *N*-terminal-His_6 fusion was provided by Prof. Jon Thorson (University of Kentucky). Recombinant SirD with *N*-terminal-His_6 (herein referred to simply as SirD), was expressed in a *E. coli* BL21(DE3) host in the presence of 50 μg mL^{-1} of kanamycin at 37 °C to an OD_{600} of ~0.6, reduced the temperature to 20 °C, induced with 0.5 mM IPTG, and continued to grow at 20 °C for another 16 h. The cells were harvested by centrifugation (30 min, 5000 rpm), resuspended in buffer A (20 mM NaH_2PO_4, 300 mM NaCl, 10 mM imidazole, pH 7.8). The cells were lysed for 30 min on ice by sonication (Fisher Scientific Model FB505; Thermo Fisher Scientific, Waltham, MA; 500 W, 4 x 30 s pulses, ~1 min between pulses) on ice. SirD was purified via affinity chromatography (5 mL HiTrap Ni-NTA chelating column, GE Healthcare, Piscataway, NJ) following standard linear gradient (50 mM NaH_2PO_4, 300 mM NaCl, pH 8.0 with a linear gradient of imidazole of 10-500 mM) using an NGC™ liquid chromatography systems (Bio-Rad, USA). Buffer exchange of pooled fractions containing the purified protein was accomplished using a PD-10 column (GE Healthcare) eluted with 25 mM Tris-HCl, 50 mM KCl, pH 8. Protein concentrations were determined by Bradford assay (Bio-Rad, Hercules, CA, USA) using BSA as a standard. All studies were conducted with SirD, that retained the *N*-terminal-His_6 affinity tag.

In-vitro SirD assay

In vitro SirD reactions were conducted in a volume of 20 μl with 1.2 mM alkyl-pyrophosphate analog (compound **A1** – **A21**), 1 mM L-Tyr and 5 μM purified SirD in 25 mM Tris buffer pH 8.0, 5 mM $MgCl_2$, 50 mM KCl, incubated at 35 °C for 16 h.

Reactions were quenched by adding an equal volume of methanol followed by centrifugation (10,000 x g for 15 min) to remove the precipitated protein and product formation for each reaction was subsequently analyzed by RP-HPLC using method A. For each reaction, percent yield was based upon the integration of species at 254 nm and calculated by dividing the integrated area of product by the sum of integrated area of product and/or and the remaining substrate. All putative products were subsequently confirmed by HRMS with positive (+) and/or negative (-) mode. Kinetic parameters were assessed using 1 mM L-Tyr and variable alkyl-PP analogues (0.1 - 5 mM). Assays were conducted in triplicate and all rates were confirmed to be linear. The kinetic curves were fit to Michaelis-Menton kinetics using Prism 5.04 (GraphPad Software, Inc. La Jolla, CA 92037 USA). The reactions with > 25% product yield were scaled (>500 μM L-Tyr), purified by semi-prep HPLC using method B and the putative new products were confirmed by NMR.

SirD structural model

A SirD BLAST search against the structural database, PDB revealed SirD to have 30% sequence identity with Trp-*C*4-PT, FgaPT2 (PDB 3I4X). A SirD homology model was constructed based upon FgaPT2 using Swiss-Model.[74] Atomic coordinates of the ligands, L-Trp and DMSPP were obtained from FgaPT2 structure (PDB 3I4X). L-Tyr model was generated by manual editing of the L-Trp using the builder module of PyMol (http://www.pymol.org) with no additional energy minimization performed on the structures. Both L-Tyr and DMSPP were subsequently modeled in the active site of SirD in a manner consistent with the conserved interactions observed for other ABBA-PTs. [24, 36, 40, 41, 47, 49] The conserved interactions used for modeling-in the

ligands include the stacking interaction of L-Tyr with the prenyl moiety of DMSPP and the hydrogen bonding interactions of amine side chain of conserved basic residues (R128, K209, R282 and K284) with the pyrophosphate moiety. Figures were generated with PyMol.

Chapter 3. Determination of Alkyl-Donor Specificity of a Tryptophan-*C4*- Prenyltransferase FgaPT2 from *Aspergillus fumigatus.*[b]

Introduction

Filamentous fungi, such as *Aspergillus*, possess some of the most impressive chemical factories known in biology and are an incredible source of biologically active natural products.[27] Even more, their natural products are being used as scaffolds for more focused diversity oriented pharmacological and drug libraries.[75] In the biosytnthesis of ergot alkaloids, DMATS has been identified to catalyze the first pathway-specific reaction, attaching a prenyl moiety onto L-tryptophan.[76] In 2005 a DMATS gene *fgaPT2,* was identified in the genome sequence for *A. fumigatus.* FgaPT2 is a soluble indole PT responsible for catalyzing the transfer of a prenyl group onto the C-4 position of L-tryptophan, which is the first step in the biosynthesis of many indole alkaloids such as the fumigaclavines (Figure 12).[77] This prenyl group can then be incorporated into a polycyclic carbon scaffold giving rise to diverse active natural products.

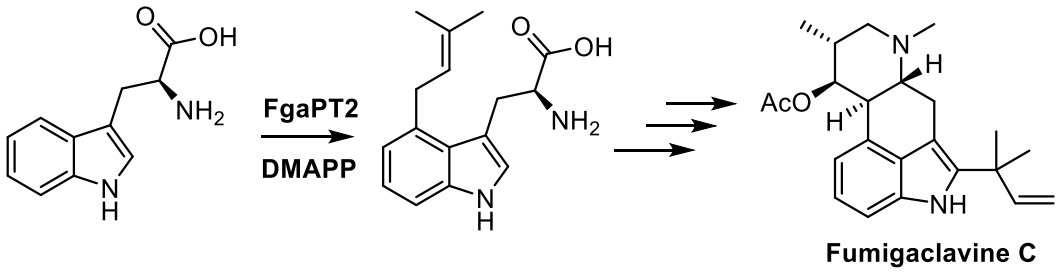


Figure 12. The role of FgaPT2 in fumigaclavine C biosynthesis

---

[b] Reprinted with permission from: Royal Society of Chemistry and MedChemComm, Authors Chandrasekhar Bandari, Erin M. Scull, Tejaswi Bavineni, Susan L. Nimmo, Eric D. Gardner, Ryan C. Bensen, Anthony W. Burgett and Shanteri Singh. "FgaPT2, a biocatalytic tool for alkyl-diversification of indole natural products*"* *MedChemComm* ***2019,*** MD-RES-03-2019-000177.R2. Copyright 2019 MedChemComm. https://pubs.rsc.org/en/journals/journalissues/md#!issueid=md010006&type=current&issnprint=2040-2503

FgaPT2 is the first DMATS structure to be solved, shortly after the bacterial aromatic PT enzyme NphB structure was published.[36] FgaPT2 shares the PT barrel fold, common among all aromatic PTs, which contains 5 repeating ααββ units. The significant differences between NphB and FgaPT2 structures can be found in the connecting extended loop regions and extra α-helices in FgaPT2. The structure of FgaPT2 complexed with the native substrate tryptophan and DMSPP revealed the architecture of the catalytic binding site and insight into understanding the mechanism of alkylation (Figure 13). L-tryptophan binds to a mostly hydrophobic pocket, forming a hydrogen bond between the indole NH and E89. [35] This likely enhances the reactivity toward the carbocation by stabilizing the positively charged intermediate. This hydrogen bond combined with several others is responsible for orienting the tryptophan within the catalytic chamber, ultimately determining its regioselectivity. Tryptophan forms hydrogen bonds with the side chains of Y191 and R244, and with main chain atoms of I80 and L81.[35] The basic side chain on K174 is located perfectly to help abstract the proton after C4 alkylation. Divalent cations Mg^{2+} and Ca^{2+} enhance the rate of FgaPT2 but are not required.[77] The negative charge of the pyrophosphate binds to the positively charged residues R100, K187, R257, K259, and R404. The oxygen atoms are able to hydrogen bond with Y189, Y261, Y345, Y413, and Q343 (Figure 14).[35] The carbocation that is formed is stabilized by the π electrons of the substrate indole ring and Y345. The carbocation is shielded from reacting with water by Y189, Y261, Y345, Y398, and Y413.[35]

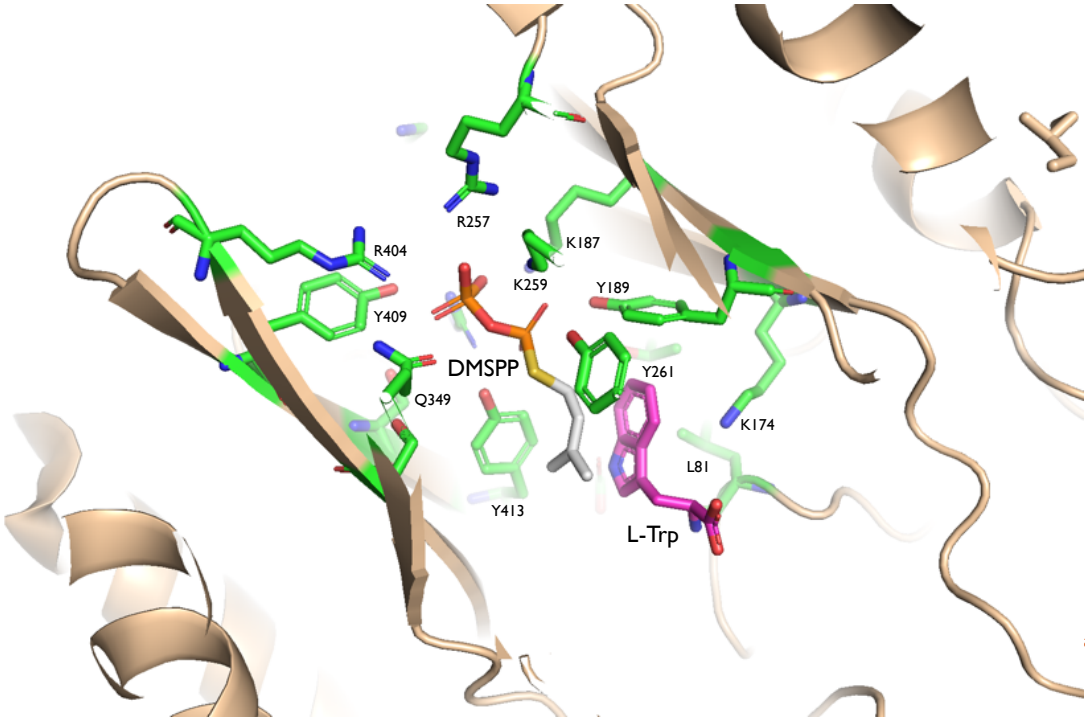


Figure 13. Active site of FgaPT2
DMSPP in the active site side chains binding with pyrophosphate moiety. Residues in the active site interacting with L-tryptophan and carbon chain of DMSPP[35]

In addition to its native catalytic function, FgaPT2 also accepts a variety of alternative substrates (Figure 16). For example, the enzyme can transfer a prenyl group to the 3 position of tyrosine, the 5 position of ortho-tyrosine, and the 4 and 6 position of meta-tyrosine.[78] Tyrosine and 4-amino-phenylalanine are accepted by FgaPT2 resulting in C3 prenylation, 6.2% and 67% yield respectively.[79] Indole-3-propionic acid and L-β-homotryptophan were C4 prenylated by whole cells overexpressing FgaPT2.[80] Cyclo-L-homotryptophan-D-valine was well accepted as a substrate resulting in a 1:1 ratio of C4 and C5 prenylated products.[81] 1-naphthol has also been successfully prenylated with FgaPT2.[82] Daptomycin is also accepted by FgaPT2 to generate a indole N-1 prenylated product.[83]

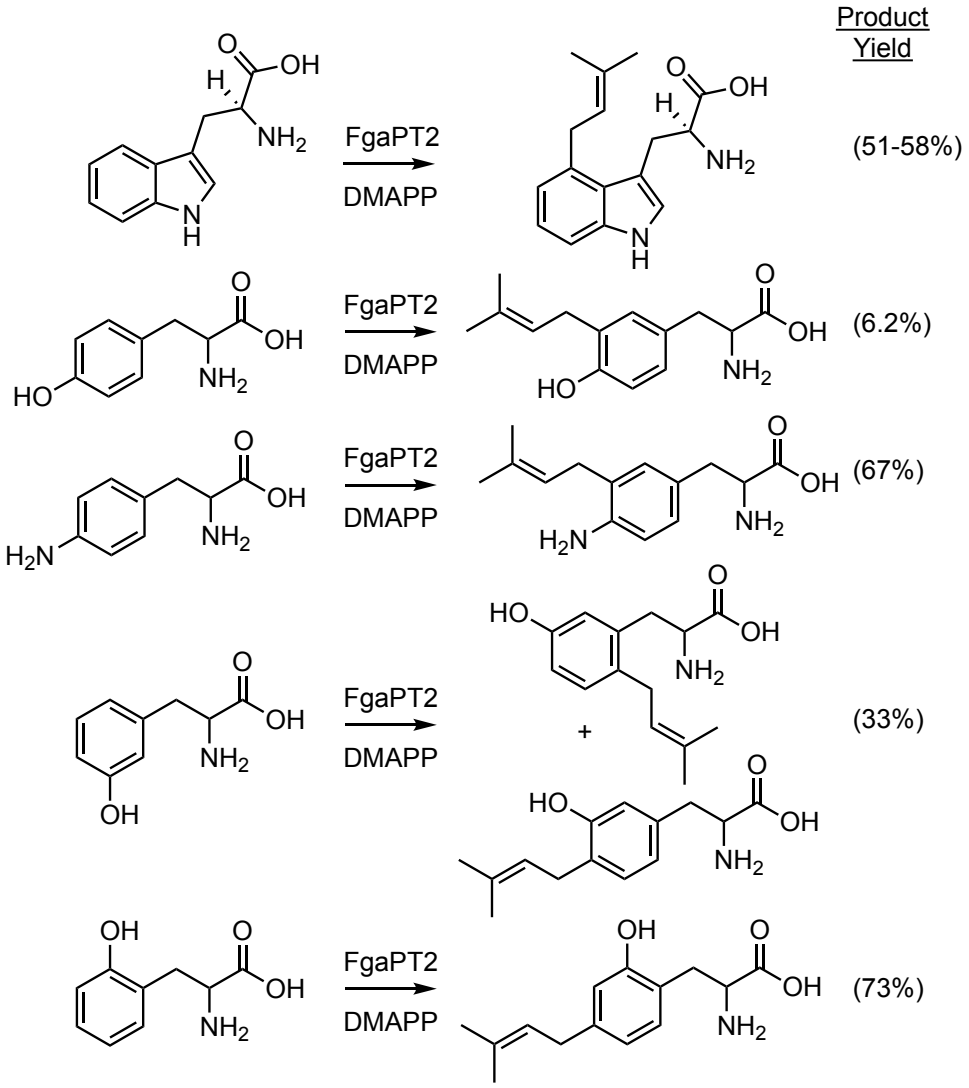


Figure 14. Accepted aromatic substrates by FgaPT2.
Known reactions catalyzed by FgaPT2 and non-native substrates

DMAPP is the natural donor substrate for FgaPT2, however a couple of unnatural pyrophosphates have been successfully transferred using this enzyme. Monomethylallyl pyrophosphate (MAPP) gave a 1:1 mixture of C4 and C5 alkylated tryptophans, while 2-pentenyl pyrophosphate alkylated the 5 position exclusively.[60] Benzyl pyrophosphate was also a substrate for FgaPT2 when incubated with tryptophan analogues, result in predominantly in C5 benzylation. The only 5 substituted indole accepted was 5-OH-Trp which was C6 benzylated by FgaPT2.[68] Native FgaPT2

cannot accept GPP or FPP as donors, however certain mutants have been engineered to accept longer chain donors. The FgaPT2 M328G/R244Q mutant was able to geranylate cyclo-L-Trp-L-Trp at the C4 position.[84] Met328 plays a major role in determining the maximum size of the donor molecule, with many of the smaller side chain mutants (C,A,T,S,G,V,N) having significant activity with GPP. FgaPT2 M328A was also able to accept FPP, although with very low turnover.[85] Site saturation mutagenesis was done on T102, K174, and R244 in attempt to increase the catalytic efficiency of FgaPT2 and alter substrate specificity.[86, 87] FgaPT2 K174F had almost no tryptophan activity but efficiently C3 prenylated L-tyrosine.[79] The related double mutants K174F/R244X (X= L,N,Q,Y) were able to reverse prenylate L-Trp cyclic dipeptides at the C3 position, resulting in cyclization (Figure 15).[87] FgaPT2 mutants R244N, R224L, R224Y and R244Q had substantially higher activity on a variety of L-Trp cyclic dipeptides while maintaining C4 prenylation selectivity.[86] The R244L mutant had the best overall substrate tolerance, converting 20-50% of most dipeptides screened. R244Y was the only mutant particularly good at prenylating cyclo-L-Trp-L-Phe.[86] FgaPT2 mutants K187E, K259E, and R257G all had >95% reduced activity because these residues are known to interact with the diphosphate group.[88]

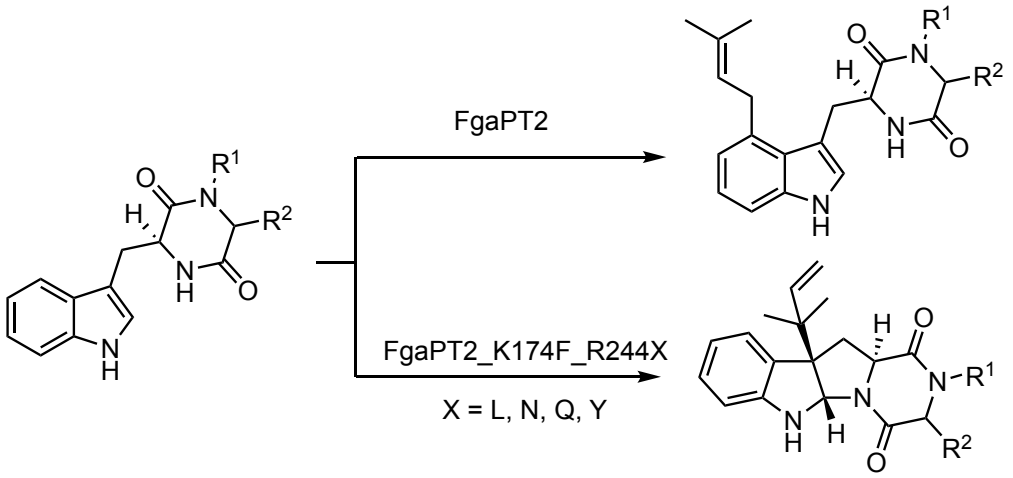


Figure 15. FgaPT2 mutants reactions.
FgaPT2 mutants have been engineered to alter the regioselectivity and substrate preference[87]

Research Objectives

Studies thus far have revealed that FgaPT2 has a broad and diverse acceptor substrate scope including, substituted tryptophans, L-Trp containing cyclic dipeptides, isomers of L-tyrosine, indolocarbazoles, as well as phenolic molecules.[78, 89-94] A few alternative alkyl donors have also been reported with FgaPT2 including the C_{10} geranyl pyrophosphate (GPP), 2-butenyl pyrophosphate, 2-pentenyl pyrophosphate, and benzyl pyrophosphate.[60, 68] Based on our recent studies using tyrosine-*O*-prenyltransferase, SirD that demonstrated relaxed alkyl-donor substrate specificity, [95] in this chapter we describe the alkyl-donor substrate scope of FgaPT2 using 34 synthetic allylic, and benzylic alkyl donors with varying carbon chain length, and substituents. The alkyl donor analogues include 21 allylic analogues described in Chapter 2, and 13 additional benzylic analogues. For the sake of the flow of the manuscript (submitted to MedChemComm) all analogues have been renumbered as described in Figure 16. The study involves assessment of FgaPT2 catalyzed alkylation reaction using RP-HPLC and

HRMS studies, systematic analysis of kinetic parameters and identification of the regio-specificity of the alkylated products using NMR spectroscopy.

Contribution

The library of alkyl-donors (Figure 16) was synthesized by Dr. Chandrashekar Bandari, Johanna Masterson and Rachel Tran. The large-scale tryptophan alkylation reaction and HRMS analysis was carried out by Dr. Chandrashekar Bandari, NMR characterization of alkyl-tryptophan products was performed by Dr. Bandari and Dr. Susan Nimmo. My contributions involve expression and purification of FgaPT2, RP-HPLC based assessment of alkyl-donor specificity of FgaPT2, and determination of kinetic parameters for FgaPT2 catalyzed reaction with diverse alkyl-donors. Most of the contents including text, tables and figures for this chapter were directly taken from the manuscript submitted for publication to MedChemComm.

Results and Discussion

In order to assess the ability of FgaPT2 to accept diverse unnatural alkyl-PP analogues, the recombinant FgaPT2 was overproduced in *Escherichia coli* BL21(DE3) cells transformed with codon-optimized synthetic *FgaPT2* gene in pET28a vector. The resulting FgaPT2 with *N*-terminal His_6-fusion protein was purified to homogeneity via Ni-NTA affinity chromatography as described previously,[40] yielding ~40 mg L^{-1} of pure *N*-terminal His_6-fusion protein.

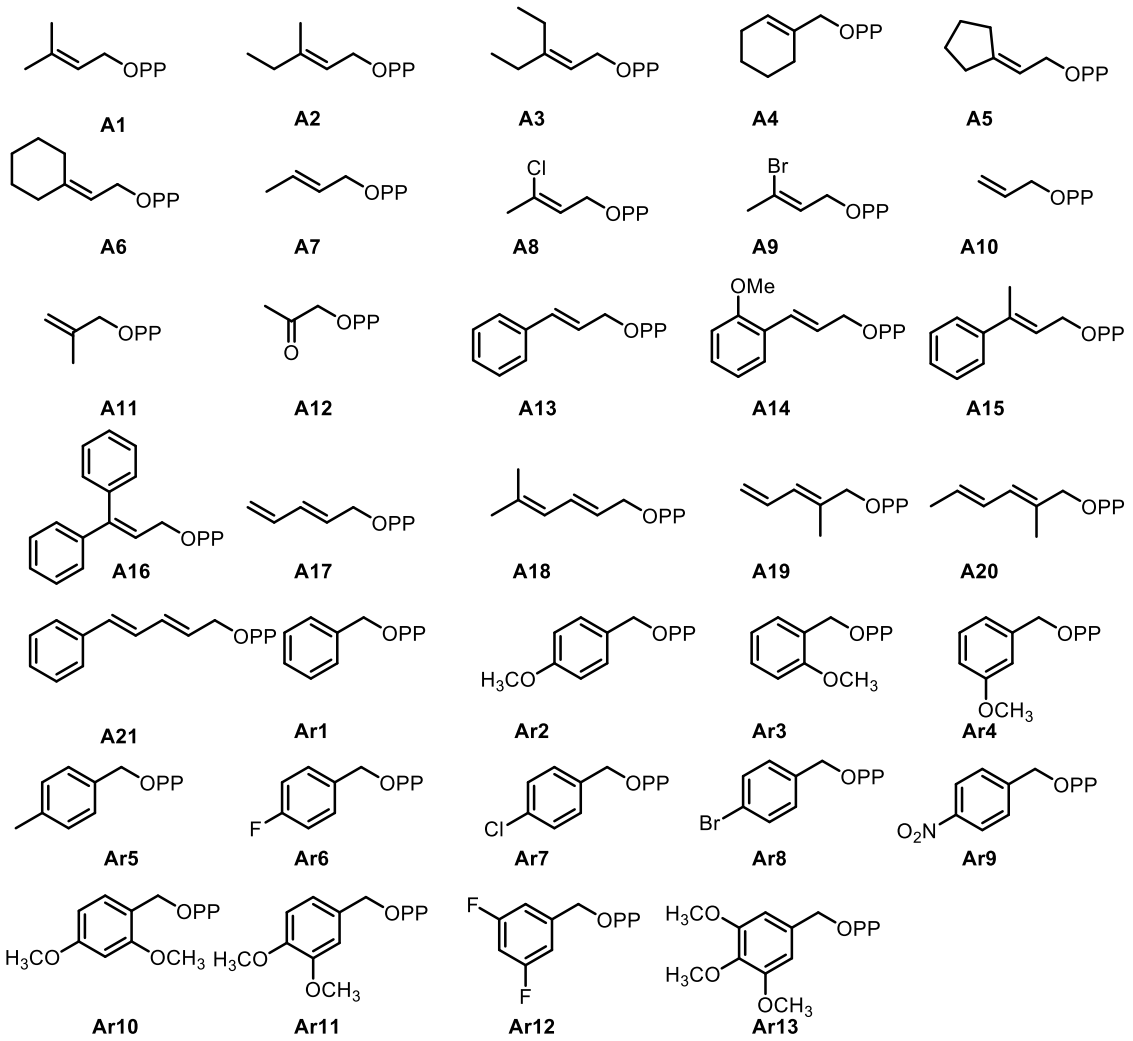


Figure 16. Synthetic alkyl-PP analogues used in this study.

RP-HPLC and HRMS Studies

Standard uniform assay conditions (1.2 mM alkyl-PP analog, 1 mM L-Trp, 5 μM FgaPT2, 25 mM Tris, 5 mM $MgCl_2$, 50 mM KCl, pH 7.5, 16 h at 35 °C) were adopted to facilitate the initial assessment of donor substrate specificity of the FgaPT2 with synthetic alkyl-PP analogues. Production of alkyl-L-Trp derivatives was determined by the difference in the retention time of L-Trp and alkyl-L-Trp product using a reverse phase high-pressure liquid chromatography (RP-HPLC) endpoint assay (Figure 17) with

subsequent confirmation by HRMS coupled with liquid chromatography (LC) analysis for all positive reactions (Table 3) to afford complete analysis of the desired product.

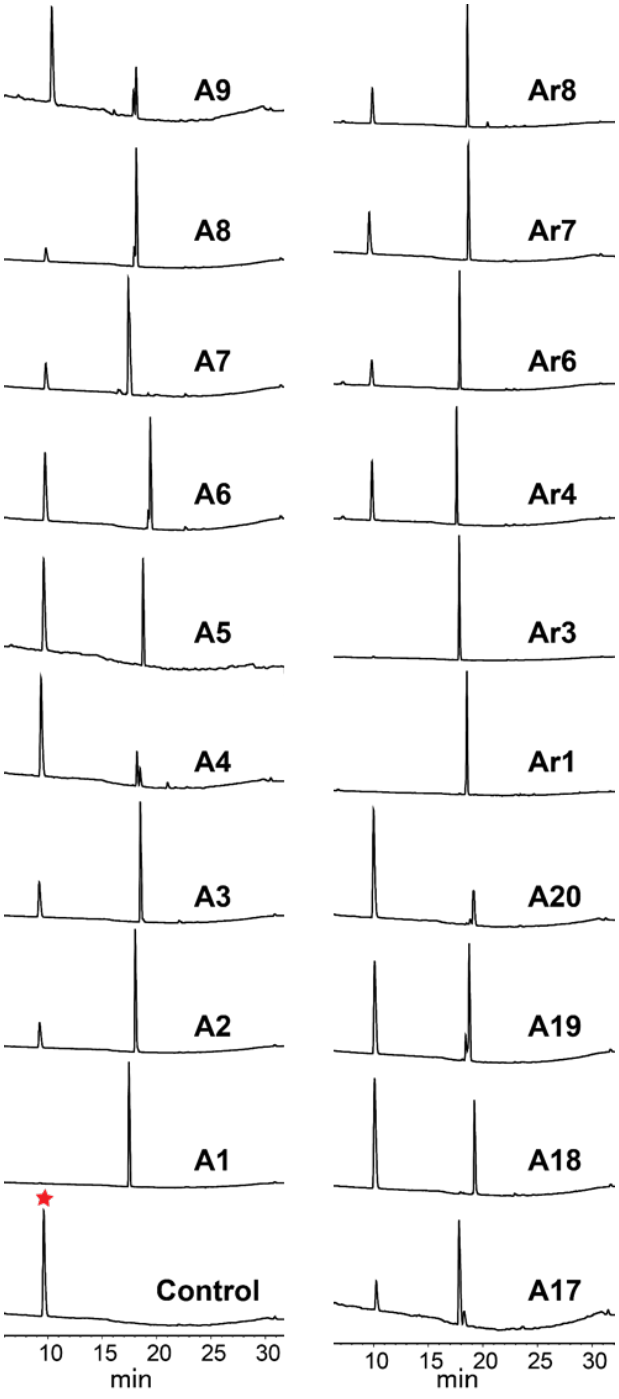


Figure 17. RP-HPLC chromatograms of FgaPT2 catalyzed reactions.
FgaPT2 was incubated with L-Trp and alkyl-PP analogues that led to the formation of corresponding alkyl-L-Trp analogues. The peak at retention time 10 min is L-Trp and the product peaks are after 15 min in the chromatograms respectively.

Table 3. Summary of HRMS data of alkyl-Trp analogues.
FgaPT2 catalyzed alkylation reaction with L-Trp and synthetic alkyl-PP analogues. The subscript '2' represents the second product based on HPLC retention time.

Enzyme Product	Chemical Formula	Calculated Mass (Da)	Observed Mass (Da)
A1-Trp	$C_{16}H_{21}N_2O_2$ $[M+H]^+$	273.1603	273.1602
A2-Trp	$C_{17}H_{23}N_2O_2$ $[M+H]^+$	287.1760	287.1754
A3-Trp	$C_{18}H_{25}N_2O_2$ $[M+H]^+$	301.1916	301.1916
A4-Trp	$C_{18}H_{23}N_2O_2$ $[M+H]^+$	299.1760	299.1756
A4-Trp$_2$	$C_{18}H_{23}N_2O_2$ $[M+H]^+$	299.1760	299.1761
A5-Trp	$C_{18}H_{23}N_2O_2$ $[M+H]^+$	299.1760	299.1768
A6-Trp	$C_{19}H_{25}N_2O_2$ $[M+H]^+$	313.1916	313.1913
A6-Trp$_2$	$C_{19}H_{25}N_2O_2$ $[M+H]^+$	313.1916	313.1911
A7-Trp	$C_{15}H_{19}N_2O_2$ $[M+H]^+$	259.1447	259.1449
A7-Trp$_2$	$C_{15}H_{19}N_2O_2$ $[M+H]^+$	259.1447	259.1444
A8-Trp	$C_{15}H_{18}ClN_2O_2$ $[M+H]^+$	293.1057	293.1061
A8-Trp$_2$	$C_{15}H_{18}ClN_2O_2$ $[M+H]^+$	293.1057	293.1062
A9-Trp	$C_{15}H_{18}BrN_2O_2$ $[M+H]^+$	337.0552	337.0552
A9-Trp$_2$	$C_{15}H_{18}BrN_2O_2$ $[M+H]^+$	337.0552	337.0547
A10-Trp	$C_{14}H_{17}N_2O_2$ $[M+H]^+$	245.1290	245.1294
A13-Trp	$C_{20}H_{21}N_2O_2$ $[M+H]^+$	321.1603	321.1601
A14-Trp	$C_{21}H_{23}N_2O_3$ $[M+H]^+$	351.1709	351.1711
A15-Trp	$C_{21}H_{23}N_2O_2$ $[M+H]^+$	335.1760	335.1757
A16-Trp	$C_{26}H_{25}N_2O_2$ $[M+H]^+$	397.1916	397.1912
A17-Trp	$C_{16}H_{19}N_2O_2$ $[M+H]^+$	271.1447	271.1442
A17-Trp$_2$	$C_{16}H_{19}N_2O_2$ $[M+H]^+$	271.1447	271.1444
A18-Trp	$C_{18}H_{23}N_2O_2$ $[M+H]^+$	299.1760	299.1768
A19-Trp	$C_{17}H_{21}N_2O_2$ $[M+H]^+$	285.1603	285.1602
A19-Trp$_2$	$C_{17}H_{21}N_2O_2$ $[M+H]^+$	285.1603	285.1605
A20-Trp	$C_{18}H_{23}N_2O_2$ $[M+H]^+$	299.1715	299.1751
A20-Trp$_2$	$C_{18}H_{23}N_2O_2$ $[M+H]^+$	299.1715	299.1749
A21-Trp	$C_{22}H_{23}N_2O_2$ $[M+H]^+$	347.1760	347.1767
Ar1-Trp	$C_{18}H_{19}N_2O_2$ $[M+H]^+$	295.1447	295.1430
Ar3-Trp	$C_{19}H_{21}N_2O_3$ $[M+H]^+$	325.1552	325.1547
Ar4-Trp	$C_{19}H_{21}N_2O_3$ $[M+H]^+$	325.1552	325.1540
Ar6-Trp	$C_{18}H_{18}FN_2O_2$ $[M+H]^+$	313.1352	313.1338
Ar7-Trp	$C_{18}H_{18}ClN_2O_2$ $[M+H]^+$	329.1057	329.1039
Ar8-Trp	$C_{18}H_{18}BrN_2O_2$ $[M+H]^+$	373.0552	373.0531

The initial assessment of FgaPT2 catalyzed alkylation of L-Trp with 34 synthetic alkyl-PP analogues based upon RP-HPLC of analytical scale reaction is illustrated in Figure

17, wherein 25 of the 34 synthetic analogues (Figure 16) in FgaPT2 catalyzed reaction produced corresponding alkyl-L-Trp. All products were subsequently confirmed to be mono-alkylated products from HRMS coupled with liquid chromatography (LC) analysis (Table 3).

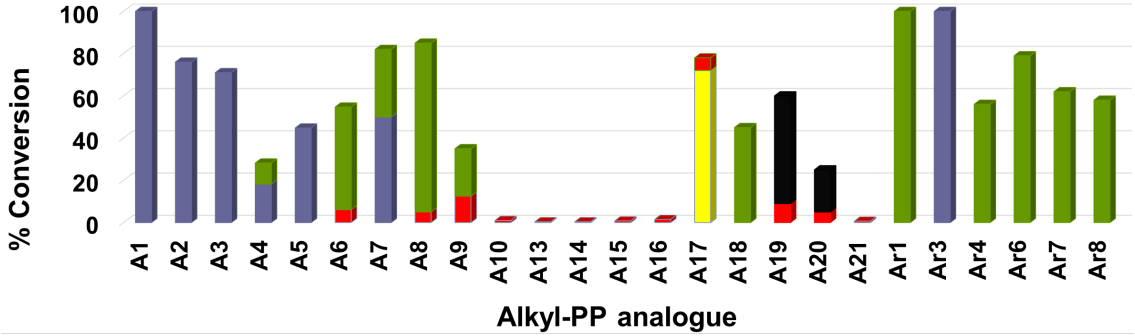


Figure 18: The percent conversion of alkyl-PP analogues.
Percent conversion of alkyl-L-Trp catalyzed by FgaPT2 based upon RP-HPLC. Reactions were performed with 1.2 mM alkyl-PP analog, 1 mM L-Trp, 5 μM FgaPT2, 25 mM Tris, 5 mM $MgCl_2$, 50 mM KCl, pH 7.5, 16 h at 35 °C. No product formation was observed in the absence of FgaPT2 or alkyl-PP analog. The blue, green, yellow, and black colors in the bar diagram denote C4, C5, C3, and N1 alkyl-L-Trp regio-isomers as confirmed by NMR, whereas the red color represents alkyl-L-Trp isomer with undetermined regio-chemistry.

Of the 25 positive reactions, 12 led to appreciable (>50%) conversion, an additional seven led to moderate (20-50%) conversion, while six offered detectable product formation (<5%) under the conditions described (Figures 19 and 20). Analysis of HPLC and HRMS results suggested more than one product for eight (**Figure 18**, **A4**, **A6**–**A9**, **A17**, **A19**, **A20**) of the 19 analytical scale reactions with product yield > 20% (Figure 16, **A1**–**A9**, **A17**–**A20**, **Ar1**, **Ar3**, **Ar4**, **Ar6**–**A8**). Notably, the 3-carbon allyl pyrophosphate **A10** was accepted as a substrate although with a very low conversion rate of 1%, resulting in the formation of allyl-L-Trp. However, **A11** with a methyl

group substituted at the β-carbon of allyl pyrophosphate was not accepted by FgaPT2. No product formation was observed for **A12** that has a carbonyl group at β-carbon. The bulky cinnamyl analog (**A13**) and its derivatives (**A14, A15, A16**, and **A21**) produced only a trace amount of the alkylated product with low yield (< 2%). In addition, while *o*-methoxy (**Ar3**), *m*-methoxy (**Ar4**) and *p*-halogen (**Ar6**-**Ar8**) substituted benzyl analogues were accepted by FgaPT2, introduction of bulky groups at the para-position, including *p*-methoxy (**Ar2**), *p*-methyl (**Ar5**), *p*-nitro (**Ar9**) and di- and tri-substituted benzyl analogues (**Ar10 – Ar12**, and **A13**) did not serve as substrates for FgaPT2 catalyzed reaction with L-Trp due to the potential steric hindrance in the active site of the enzyme. These results suggest the FgaPT2 catalyzed reaction with L-Trp is sterically limited by bulky substitution on the alkyl-donor.

Kinetic studies

Michaelis−Menten kinetic parameters for all 19 alkyl-PP analogues with product conversion > 20%, (Table 4) and for L-Trp with representative alkyl-PP analogues were carried out. The kinetic parameters, rates (k_{cat}) and Michaelis constants (K_M) were determined from a nonlinear regression fit of initial velocities versus concentration of alkyl-PP analog by GraphPad Prism 5.04 (Figure 19) . Interestingly, the K_M of L-Trp for FgaPT2 with various alkyl-PP donors did not change drastically by the nature of the alkyl donors and remained within the range of 0.20 ± 0.08 mM. Consistent with our previous observations with tyrosine-*O*-prenyltransferase SirD,[95] the alkyl-PP analogues that contained groups to enhance the stability of the carbocation via increased conjugation and resonance stabilization correlated with the increased turnover of the product. For example, the k_{cat} values of the reaction correlated with conjugation by a

methyl group in the order, **A1** > **A2** > **A3** > **A7** (**Table 4**). In addition, the K_M values increased with the increased length of the carbon chain in the order **A1** < **A2** ≅ **A3** ≅ **A5** < **A6** and **A17** < **A18** ≅ **A19** ≅ **A20**. Removing one methyl group of **A1** decreased the efficiency (k_{cat}/K_M) of **A7** by 88-fold compared to **A1**.

Table 4. Kinetic parameters for FgaPT2 with L-Trp.
*1.2 mM L-Trp, and varied concentration of alkyl-PP analogues in 25 mM Tris, 5 mM $MgCl_2$, 50 mM KCl, pH 7.5, 35 °C. (*Relative catalytic efficiency is defined as the percent k_{cat}/K_M when compared to **A1**)*

Alkyl-PP analog	K_{cat} (min^{-1})	K_M (mM)	k_{cat} / K_M ($mM^{-1}min^{-1}$)	Relative catalytic efficiency*
A1	50 ± 1	0.14 ± 0.01	357	100
A2	9.9 ± 0.4	0.48 ± 0.06	21	5.88
A3	6.5 ± 0.1	0.37 ± 0.02	18	5.04
A4	0.160 ± 0.006	0.16 ± 0.02	1	0.28
A5	5.04 ± 0.18	0.31 ± 0.03	16	4.48
A6	3.2 ± 0.4	1.4 ± 0.2	2.28	0.64
A7	0.57 ± 0.02	0.14 ± 0.01	4.07	1.14
A8	1.3 ± 0.1	0.53 ± 0.08	2.5	0.70
A9	0.47 ± 0.01	0.35 ± 0.03	1.3	0.38
A17	26 ± 1	0.66 ± 0.06	39	10.92
A18	28 ± 1	1.1 ± 0.1	25.5	7.14
A19	20.2 ± 0.9	1.3 ± 0.1	15.5	4.34
A20	16.9 ± 2	1.39 ± 0.2	12.1	3.39
Ar1	1.36 ± 0.02	0.22 ± 0.01	6.2	1.74
Ar3	1.93 ± 0.05	0.57 ± 0.04	3.4	0.95
Ar4	0.170 ± 0.005	0.73 ± 0.06	0.23	0.064

Ar6	0.276 ± 0.004	0.4 ± 0.02	0.69	0.19
Ar7	0.196 ± 0.004	0.43 ± 0.03	0.46	0.13
Ar8	0.134 ± 0.003	0.32 ± 0.03	0.42	0.12

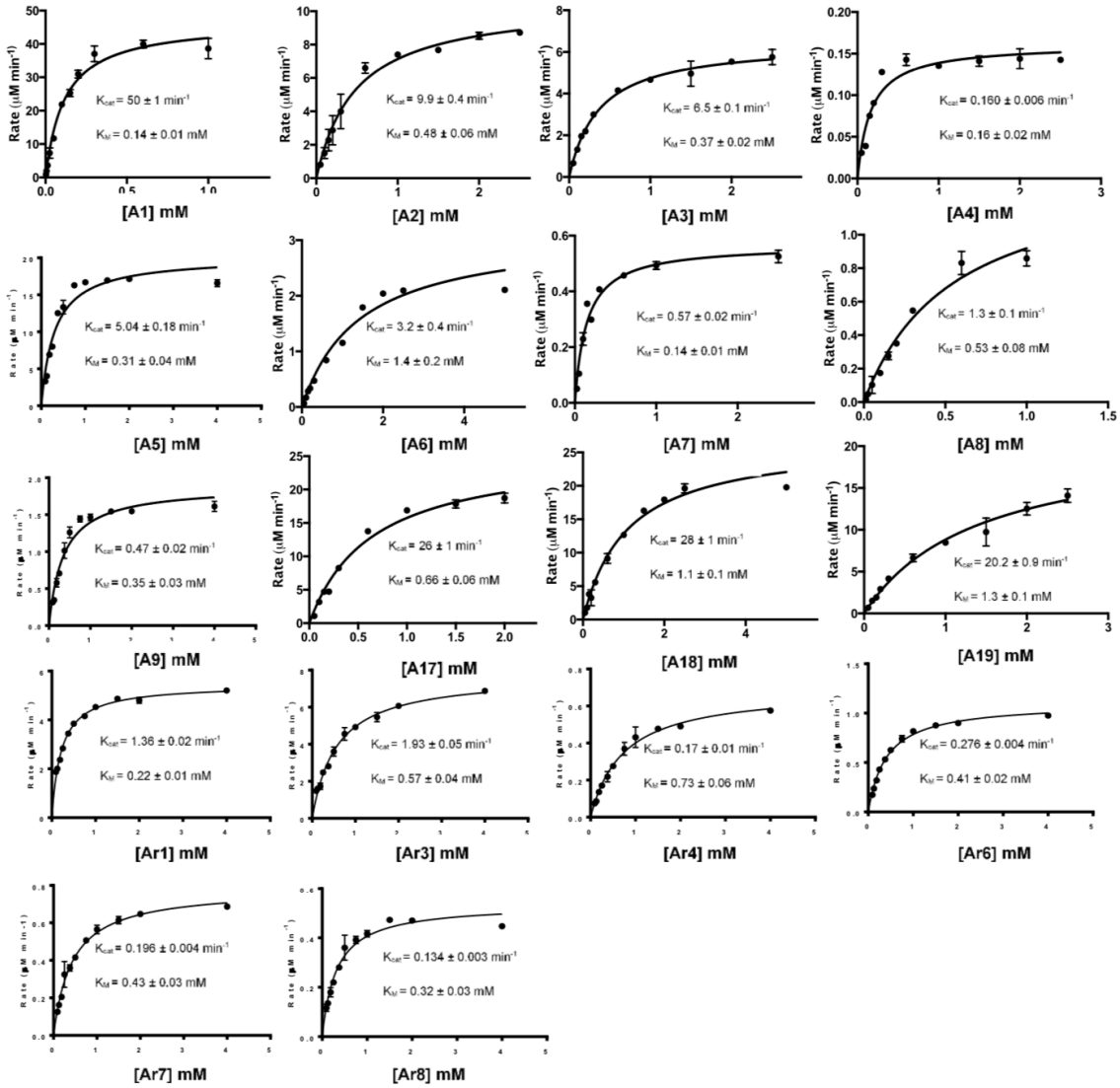


Figure 19. Michaelis-Menten inetic plots for FgaPT2 reactions
Kinetic parameters detemered by Michaelis-Menten plots with 1mM tryptophan and varying concentrations of pyrophosphate analogues incubated at 35℃

Further, changing one or both methyl groups of **A1** to an ethyl group (**A2** and **A3**) lowered the enzyme efficiency 17-20 times compared to **A1**. Similarly, the k_{cat} values of the reaction correlated with resonance stabilization in the order **A17** > **A7**; **Ar1** > **A4**; **Ar1** > **Ar6** > **Ar7** > **Ar8**. Furthermore, a 9-fold higher k_{cat} value of **Ar1** compared to **A4** suggests resonance stabilization of the carbocation by the benzylic group contributes to the rate of the reaction. However, the k_{cat} value of the cyclohexyl (**A4**) and benzyl analogues (**Ar1**) were nearly 310 and 36, fold lower than **A1**. When an electron withdrawing group such as chloro (**A8**) or bromo (**A9**) replaced one of the methyl groups of **A1**, the efficiency of the enzyme was lowered nearly 150–250 fold compared to the natural alkyl donor, **A1**, which explains the importance of methyl group in stabilizing the carbocation. Surprisingly, the dienyl analogues (**A17**, **A18**, **A19**, and **A20**) displayed relatively higher rates with just ~2 fold lower k_{cat} values compared to the natural alkyl donor, **A1**, implying extended resonance stabilization of the carbocation favors the FgaPT2 catalyzed reaction. However, the K_M values of the dienyl analogues were 5-10-fold higher than the natural alkyl donor, **A1** and the trend of K_M values correlated with the increasing length of the carbon chain (C5–C7), in the order, **A17** < **A19** < **A20**, again pointing at the steric factors and the orientation of the alkyl group in the active site of the enzyme to contribute to the enzyme efficiency. All mono*o*-substituted benzylic analogues (**Ar3**, **Ar4**, **Ar6**, **Ar7**, **Ar8**) displayed a similar K_M value, which was 2–3 fold higher than the benzyl analog, **Ar1**. The 10-fold higher k_{cat} value of *o*-methoxy (**Ar3**) compared to the *m*-methoxy (**Ar4**), suggests benzylic cation stabilization by an *o*-methoxy group increases the efficiency of the FgaPT2 catalyzed alkylation reaction. Among the para-substituted halogens, the k_{cat} values followed the

order *p*-fluoro (**Ar6**) > *p*-chloro (**Ar7**) ≅ *p*-bromo (**Ar8**), suggesting a combination of steric factors and possible stabilization of carbocation of the **Ar6** carbocation via back donation of the non-bonded electron pairs of the fluorine atom to the **Ar6** carbocation through effective 2p-2p orbital interaction. The observed k_{cat} values of para-substituted halogens were ~5-10 fold lower than **Ar1**, which is consistent with the inductive effect of the halogens. Surprisingly, while the para-substituted halogens were accepted by FgaPT2, the *p*-methoxy and *p*-methyl were not substrates for FgaPT2 catalyzed reaction even with their ability to contribute to the stabilization of the benzylic cation, likely due to the steric factors in the active site of the enzyme. These results emphasize the fact that the FgaPT2 catalyzed Friedel-Craft alkylation reaction proceeds via stabilized carbocation,[60] and the steric factor and the orientation of alkyl group in the active site has a major role in the ability of FgaPT2 to utilize alkyl donors.

NMR Studies

To assess the regio-specificity of FgaPT2 catalyzed alkyl-transfer, the 19 analytical scale reactions with an alkyl-tryptophan yield > 20% (reaction involving **A1**-**A9**, **A17**-**A20**, **Ar1**, **Ar3 Ar4**, **Ar6**-**Ar8**, **Figure 16**) were scaled up, purified via RP-HPLC, and characterized via ^{1}H and 2D NMR experiments by Dr. Chandrashekar Bandari. While eight of the 19 alkyl-transfer reactions involving alkyl donors **A4**, **A6**, **A7**, **A8**, **A9**, **A17**, **A19** and **A20** yielded two or more mono-alkylated products based on RP-HPLC and HRMS analysis, regio-specific alkyl-group attachment of minor products of reactions involving **A6**, **A8**, **A9**, **A17**, **A19**, and **A20** could not be obtained due to insufficient intensity of NMR signals. The regiospecificity of 21 alkyl-tryptophan analogues was determined using detailed 2D NMR analysis (Figure 20). Among the 21

alkyl-tryptophan analogues characterized by NMR , the alkyl group of seven were at C4 (derived from **A1**-**A5**, **A7**, and **Ar3**), 11 at C5 (derived from **A4**, **A6**, **A7**, **A8**, **A9**, **A18**, **Ar1**, **Ar4**, **Ar6**-**Ar8**), one at C3 (derived from **A17**) forming hexahydro-pyrroloindoline product as verified by UV (Figure 21), and two were at the N1 (derived from **A19**, **A20**) position of tryptophan respectively (Figure 20).

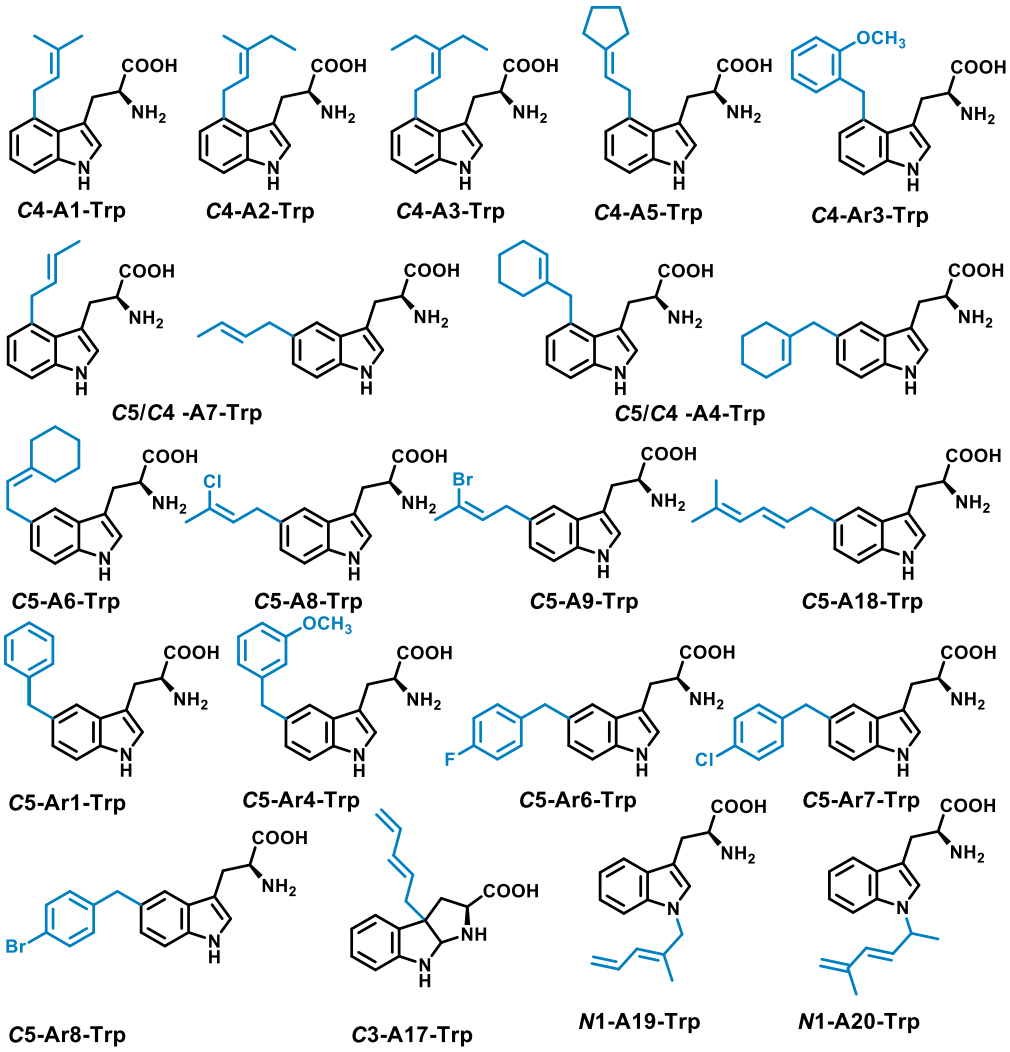


Figure 20. NMR characterized structures
Structure of isolated alkyl-tryptophan products obtained from FgaPT2 reaction with L-Trp and alkyl-PP analogues determined by NMR analysis.

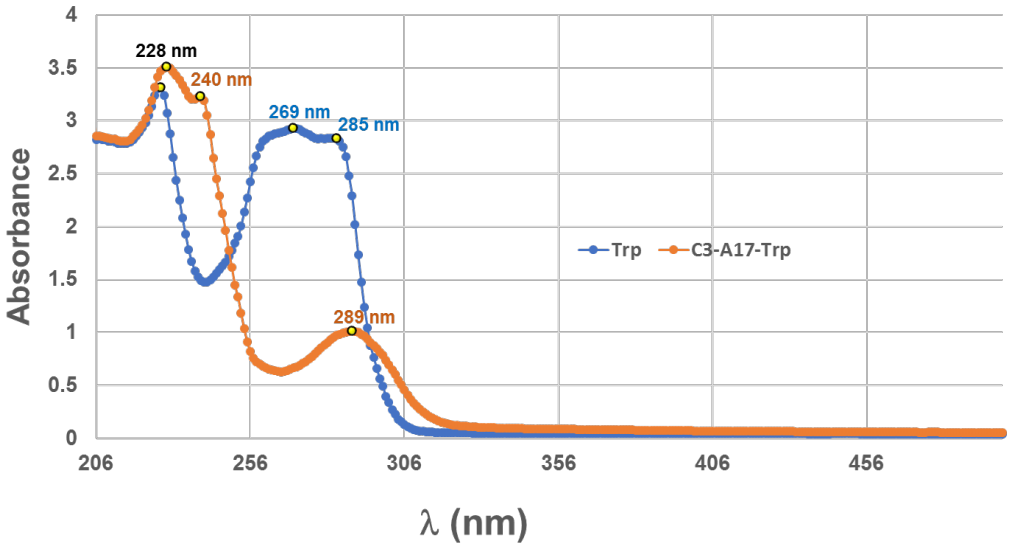


Figure 21: UV absorption spectra of L-Trp and C3-A17-Trp.
Showing signature absorption maxima for hexahydro-pyrroloindoline tryptophan product.

Intriguingly, apart from the strict C4 alkylation of tryptophan by FgaPT2 using the natural alkyl donor **A1**, the unnatural alkyl donors, **A2**, **A3** and **A5,** which contained an ethyl group (**A2** and **A3**) in place of one or both methyl group/s of **A1,** or the similarly sized conformationally restricted cyclopentyl analog (**A5**) selectively added the alkyl group at the C4 position of tryptophan. Alkyl-PP analogues with smaller alkyl chain in the linear direction compared to **A1** (**A4** and **A7**) resulted in a mixture of C4 and C5 regio-isomers, and alkyl-PP analogues with a methyl group of **A1** replaced with a halogen (**A8** and **A9**) or larger alkyl chain (**A6** and **A18**) predominantly produced the C5 alkylated product. While most of the unnatural benzylic analogues (**Ar1**, **Ar4**, **Ar6**, **Ar7,** and **Ar8**) produced selectively C5 alkylation of tryptophan, the *o*-methoxy benzyl analog (**Ar3**) produced a single C4-alkylated tryptophan. Careful analysis of the C4 alkylating analogues (**A1**, **A2**, **A3**, **A5**, and **Ar3**) suggests that C4 substitution is

preferred when the carbon chain length is less than 6 while C3' is also disubstituted to facilitate stacking interaction with the indole ring. Therefore, the active site steric factors in combination with improper stacking interaction of the alkyl group with the indole ring conceivably displaces the carbocation resulting in a direct addition of alkyl group to C5 of tryptophan as seen for 11 of the C5-alkyl-Trp products. The addition of alkyl groups at the C5 position of tryptophan by most of the alkyl-PP analogues is consistent with the orientation of DMASPP with respect to the indole ring in the active site of the FgaPT2 crystal structure,[51] where C5 of tryptophan is just at 3.5 Å from the C1' of the alkyl group compared to a distance of 3.8 Å between C4 of tryptophan to the C1' of the alkyl group (Figure 22).

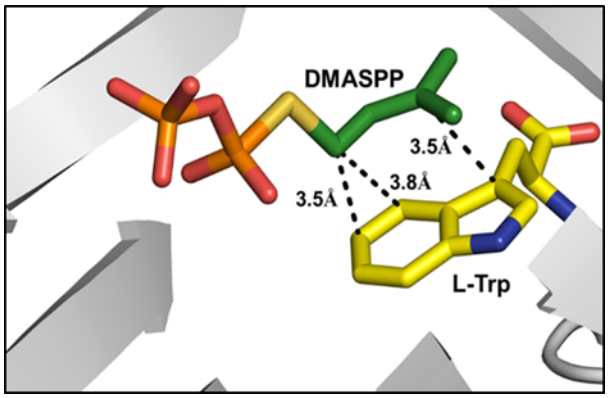


Figure 22: The active site of FgaPT2 structure (PDB:3I4X)
FgaPT2 in complex with L-Trp and DMASPP displaying distances between C1' of DMASPP and C4 and C5 of L-Trp; and C3' of DMASPP and C3 of L-Trp.

Conclusions

In conclusion, this work has revealed that FgaPT2 has a remarkable ability to accept diverse allylic and benzylic unnatural alkyl-donor substrates. While FgaPT2 can transfer alkyl groups at C4, C5, N1 and C3 position of L-Trp, the C5 position is the

preferred alkylation position for FgaPT2 with unnatural alkyl-donors. Thus, these studies highlight the potential utility of FgaPT2 for broader applications such as alkyl-diversification of indole-containing natural products for drug discovery and other synthetic applications. Future enzyme mutational studies along with substrate engineering is expected to drive the development of more efficient and selective FgaPT2-based biocatalysts.

Experimental

General materials

Unless otherwise stated, all chemicals and reagents were purchased from Sigma-Aldrich (St. Louis, MO, USA), Acros (New Jersey, USA), Alfa-Aesar (Ward Hill, MA, USA) or TCI (Portland, OR, USA) and were reagent grade or better. PD-10 column and Ni-NTA superflow columns were purchased from GE Healthcare (Piscataway, NJ).

General methods

HPLC was accomplished using Agilent 1220 system equipped with a DAD detector. High-resolution mass spectrometric (HRMS) data and liquid chromatography mass spectrometric (LCMS) were obtained on Agilent 6545-QTOF W/1290 HPLC mass spectrometer at the University of Oklahoma, Department of Chemistry and Biochemistry. NMR spectra were obtained on Varian VNMRS 400 or 500 MHz instruments at the NMR facility of the Department of Chemistry and Biochemistry at the University of Oklahoma using 99.9% DMSO-d_6 with 0.05% v/v TMS, or 99.9% D_2O or 99.8% MeOH-d_4, 99.9% Acetone-d_6 (Cambridge Isotope Laboratories, MA, USA.

***In-vitro* FgaPT2 assay**

The recombinant FgaPT2 was overproduced in *Escherichia coli* BL21(DE3) cells transformed with codon-optimized synthetic *FgaPT2* gene in pET28a vector. The resulting FgaPT2 with *N*-terminal His_6-fusion protein was purified to homogeneity via Ni-NTA affinity chromatography as described previously.[40] *In vitro* FgaPT2 reactions were conducted in a volume of 20 μl with 1.2 mM alkyl-PP analog (**A1** – **A21**, **Ar1** – **Ar13**), 1 mM L-Trp and 5 μM purified FgaPT2 in 25 mM Tris buffer pH 7.5, 5 mM $MgCl_2$, 50 mM KCl, incubated at 35 °C for 16 h. Reactions were quenched by adding an equal volume of methanol followed by centrifugation (10,000 x*g* for 15 min) to remove the precipitated protein and product formation for each reaction was subsequently analyzed by RP-HPLC using **Method A** or **Method C**. For each reaction, percent yield was based upon the integration of species at 254 nm and calculated by dividing the integrated area of the product by the sum of the integrated area of product and/or and the remaining substrate. All putative products were subsequently confirmed by HRMS with positive (+) and/or negative (-) mode. Kinetic parameters were assessed using 1.2 mM L-Trp and variable alkyl-PP analogues (0.1 - 6 mM). Assays were conducted in triplicate and all rates were confirmed to be linear. The kinetic curves were fit to Michaelis-Menton kinetics using Prism 5.04 (GraphPad Software, Inc. La Jolla, CA 92037 USA). The reactions with > 20% product yield were performed in 2-5 mL volume under standard condition, purified by semi-prep HPLC using **Method B** and the putative new products were confirmed by NMR. **Method A:** To monitor FgaPT2 reactions of L-Tryptophan, analytical reverse-phase (RP) HPLC employed a Gemini-NX, C-18 (5 μm, 4.6 mm × 250 mm) column (Phenomenex, Torrance,

California, USA) [gradient of 10% B to 25% B over 10 min, 25% B to 100% B over 15 min, 100% B for 3 min, 100% B to 10% B over 0.1 min, 10% B for 7 min (A = ddH_2O with 0.1% TFA; B = acetonitrile) flow rate = 1 mL min^{-1}; A_{254}]. The reaction was monitored by the retention time difference between starting material and product. **Method B :**Semi-preparative RP HPLC was conducted on a Gemini-NX, C-18 (5 μm, 10 mm × 250 mm) column (Phenomenex, Torrance, California, USA) to purify the L-Trp analogues [gradient of 10% B to 25% B over 10 min, 25% B to 100% B over 15 min, 100% B for 3 min, 100% B to 10% B over 0.1 min, 10% B for 7 min (A = ddH_2O with 0.1% TFA; B = acetonitrile) flow rate = 2 mL min^{-1}; A_{254}].

Chapter 4. Alkyl donor specificity of a Naptherpin prenyltransferase, NphB

Introduction

NphB, previously referred to as orf2, is a soluble aromatic PT with significant Mg^{2+} dependent activity found in the Naphterpin biosynthetic pathway.[96] Naphterpin is a powerful antioxidant produced in the microorganism *Streptomyces* sp CL190. The core is comprised of a naphthoquinone moiety with an attached 10-carbon geranyl group forming a cyclohexene ring with a geminal dimethyl group.[97] Briefly, the biosynthesis begins with the polyketide 1,3,6,8-tetrahydroxynaphthalene (THN), formed from the malonyl-CoA by a type III polyketide synthase, which undergoes an oxidative transformation to flaviolin. The resulting THN, flaviolin, or THN-derived metabolite are tailored by addition of a geranyl co-substrate and further modified by subsequent cyclization. The gene cluster responsible for naphterpin production revealed an open reading frame (*orf2*) with a high degree of homology to the characterized PTs CloQ and NovQ, leading to the proposal that *orf2* encodes for the PTase responsible for the transfer of the geranyl group on THN or THN derivative (Figure 23). [36] Although the precise native substrate of NphB currently remains ambiguous, in common practice 1,6 dihydroxynapthalene is used as a surrogate acceptor substrate.

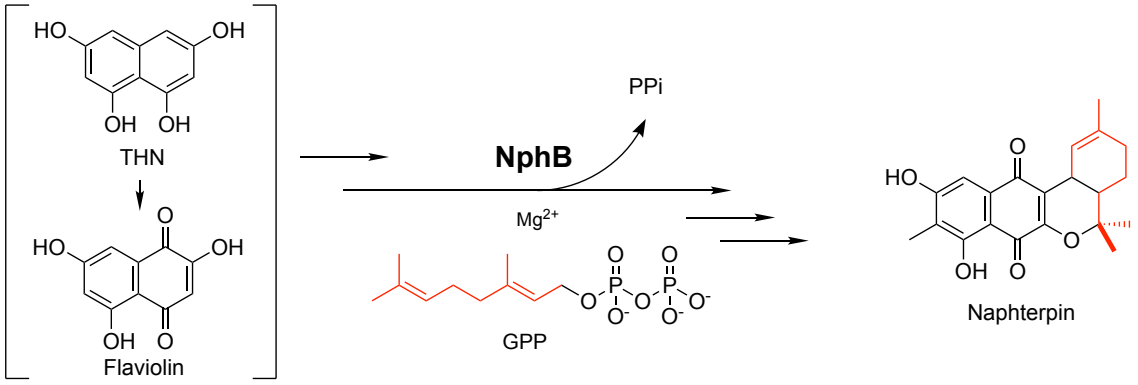


Figure 23. NphB catalyzed step in the biosynthesis of naptherpin[36]

As mentioned, the true biological substrate has not been identified; however, various aromatic acceptors have been tested revealing a highly promiscuous nature towards aromatic substrates. Initially, enzyme activity was assessed by incubating with prenyl donors, DMAPP, GPP, or FPP, in the presence of aromatic acceptors; further, this was later tested with an azido-substituted GPP.[36, 54] For the isoprenoid pyrophosphate substrates, NphB did not display any enzymatic activity with DMAPP, as isoprenoid pyrophosphate substrate. There was detectable activity with FPP and azido-GPP and the highest activity with GPP.[36, 98]

NphB has been assayed for utilization of various aromatic substrates including flavonoids, isoflavonoids, plant polyketides and 1,3,6,8-tetrahydroxynaphthalene (THN) analogues. The enzyme is capable of GPP additions on several positions of the aromatic ring including C- and O- geranylations yielding several different alkylated products. A comparison of the reaction products showed that most contain a geranyl group in the ortho position relative to the hydroxyl group.[54, 99] With the flavonoids, NphB performed an O-prenylation of a hydroxyl group as well as the C6 position of

naringenin and apigenin and the C8 position of daidzein[36, 54]. This demonstrates that, consistent with other PTs, NphB catalyzes donor-dependent prenylation reactions. The structure of NphB consists of a single domain PT- fold with some variability in the overall ααββ repeating motif resulting in missing the α9 helix between strands β8 and β9. Additionally, NphB has three helices outside of the PT-fold. The first helix, 3_{10}, is found between β1- β2 strands and positioned above the metal binding site within the barrel. The second additional helix follows the end of strand β4 and partially overlaps with the opening at the C-terminal end of the β-barrel. NphB also has an extra C-terminal α-helices, that fully extends across the aromatic binding domain opening of the barrel. The interior of the barrel contains a number of hydrophobic residues used to sequester the geranyl tail of GPP, with the head groups positioned towards the polar end of the barrel thus allowing contact with the coordinated Mg^{2+} cation. Notably, the sequence does not contain the (N/D)DXXD recognition motif found in most Mg^{2+} dependent isoprenoid diphosphate enzymes.

Research Objective

The aim of this study is to define the alkyl pyrophosphate donor scope of the polyketide prenyltransferase NphB, using an extensive synthetic library of 65 pyrophosphate analogues, in the presence of the native substrate 1,6-DHN or of the drug compound sulfabenzamide. The library includes 44 new synthetic analogues added from the work reported in Chapter 3, and all analogues have been renumbered as described in Figure 24. In this chapter we report an extensive alkyl pyrophosphate donor scope of polyketide prenyltransferase NphB with 1,6-DHN and sulfabenzamide, and structure-

based engineering of NphB. Interestingly, a comparison of the *in vitro* activity assays with 1,6-DHN or with sulfabenzamide indicated a strong donor dependent alkylation reaction. In the presence of 1,6-DHN or sulfabenzamide, NphB was able to catalytically transfer 26 and 29 out of the 65 diverse pyrophosphate donors, respectively. Through the structural elucidation of the alkyl-diversified sulfabenzamide compounds, we observed a previously unreported functionality of NphB to perform regio specific N-alkylations. Moreover, we accomplished structure-based rational engineering of NphB to increase substrate acceptance capabilities, producing a gernalyated sulfabenzamide derivative.

Contributions

All alkyl pyrophosphate analogues were synthesized by Dr. Chandrasekhar Bandari, Tejaswi Bavineni, Johanna Masterson, Rachel Tran, and Eric Gardener. Large-scale enzymatic reaction and subsequent purification was carried out in part by me and Andrea Batchev. Structural characterization of sulfabenzamide derivatives by NMR spectroscopy was performed in part by me, Dr. Susan Nimmo and Andrea Batchev. My contributions also involved expression and purification of NphB , RP-HPLC and HRMS based assessment of alkyl-donor specificity of NphB, and determination of kinetic parameters for NphB catalyzed reaction with diverse alkyl-donors. Some contents from this chapter including text, tables and figures will be directly used for a publication in a peer-reviewed journal.

Results

Description of the alkyl pyrophosphate library.

In this study, we investigated the NphB catalyzed alkylation reaction of 1,6-DHN and sulfabenzamide, an antimicrobial compound with promising anti-tumor/ anti-cancer properties[96], against an internally-generated library of synthesized pyrophosphates. The library contains 65 electronically and structurally diverse compounds, designed to probe the donor permissiveness of the enzyme as well as potentially generating compounds with increased bioactivity (Figure 24). We have organized the compounds according to their chemical space and potential functionality, including; allylic-, benzylic- and heterocyclic analogues as well as analogues with chemo selective functionally.

Compounds were designed with two different chemical handles; allylic analogues (**PP1-PP35**) and benzylic analogues (**PP36-PP48**). Amongst the allylic analogues, features including chain length, methylation positions, cyclization, degree of saturation, and functional groups were varied. In order to better understand the effect of chain length on substrate preference, compounds were synthesized with various lengths ranging from an allyl pyrophosphate (C_3) (**PP1**) to farnesyl pyrophosphate (C_{15}) (**PP35**). Derivatives of dimethyl allyl were created with assorted terminal saturated aliphatic chains (**PP6-PP12**), altering the overall length as well as bulk of the donor compound. Presumably, the saturated carbon chains could add more flexibility to the general structure when compared to polyunsaturated chains. Further, carbocation stability of the activated allylic group was investigated through conjugated system and the loss of the C3 methyl group, thought to stabilize the carbocation through hyper-conjugation. The necessity of

this methyl on the C3 carbon was investigated by either removal (**PP3, PP14, PP16, PP17**, and **PP26-PP28**), rearrangement on the C2 carbon position (**PP4, PP15, PP18**) or by replacement by a chloro- (**PP22**) or bromo- (**PP23**) halogen atom. Additionally, conjugated compounds were synthesizing in either linear (**PP13-PP18**) or aromatic (**PP24-PP28**) form. Our library also includes several geranyl derivatives, formed by the addition of a methyl group (**PP31**), ester linked benzyl group (**PP33**), alcohol group (**PP34**) or alkene group (**PP32**) on the terminal methyl. Additionally, a subset of the library consists of benzylic analogues substituted with either electron-donating (methyl or methoxyl) or electron-withdrawing (fluoro-, chloro-, bromo- or nitro-) substituents. To investigate the reactivity influenced by substituent orientation and degree of substitution, we synthesized ortho- and meta-methoxy (**PP38** and **PP39**), di-methoxy (**PP45** and **PP46**), di-fluoro (**PP48**) and tri methoxy (**PP48**) derivatives on the benzyl ring.

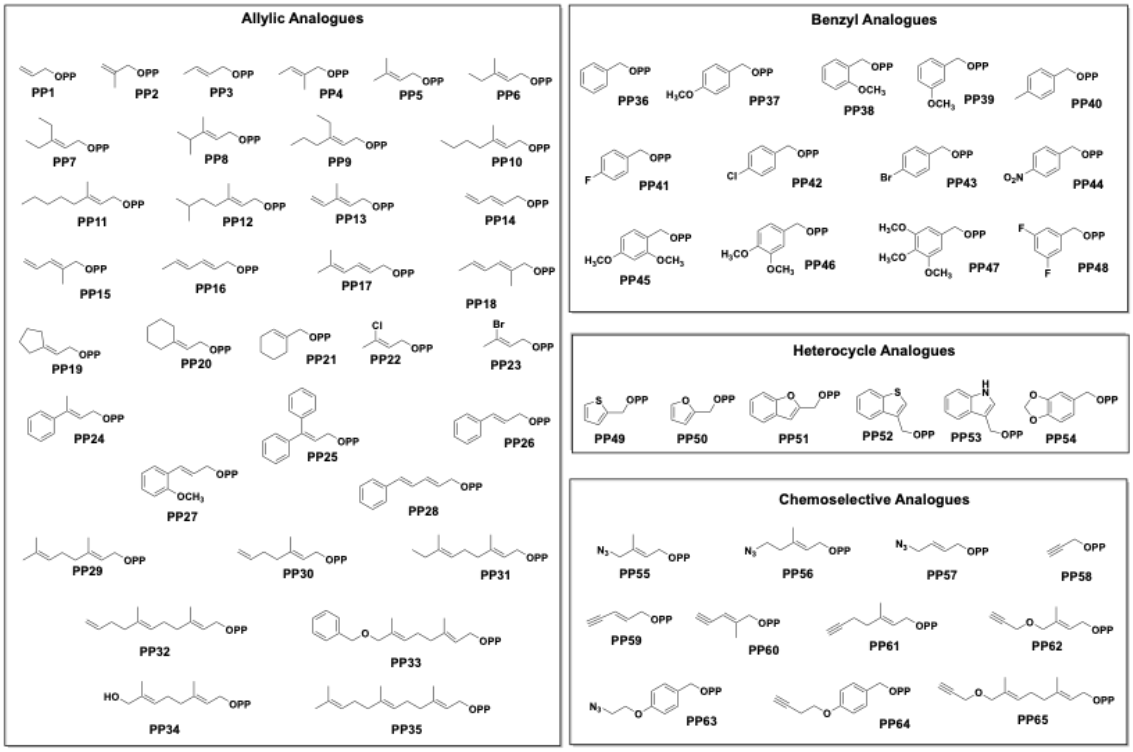


Figure 24. Library of synthetic alkyl-PP analogues.
Analogues were assessed with NphB catalyzed reaction with 1,6-DHN or sulfabenzamide

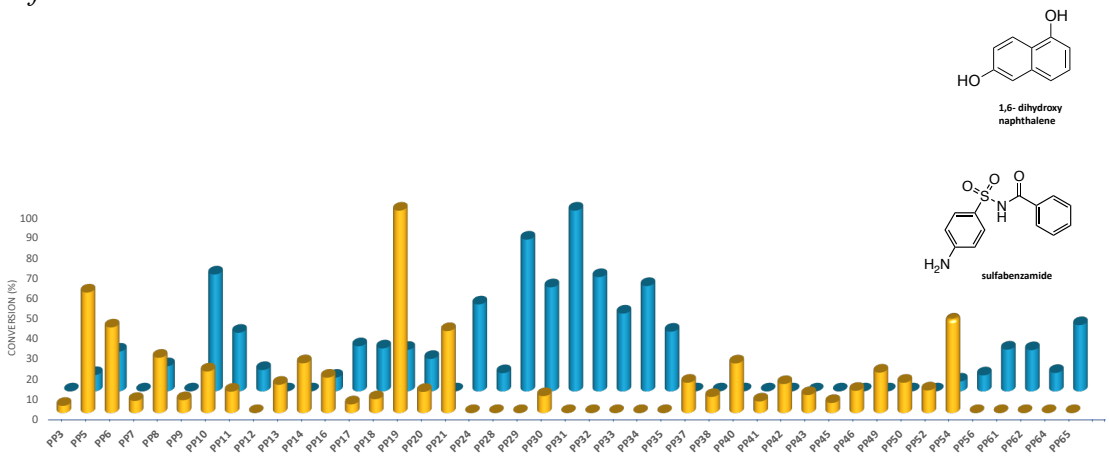


Figure 25. Percent conversion.
Percent conversion of library of alkyl pyrophosphate using 1,6-DHN (blue) or sulfabenzamide (orange). Assays were performed under standard condition, 1.2 mM alkyl pyrophosphate, 1 mM sulfabenzamide or 1,6-DHN, NphB, 25 mM Tris pH 7.8 5mM $MgCl_2$, 50 mM KCl and incubated for 16hrs at 35 ℃ and evaluated by RP-HPLC.

Table 5. Summary of HRMS data of 1,6-DHN analogues from NphB catalyzed alkylation reaction with 1,6-DHN and synthetic alkyl-PP analogues.

Enzyme Product	Chemical Formula	Calculated Mass (Da)	Observed Mass (Da)
1,6-DHN	$C_{10}H_8O_2$ $[M-H]^-$	159.0452	159.0457
***1,6-DHN*-PP5**	$C_{15}H_{16}O_2$ $[M-H]^-$	227.1078	227.1079
***1,6-DHN*-PP6**	$C_{16}H_{18}O_2$ $[M-H]^-$	241.1234	241.1237
***1,6-DHN*-PP8**	$C_{17}H_{20}O_2$ $[M-H]^-$	255.1390	255.1394
***1,6-DHN*-PP10**	$C_{18}H_{22}O_2$ $[M-H]^-$	269.1547	269.1548
***1,6-DHN*-PP11**	$C_{19}H_{24}O_2$ $[M-H]^-$	283.1703	283.2645
***1,6-DHN*-PP16**	$C_{16}H_{16}O_2$ $[M-H]^-$	239.1078	239.1081
***1,6-DHN*-PP17**	$C_{17}H_{18}O_2$ $[M-H]^-$	253.1234	253.1230
***1,6-DHN*-PP18**	$C_{17}H_{18}O_2$ $[M-H]^-$	253.1234	253.1238
***1,6-DHN*-PP19**	$C_{17}H_{18}O_2$ $[M-H]^-$	253.1234	253.1235
***1,6-DHN*-PP20**	$C_{18}H_{20}O_2$ $[M-H]^-$	267.1391	267.1379
***1,6-DHN*-PP24**	$C_{20}H_{18}O_2$ $[M-H]^-$	289.1234	289.1232
***1,6-DHN*-PP28**	$C_{21}H_{18}O_2$ $[M-H]^-$	301.1234	301.1235
***1,6-DHN*-PP29**	$C_{20}H_{24}O_2$ $[M-H]^-$	295.1703	295.1704
***1,6-DHN*-PP30**	$C_{18}H_{20}O_2$ $[M-H]^-$	267.1390	267.1391
***1,6-DHN*-PP31**	$C_{21}H_{26}O_2$ $[M-H]^-$	309.1860	309.1859
***1,6-DHN*-PP32**	$C_{23}H_{28}O_2$ $[M-H]^-$	355.2016	355.2098
***1,6-DHN*-PP33**	$C_{27}H_{30}O_3$ $[M-H]^-$	401.2122	401.2132
***1,6-DHN*-PP34**	$C_{20}H_{24}O_3$ $[M-H]^-$	311.1653	311.1660
***1,6-DHN*-PP35**	$C_{25}H_{32}O_2$ $[M-H]^-$	363.2329	363.2339
***1,6-DHN*-PP37**	$C_{18}H_{16}O_3$ $[M-H]^-$	279.1027	279.1026
***1,6-DHN*-PP54**	$C_{18}H_{14}O_4$ $[M-H]^-$	293.0819	293.0821
***1,6-DHN*-PP56**	$C_{16}H_{17}N_3O_2$ $[M-H]^-$	282.1248	282.125
***1,6-DHN*-PP61**	$C_{18}H_{18}O_2$ $[M-H]^-$	265.1234	265.1244
***1,6-DHN*-PP62**	$C_{18}H_{18}O_3$ $[M-H]^-$	281.1183	281.1179
***1,6-DHN*-PP64**	$C_{20}H_{16}O_3$ $[[M-H]^-$	303.1027	303.1031
***1,6-DHN*-PP65**	$C_{23}H_{26}O_3$ $[M-H]^-$	349.1809	349.1801

Chemoenzymatic syntheses of alkylated 1,6 dihydroxy naphthalene

NphB was heterologously expressed in *Escherichia coli* BL21 (DE3) cells as a N-terminal His-tagged fusion protein and purified to homogeneity by Ni-NTA affinity chromatography. Although the true native substrate for NphB is unknown, 1,6-DHN is used as a surrogate substrate to assess donor specificity. The purified recombinant

enzyme was incubated with 1,6-DHN and the synthesized alkyl pyrophosphate donors at standard assay conditions (1.2mM alkyl-PP, 1mM aromatic acceptor, 50uM NphB, 25mM Tris, 5mM $MgCl_2$, 50mM KCl, pH 7.8, 16 h at 35 C). The formation of alkylated products was analyzed using reverse phase high-performance liquid chromatography (RP-HPLC) and confirmed by high resolution mass spectroscopy (HRMS) (Figure 25 and 28; Table 5).

Analysis of the analytical scale reactions demonstrated that 27 of the 65 pyrophosphate analogues were able to be catalytically transferred by NphB onto the aromatic substrate, 1,6-DHN (Figure 25). Although the HRMS data indicates only monoprenylated products for all of the reactions, the HPLC chromatograms for 20 of the 27 catalyzed reactions indicated the presence of three different isomer products based off their retention times. Similarly, previous studies have determined the formation of three different geranylated products upon the incubation of NphB with 1,6-DHN and GPP[54].

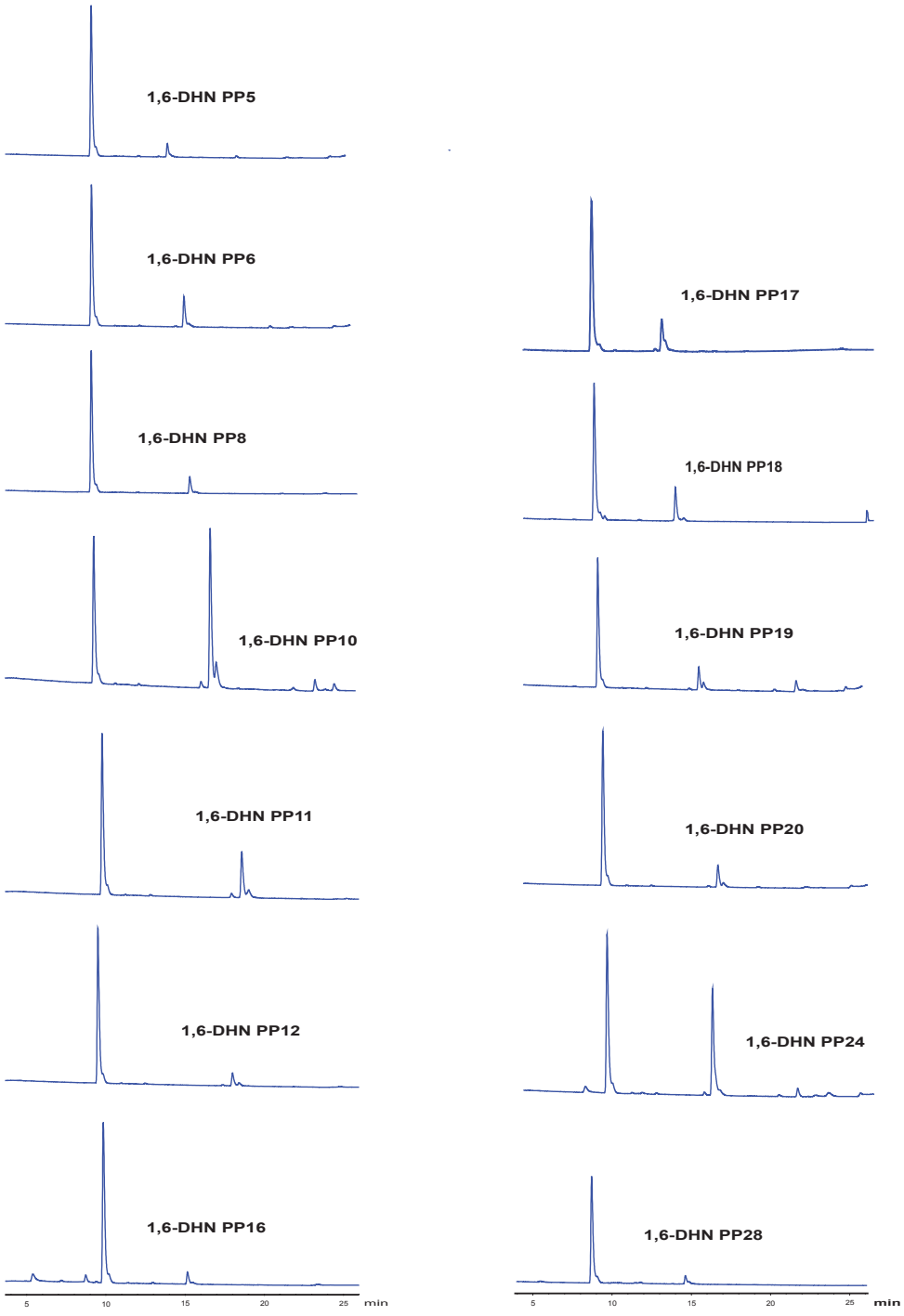
Of the 26-catalyzed reaction 16 displayed significant product formation (>20%) and six showed a >50% product formation. The six highest producing reactions included the native substrate GPP (**PP29**), **PP10, PP30-PP32** and **PP34**. As expected, the reaction containing GPP significant conversion of 75% when incubated for 16h. Both **PP10** (58% conversion) and **PP30** (51% conversion) are seven carbons in length and show a similar product conversion, **PP10** is a butane derivative of DMAPP and **PP30** is a butene derivative with a terminal alkene. **PP31** and **PP32** both have added aliphatic groups onto the terminal methyl of GPP. Interestingly, **PP31** with an additional methyl added and was able to show 90% product conversion, overall greater conversion

compared to the native substrate, GPP. However, **PP32** with an additional terminal allyl group, resulted in a decreased the conversion to only 57%. Analogue **PP34** features a terminal alcohol group on the geranyl tail and displays an impressive 52% product conversion.

The remaining 10 compounds that showed an appreciable >20% conversion have a large distribution in the length of the alkyl moiety. The smallest compound that was catalytically transferred onto 1,6-DHN was an the allylic cyclopentane **(PP19** (21%)), while the longest were the ether linked benzyl GPP derivative **(PP33** (39%)**)** and FPP (**PP35** (30%)). FPP has previously been reported has a substrate for 1,6DHN[36] and showed a 30% conversion when incubated for 16h under the stated assay conditions. Additional allylic analogues, **PP6**, **PP11, PP18,** and **PP24** showed 20%, 29%, 21%, 43% conversion respectively. **PP6** is an ethyl DMAPP derivative, **P11** is a pentyl DMAPP derivative, while **PP18** is a C2 methylated 2,4-hexadiene. **PP24**, like **PP18**, has a conjugated system; however, it is in the form of a benzyl substituted DMAPP and mediated twice the product conversion compared to **PP18**. Furthermore, three propargyl containing analogues (**PP61, PP62 and PP65),** ranging in linear length between 7 and 12 atoms, displayed appreciable conversion. **PP61** is a propargyl derivative of DMAPP with a terminal propargyl group showing and it underwent a 21% conversion. Both **PP62** and **PP65** are ether linked propargyl derivatives of DMAPP and GPP respectively, **PP62** underwent 20% conversion while **PP65** had a 33% conversion.

The remaining enzyme reactions produced <20% conversion. They included allylic analogues of varying length, methylation and conjugation; **PP5** (DMAPP) (8%)**, PP8 (**12%)**, PP12(**11%)**, PP16** (7%)**, and PP17** (13%)**.** Additionally, **PP20**, allylic

cylcohaxane, and **PP28**, five-carbon chain aromatic displayed 16%, and 9% conversion. Of the 13 synthesized benzyl analogues only one was accepted as substrate; **PP37,** a para-methoxy substituted benzyl analogue, with a 18% conversion. Two additional chemoselective analogues, **PP64**, a para-propargyl ether substituted benzyl compound, and **PP56**, an azido DMAPP derivative showed slight product formation at 9% and 5% respectively. Finally, only one heterocycle analogue was accepted using 1,6-DHN as the substrate, **PP54**, a piperonyl pyrophosphate baring a 3, 4 methylene dioxy moiety, which exhibited a 14% conversion.


1,6-DHN PP5
1,6-DHN PP6
1,6-DHN PP8
1,6-DHN PP10
1,6-DHN PP11
1,6-DHN PP12
1,6-DHN PP16
1,6-DHN PP17
1,6-DHN PP18
1,6-DHN PP19
1,6-DHN PP20
1,6-DHN PP24
1,6-DHN PP28
5
10
15
20
25
min

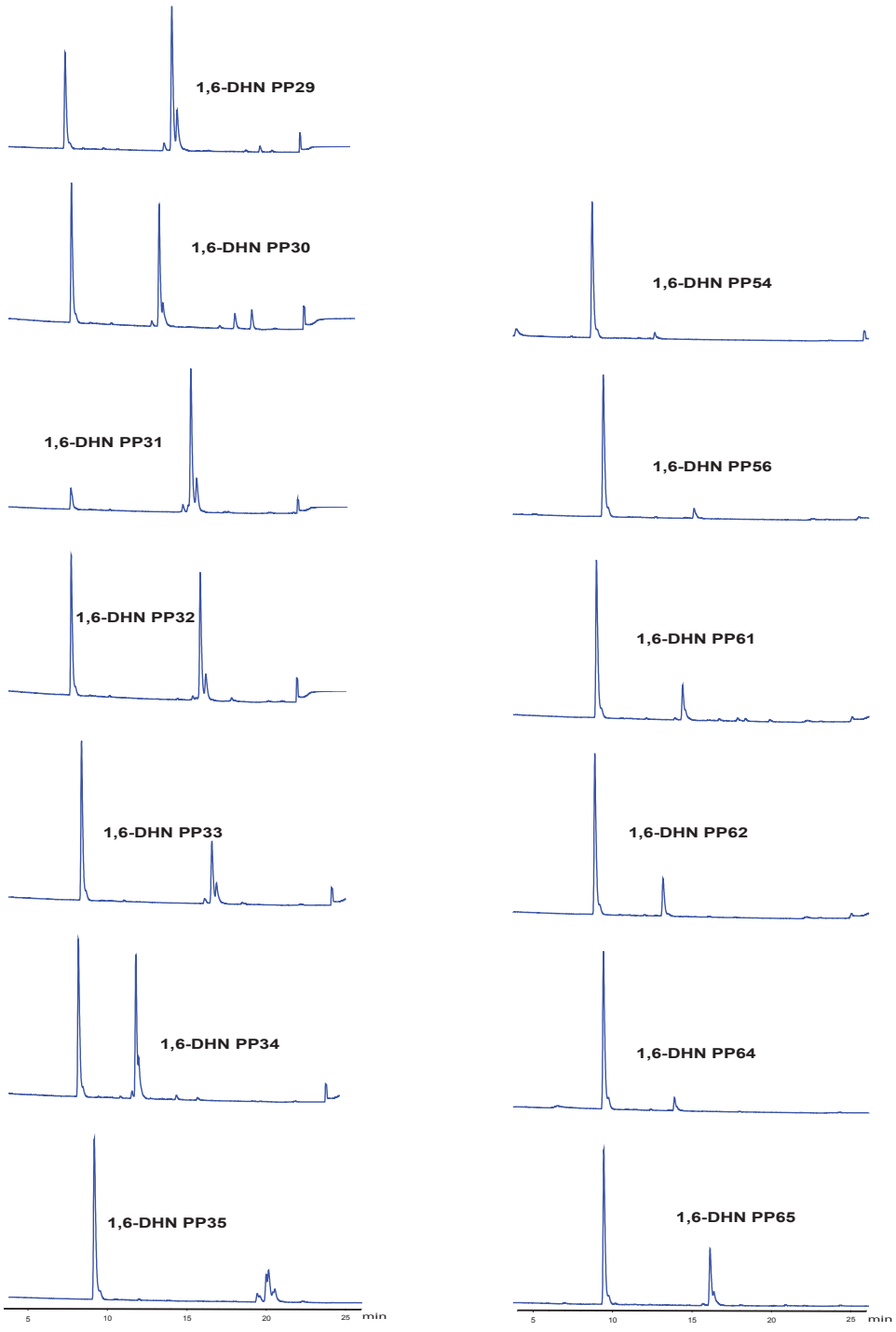


Figure 26 RP- HPLC chromatograms.
RP- HPLC chromatogram of incubation mixtures of 1,6-DHN with pyrophosphate analogues which lead to the NphB catalyzed formation of alkylated sulfabenzamide derivatives. The peak at approximately 9.5 min is 1,6-DHN and the product peaks are after 10 min in the chromatogram.

Chemoenzymatic syntheses of alkylated sulfabenzamide

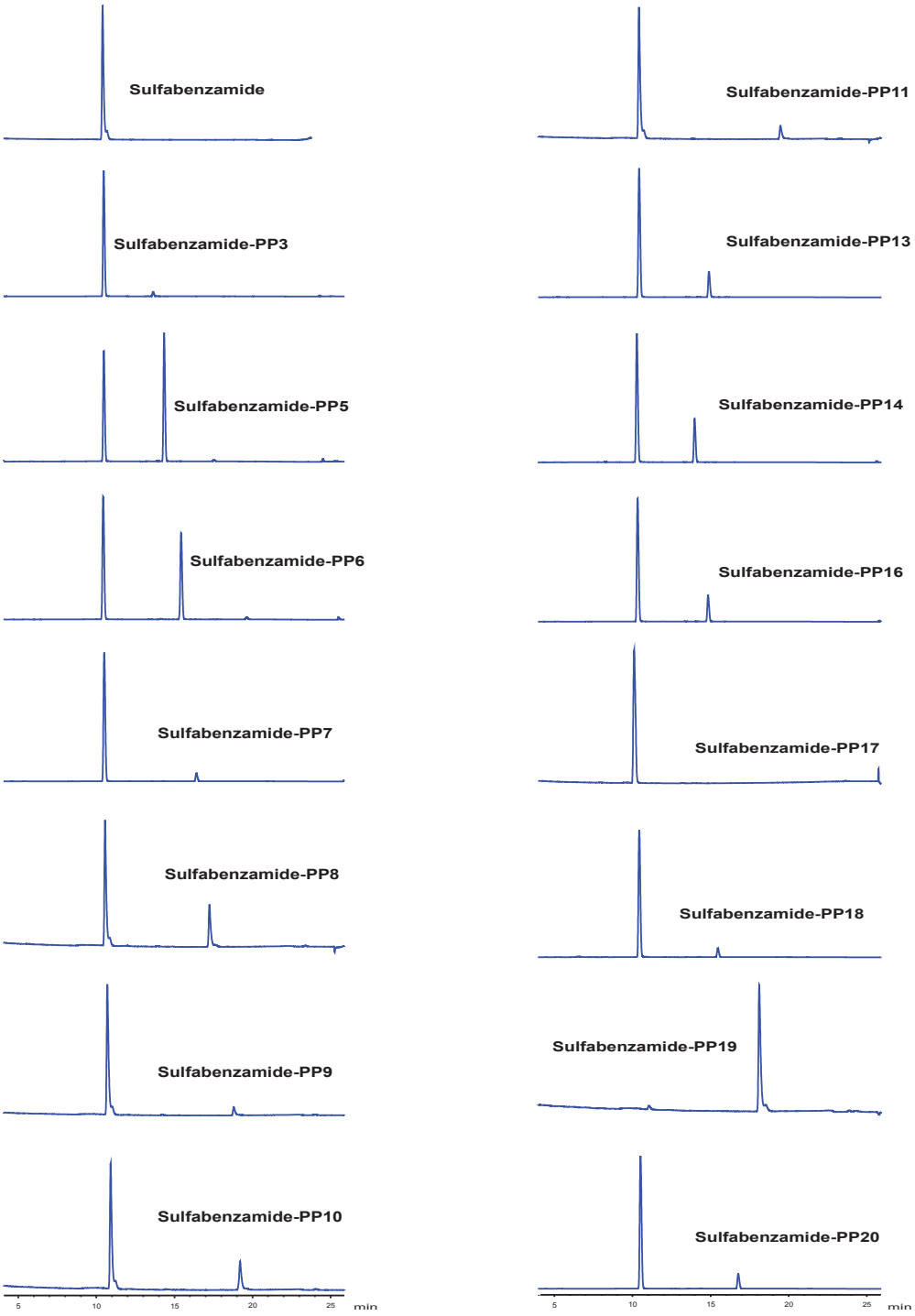
Next, to investigate the utility of NphB to perform catalytic modification of synthetic aromatic substrates, 11 known drug compounds (amoxicillin, methotrexate, tamoxifen, catharanthine, puromycin, camptothecin, yohimbine, sulfadoxin, chloramphenicol, ethynylestradiol and sulfabenzamide) containing aromatic moieties were incubated with prenyl pyrophosphates GPP and DMAPP. The HPLC and HRMS analysis of the enzyme reaction revealed that NphB accepted sulfabenzamide as a prenyl acceptor. In contrast to the native behavior of NphB, no product formation was detected with GPP as the donor substrate when sulfabenzamide is the aromatic acceptor. On the other hand, DMAPP was able to be catalytically transferred onto sulfabenzamide producing a prenylated derivative. The drastic shift in donor substrate preference prompted us to test the catalytic capability of NphB to transfer non-native alkyl pyrophosphates using our library of synthetic pyrophosphates, generating sulfabenzamide derivatives with potentially altered biological activity.

Similar to the analytical reactions involving 1,6-DHN aromatic acceptor, analysis of the product formation was performed using HPLC and HRMS. This revealed that 29 out of the 65 alkyl-PP enzymatic reactions resulted in alkylated sulfabenzamide products (Figure 25 and 29; Table 6). A variety of distinctive analogues were accepted as alkyl donors; markedly, of the 29 accepted donors, less than 50% were seen to be accepted using 1,6-DHN. Overall, the linear length of the accepted donors ranges from a four-carbon chain (**PP5 (DMAPP)** (60%), **PP19** (100%) and **PP3** (4%)) to a seven-carbon chain (**PP10)** (20%)). Of the 29 positive reactions, ten pyrophosphate analogues (**PP5, PP6, PP19, PP21, PP14, PP10, PP8, PP40, PP49, PP54)** show an appreciable (>20%)

product conversion. Notably, of the analogues showing greater than 20% product conversion, half of these contain an aromatic (**PP40** (25%), **PP54** (46%), **and PP49** (20%)) or non-aromatic ring structures (**PP19** (100%) and **PP21** (40%)). The remaining five analogues contain various carbon chain length, methylation and conjugation. Diversity in the overall chain length can be seen in the acceptance of a four-carbon chain DMAPP (**PP5**) and the allylic cyclopentane (**PP19**), five-carbon chain ethyl DMAPP derivative (**PP6),** and isopropyl DMAPP derivative (**PP8** (27%)), and a seven-carbon chain, butyl DMAPP derivative (**PP10** (20%)) donor substrates. The C3 methyl group can be found on **PP5**, **PP6**, **PP10** and **PP8**. Compound **PP14** (25%) lacked methyl groups; however, it is the only analogue to show appreciable product formation with a linear conjugated system. Analysis of the subset of benzyl pyrophosphate analogues revealed that NphB is capable of transferring eight out of the 13 benzyl groups onto sulfabenzamide, including; a *para*- (**PP37** (13%)) and *ortho*- (**PP38** (8%)) methoxy substituted benzyl compounds, a *para*- methyl substituted benzyl compound (**PP40**(25%)), fluorine, chlorine and bromine halogenated benzyl compounds (**PP41** (6%), **PP42** (14%), **PP43**(9%))**,** *para*- and *ortho*- methoxy di-substituted benzyl (**PP45**(11%)), and a para- and meta-methoxy di-substituded benzyl **(PP46**(8%)). Additionally, four aromatic heterocycle analogues; thiopene (**PP49**(20%)), furane (**PP50**(14%)) a benzothiophen (**PP52**(11%)) and piperonyl pyrophosphate baring a 3, 4 methylene dioxy moiety (**PP54**(46%)) pyrophosphate were also able to be transferred onto sulfabenzamide, displaying 20%, 15% 11% and 46% conversion respectively.

Table 6. Summary of HRMS data of sulfabenzamide analogues from NphB catalyzed alkylation reaction with sulfabenzamide and synthetic alkyl-PP analogues.

Enzyme Product	Chemical Formula	Calculated Mass (Da)	Observed Mass (Da)
Sulfabenzamide	$C_{13}H_{12}N_2O_3S$ $[M+H]^+$	277.0641	277.0648
Sulfabenzamide-PP3	$C_{17}H_{18}N_2O_3S$ $[M+H]^+$	331.1111	331.1120
Sulfabenzamide-PP5	$C_{18}H_{20}N_2O_3S$ $[M+H]^+$	345.1267	345.1276
Sulfabenzamide-PP6	$C_{19}H_{22}N_2O_3S$ $[M+H]^+$	359.1424	359.1442
Sulfabenzamide-PP7	$C_{20}H_{24}N_2O_3S$ $[M+H]^+$	373.158	373.1592
Sulfabenzamide-PP8	$C_{20}H_24N_2O_3S$ $[M+Na]^+$	395.1406	395.1395
Sulfabenzamide-PP9	$C_{21}H_{26}N_2O_3S$ $[M+Na]^+$	409.1562	409.1576
Sulfabenzamide-PP10	$C_{21}H_{26}N_2O_3S$ $[M+Na]^+$	409.1562	409.1577
Sulfabenzamide-PP11	$C_{22}H_{28}N_2O_3S$ $[M+Na]^+$	423.1719	423.1733
Sulfabenzamide-PP13	$C_{19}H_{20}N_2O_3S$ $[M+H]^+$	357.1267	357.1270
Sulfabenzamide-PP14	$C_{18}H_{18}N_2O_3S$ $[M+H]^+$	343.1111	343.1118
Sulfabenzamide-PP16	$C_{19}H_{20}N_2O_3S$ $[M+H]^+$	357.1267	357.1277
Sulfabenzamide-PP17	$C_{22}H_{22}N_2O_5S$ $[M+H]^+$	371.1424	371.1432
Sulfabenzamide-PP18	$C_{20}H_{22}N_2O_3S$ $[M+H]^+$	371.1424	371.1435
Sulfabenzamide-PP19	$C_{20}H_{22}N_2O_3S$ $[M+Na]^+$	393.1249	393.1266
Sulfabenzamide-PP20	$C_{21}H_{24}N_2O_3S$ $[M+H]^+$	385.158	385.1590
Sulfabenzamide-PP21	$C_{20}H_{22}N_2O_3S$ $[M+H]^+$	371.1424	371.1435
Sulfabenzamide-PP29	$C_{23}H_{28}N_2O_3S$ $[M+Na]^+$	435.1719	435.1723
Sulfabenzamide-PP30	$C_{21}H_{24}N_2O_3S$ $[M+Na]^+$	407.1406	407.1420
Sulfabenzamide-PP37	$C_{21}H_{20}N_2O_3S$ $[M+Na]^+$	419.1036	419.1029
Sulfabenzamide-PP38	$C_{22}H_{20}N_2O_3S$ $[M+H]^+$	393.1267	393.1275
Sulfabenzamide-PP40	$C_{21}H_{20}N_2O_3S$ $[M+Na]^+$	403.1093	403.1106
Sulfabenzamide-PP41	$C_{20}H_{17}FN_2O_3S$ $[M+Na]^+$	407.0842	407.0858
Sulfabenzamide-PP42	$C_{20}H_{17}ClN_2O_3S$ $[M+Na]^+$	423.0546	423.0553
Sulfabenzamide-PP43	$C_{20}H_{17}BrN_2O_3S$ $[M+Na]^+$	467.0042	467.0060
Sulfabenzamide-PP45	$C_{22}H_{22}N_2O_5S$ $[M+Na]^+$	453.1647	453.1673
Sulfabenzamide-PP46	$C_{22}H_{22}N_2O_5S$ $[M+Na]^+$	449.1147	449.1166
Sulfabenzamide-PP49	$C_{18}H_{16}N_2O_3S_2$ $[M+Na]^+$	395.0500	395.0499
Sulfabenzamide-PP50	$C_{18}H_{16}N_2O_4S$ $[M+Na]^+$	379.0729	379.0733
Sulfabenzamide-PP52	$C_{22}H_{18}N_2O_3S_2$ $[M+Na]^+$	445.0657	455.0665
Sulfabenzamide-PP54	$C_{21}H_{18}N_2O_5S$ $[M+Na]^+$	433.0834	433.0838


Sulfabenzamide
Sulfabenzamide-PP3
Sulfabenzamide-PP5
Sulfabenzamide-PP6
Sulfabenzamide-PP7
Sulfabenzamide-PP8
Sulfabenzamide-PP9
Sulfabenzamide-PP10
Sulfabenzamide-PP11
Sulfabenzamide-PP13
Sulfabenzamide-PP14
Sulfabenzamide-PP16
Sulfabenzamide-PP17
Sulfabenzamide-PP18
Sulfabenzamide-PP19
Sulfabenzamide-PP20
5
10
15
20
25
min

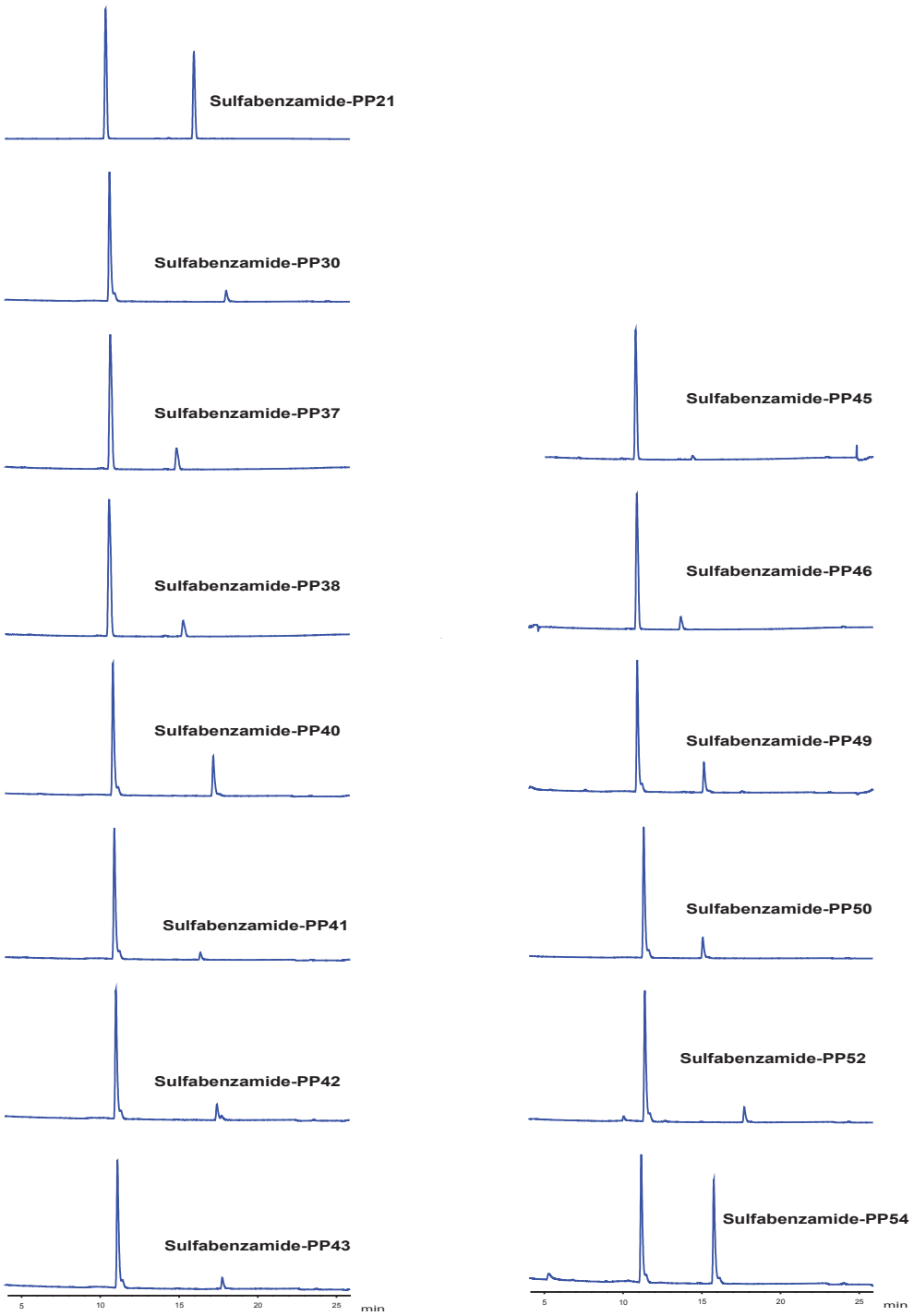


Figure 27. RP- HPLC chromatograms.
Chromatograms of incubation mixtures of sulfabenzamide with pyrophosphate analogues which lead to the NphB catalyzed formation of alkylated sulfabenzamide derivatives.

NphB mutational studies.

Based on the analysis of the existing crystal structure of NphB, complexed with geranyl S-thiodiphosphate (GSPP) and 1,6-DHN (PDB ID, 1zb6), along with previously performed prenyltransferase mutational studies, we speculated altering residues found in the prenyl binding pocket would subsequently modify the substrate specificities. [36, 56] Guided by the mutational studies on TleC, MpnD, and PagF (TleC Phe170 and Trp97, MpnD Met159 and Tyr80, PagF Phe222), we therefore focused on key residues lining the distal end of the prenyl binding pocket: Met106 and Phe123. [53, 100] To evaluate the impact of the size of the side chain, we constructed the M106V variant. Further modifications to the prenyl binding pocked were made by construction of a double mutant, M106V/F123V. Variant enzymes were assayed against the alkyl-PP library with sulfabenzamide (Figure 28D). Both the single and double mutant, M106 and M106V/F123V, were able to accept GPP as a prenyl donor (M106V/F123V k_{cat} 7.8 x 10^{-3} min^{-1}, K_M 0.4 mM; M106V 1.5 x 10^{-3} min^{-1}, K_M 0.6 mM), an activity not present in wild-type enzyme when incubated with sulfabenzamide as the acceptor (Figure 28 A-C). Furthermore, both mutants were able to transfer **PP31** (5% and 3.5%) and the double mutant accepted **PP32**, **PP33**, and **PP64** to a small degree (5%, 4%, and 11.5%). New activity shown in the NphB mutants was seen when incubated with longer pyrophosphate analogues and sulfabenzamide. Although the majority of wild-type activity was maintained in the mutants, a decrease in product formation was seen for all other reactions.

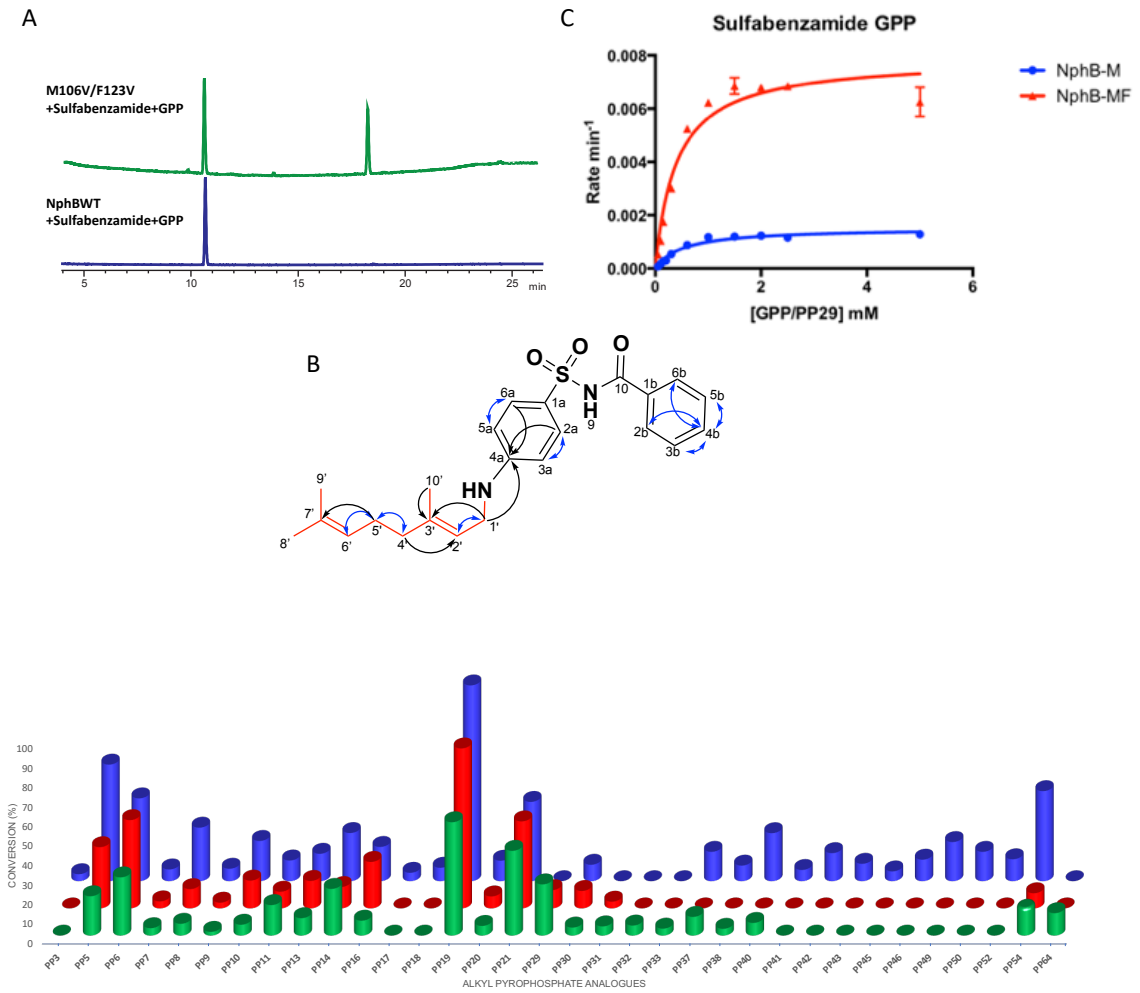


Figure 28. NphB mutation analysis.

(A) *Reverse-phase HPLC analysis of NphB wild-type (bottom) and NphB M106V/F123V (top) enzyme assays using sulfabenzamide and GPP/PP29.* ***(B)*** *NMR correlations (blue arrow, COSY correlations, black arrow, HMBC correlations) of sulfabenzamide-GPP product generated through incubation NphB M106V/F123V.* ***(C)*** *Kinetic curves showing the enzyme activities of NphB M106 and M106V/F123V with sulfabenzamide and GPP/PP29.* ***(D)*** *Percent conversion of library of alkyl pyrophosphate incubated with sulfabenzamide using NphB-WT (blue) and NphB-M106V (red) and NphB-M106V/F123V (Green) Assays were performed under standard condition and incubated for 16hrs. Alkylated sulfabenzamide products marked with an asterisk were isolated using HPLC and characterized using NMR*

Structure characterization of sulfabenzamide products.

To elucidate the structure of the alkylated sulfabenzamide products, which were generated for 12 out of 29 reactions, confirmed by HRMS and RP-HPLC to yield products, were scaled up and purified *via* a semi-preparative RP-HPLC protocol (See method B (HPLC) in Experimental Methods), and subjected to NMR analysis (Table 7). Sulfabenzamide products selected for characterization displayed >15% product conversion, as determined in the initial analytical reactions, and possess unique electronic and structural features, e.g. carbon chain length, conjugated systems, cyclization and aromaticity. Specifically, the characterized sulfabenzamide products were diversified through the attachment of allylic analogues, DMAPP (**PP5**), GPP (**PP29**), ethyl and isopropyl DMAPP derivative (**PP6** and **PP8**), as well as two diene analogues with C5 and C6 carbon chain length (**PP14** and **PP16**) and two cyclic pyrophosphates (**PP19** and **PP21**). Additionally, two benzylic derivatized sulfabenzamide compounds, (**PP37** and **PP40**), and three heterocyclic analogues (**PP49, PP50** and **PP54**) were also scaled up for characterization. The resulting purified sulfabenzamide products were subjected to 1H and 2D NMR experiments to determine the exact position of derivatization on the parent compound. In addition to the 1H experiments, all purified sulfabenzamide products have a COSY spectrum; however, due to limited available quantities, experiments such as HMBC and HSQC could only be performed on **PP29, PP8, PP19, PP49**, **PP50** and **PP54**. Previous studies have indicated that the position of the alkylation was influenced by the specific alkyl donor (Chapter 3, [56]); therefore, given the wide variety of structurally characterized

alkylated sulfabenzamide products, we expect insight into the regio selectivity and specificity of NphB catalyzed reaction.

We have concluded that all scaled up sulfabenzamide reactions resulted in the regiospecific N-alkylation (Figure 29, NMR Table **5**) as characterization by NMR analysis, including chemical shift values, integration, splitting, and COSY and/or HMBC correlations. The ^{1}H NMR of the sulfabenzamide derivatives, when compared to sulfabenzamide, revealed that all aromatic protons were accounted for on both rings of the parent compound found in the 6.0-8.0ppm range, strongly suggesting an N-substitution. Signals corresponding to the two aromatic rings on sulfabenzamide could be differentiated by their splitting pattern, as the benzamide ring displays three distinct peaks with multiplet splitting pattern integrating to a 2:2:1 ratio whereas the 4-amino benzenesufonyl has two proton peaks with a doublet splitting pattern integrating to a 1:1 ratio. Assignments of the aromatic proton signals were further supported by the COSY spectra showing correlation peaks between the H2a-H3a and H6a-H5a on the 4-amino benzenesulfonyl ring as well as correlation peaks between H2b-H3b, H3b-H4b, H4b-H5b and H5b-H6b on the benzamide ring. In some cases, the COSY spectra also showed correlation between the proton on the amino NH and the H1' of the substituent alkyl or benzyl group. For the samples with sufficient quantities of purified compound, we were able to obtain additional 2D experiments, the ^{1}H – ^{13}C HMBC and ^{1}H -^{13}C HSQC spectra were collected, displaying connectivity between H1' alkyl or benzyl group to the C4a of the 4-amino benzenesuflonyl ring, unequivocally confirming the N-alkyl addition. Each scale up reaction was additionally confirmed by HRMS data, supporting on the presence of only a mono-alkylated product. These findings verify the

novel capabilities of NphB to catalyze the N-alkylation of sulfabenzamide using natural donors DMAPP and GPP, and non-native donors including dienes, para-substituted benzyl and heterocyclic pyrophosphate donors

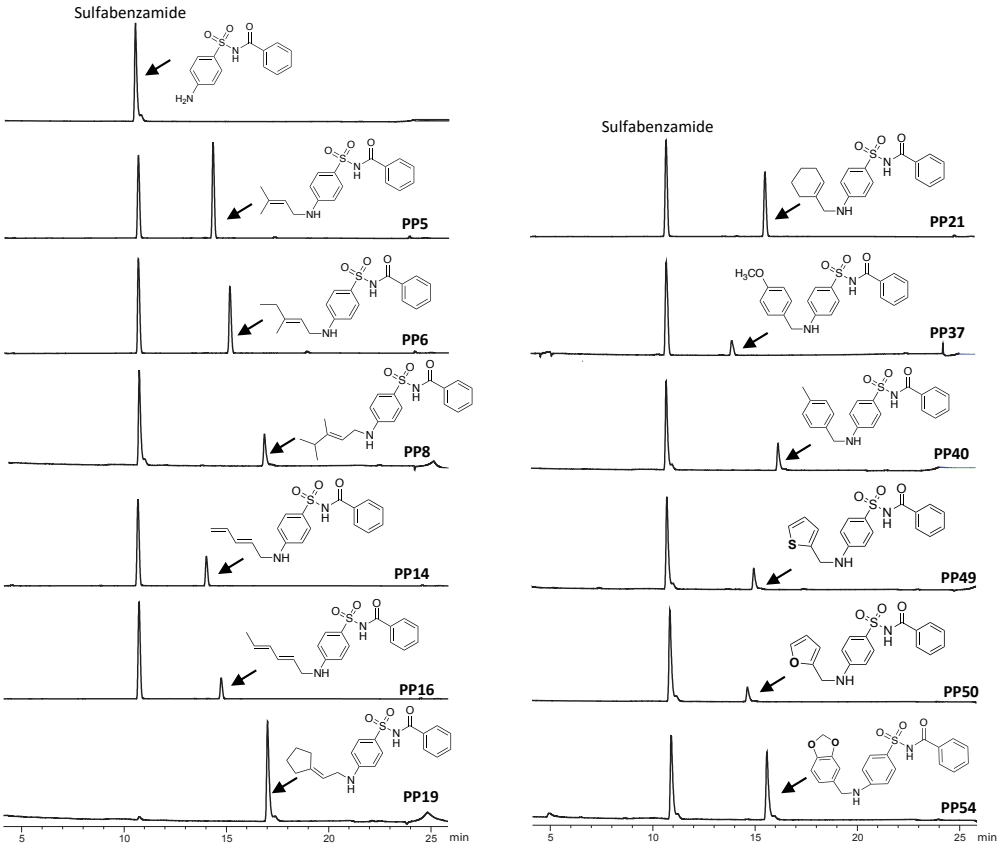
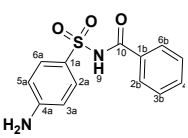
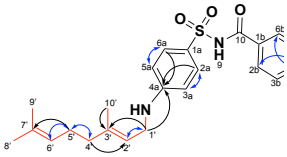
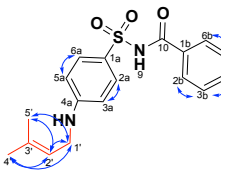
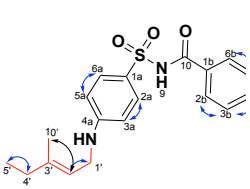
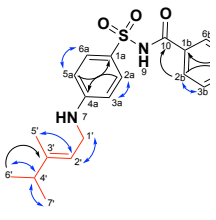
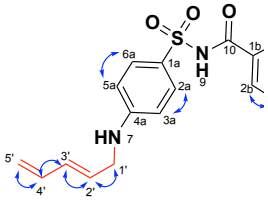
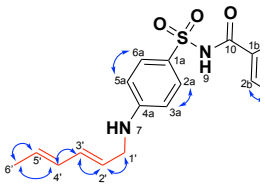
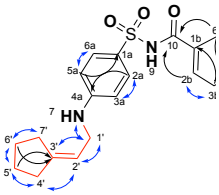
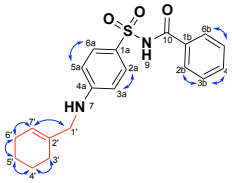
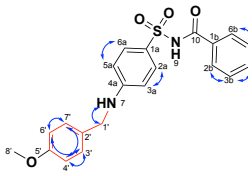
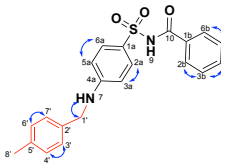
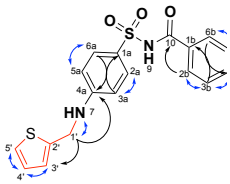


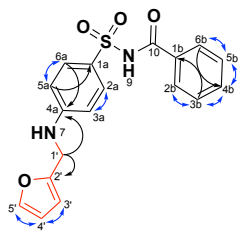
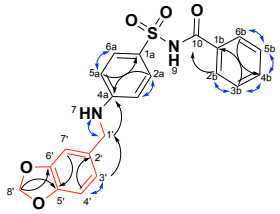
Figure 29. Sulfabenzamide derivatives.
Reverse-phase HPLC analysis of NphB wild-type catalyzed reactions that resulted in structure elucidated via NMR and RP-HRMS.

Table 7. NMR data of alkylated sulfabenzamide

				
	Sulfabenzamide	**Sulfabenzamide-GPP_PP29**	**Sulfabenzamide-PP5**	**Sulfabenzamide-PP6**
Position	**δ_H, multi (J)** **δ_C**	**δ_H, multi (J)** **δ_C**	**δ_H, multi (J)** **δ_C**	**δ_H, multi (J)** **δ_C**
NH	12.07, s		8.13, s	8.13, s
NH	6.15, s (NH_2)		6.56, s	6.52, s
1a				
2a	7.63, d (8.8) 130.6	7.78, d (8.9) 129.4	7.59, d (8.4)	7.62, d (8.7)
3a	6.61, d (8.8) 112.7	6.63 d (8.9) 110.1	6.52, d (8.4)	6.57, d (8.7)
4a		152.7		
5a	6.61, d (8.8) 112.7	6.63 d (8.9) 110.1	6.52, d (8.4)	6.57, d (8.7)
6a	7.63, d (8.8) 130.6	7.78, d (8.9) 129.4	7.59, d (8.4)	7.62, d (8.7)
1b				
2b	7.83, dd (8.4, 1.3) 128.7	7.79, dd (7.9, 1.0) 127.3		7.84, d (7.1)
3b	7.47, dd (8.4, 7.4) 128.9	7.60, t (7.9) 127.8	7.36, m	7.40, t (7.1)
4b	7.60, tt (7.4, 1.3) 133.5	7.47, tt (7.4, 1.0) 132.1	7.44, m	7.50, m
5b	7.47, dd (8.4, 7.4) 128.9	7.6 127.8		7.40, t (7.1)
6b	7.83, dd (8.4, 1.3) 128.7	7.79 127.3		7.84, d (7.1)
1’		3.73, d (6.5) 39.9	3.64, dd (6.5, 5.9)	3.67, t (5.7)
2’		5.26, t (6.5) 120.5	5.22, t (6.5)	5.22, t (5.7)
3’		137.7		
4’		2.06, m 38.7	1.68, s	1.99, q (7.8)
5’		2.11, m 25.5	1.69, s	0.96, t (7.8)
6’		5.07, t (7.1) 123.1		1.68, s
7’		130.3		
8’		1.57, s 15.8		
9’		1.57, s 15.8		
10’		1.73, s 14.5		
Solvent	DMSO-d6	CD_3OD	DMSO-d6	DMSO-d6

	 Sulfabenzamide-PP8		 Sulfabenzamide-PP14		 Sulfabenzamide-PP16		 Sulfabenzamide-PP19	
Position	**δ_H, multi (J)**	**δ_C**	**δ_H, multi (J)**	**δ_C**	**δ_H, multi (J)**	**δ_C**	**δ_H, multi (J)**	**δ_C**
NH			8.14, s		12.12, s		8.14, brs	
NH			6.56, s		6.54, s		6.37, brs	
1a		124.09						129.42
2a	7.93, d (8.9)	127.71	7.54, d (8.4)		7.63, d (8.7)		7.59, d (8.8)	129.45
3a	6.60, d (8.9)	111.44	6.49, d (8.4)		6.59, d (8.7)		6.52, d (8.8)	110.8
4a		152.8						151.8
5a	6.60, d (8.9)	111.44	6.49, d (8.4)		6.59, d (8.7)		6.52, d (8.8)	110.8
6a	7.94, d (8.9)	127.71	7.54, d (8.4)		7.63, d(8.7)		7.59, d (8.8)	129.49
1b		124.09						136.76
2b	7.79, dd (8.4,1.3)	130.97	7.84, dd (8.3, 1.6)		7.84, dd (8.3, 1.4)		7.86, d (8.0)	128.24
3b	7.44, t, (8.4, 7.4)	128.9	7.3		7.42, dd (8.3, 7.5)		7.36 t, (7.6)	128.24
4b	7.55, tt (7.5, 1.3)	133.22	7.34, m		7.53, tt (7.5, 1.4)		7.44, t (7.3)	131.49
5b	7.44, t, (8.4, 7.4)	128.9	7.30, m		7.42, dd (8.3, 7.5)		7.36 t, (7.6)	128.21
6b	7.79, dd (8.4,1.3)	130.97	7.84		7.84, dd (8.3, 1.4)		7.86, d (8.0)	128.7
1’	3.75, d (6.6)	41.24	3.75, t (5.6)		3.75, td(5.7, 1.5)		3.61, d (6.0)	42.35
2’	5.30, t (6.7)	117.84	5.79, dt (15,3, 5.6)		5.58, dt (15.1, 5.7)		5.34, p (4.1, 2.1)	
3’		146.11	6.22, dd (15.3, 10.5)		6.17, ddt (15.1, 10.5, 1.5)			145.5
4’	2.28, hept (7.3,7.0)	36.71	6.35, dt (16.9, 10.5)		6.05, ddd(15.1, 10.5, 1.5)		2.24, m	28.89

	 Sulfabenzamide-PP21		 Sulfabenzamide-PP37		 Sulfabenzamide-PP40		 Sulfabenzamide-PP49	
Position	**δ_H, multi (J)**	**δ_C**	**δ_H, multi (J)**	**δ_C**	**δ_H, multi (J)**	**δ_C**	**δ_H, multi (J)**	**δ_C**
NH	12.12, s		6.55, br s		8.41, s		8.3, brs	
NH	6.54, s				6.53, t (5.8)		6.62, t (6.0)	
1a								134.1
2a	7.60, d (8.4)		7.50, d (8.4)		7.49, d (8.5)		7.53, d (8.7)	128.68
3a	6.56, d (8.4)		6.47, d (8.4)		6.46, d (8.5)		6.55, d (8.9)	111.02
4a								150.03
5a	6.56, d (8.4)		6.47, d (8.4)		6.46, d (8.5)		6.55, d (8.7)	111.02
6a	7.60, d (8.4)		7.50, d (8.4)				7.53, d (8.7)	128.68
1b								139.64
2b	7.85, d (7.7)		7.85, d (7.1)		7.85, d (7.1)		7.87, dd (8.4,1.4)	128.74
3b	7.39, t (7.6)		7.27, t (7.1)		7.26, dd (7.1, 6.6)		7.27, tt (7.2, 1.4)	127.72
4b	7.49, m		7.32, t (7.1)		7.31, t (6.6)		7.33, tt (7.4, 1.4)	129.97
5b	7.39, t (7.6)		7.27, t (7.1)		7.26, dd (7.1, 6.6)		7.27, tt (7.2, 1.4)	127.72
6b	7.85, d (7.7)		7.85, d (7.1)		7.85, d (7.1)		7.87, dd (8.4,1.4)	128.74
1’	3.57, d (5.7)		4.20, d (5.9)		4.22, d (5.8)		4.45, d (4.45)	42.04
2’								
3’	1.94, m		7.25, d (8.1)		7.21, d (7.7)		7.03, dd (3.4, 1.1)	125.29
4’	1.57, m		6.87, d (8.4)		7.1, d (7.7)		6.94, dd (5.0,3.4)	127.19
5’	1.50, m						7.34, dd (5.1,1.3)	125
6’	1.95, m		6.87, d (8.4)		7.1, d (7.7)			

	 Sulfabenzamide-PP50		 Sulfabenzamide-PP54	
Position	**δ_H, multi (J)**	**δ_C**	**δ_H, multi (J)**	**δ_C**
NH	8.29, brs		8.16, brs	
NH	6.45, t (6.0)		6.64, brs	
1a		133.9		132.16
2a	7.53, d (8.7)	128.65	7.53, dd (8.8)	128.96
3a	6.56, d (8.8)	110.94	6.51, d (8.9)	110.93
4a		149.97		150.58
5a	6.56, d (8.8)	110.94	6.51, d (8.9)	110.93
6a	7.53, d (8.7)	128.65	7.53, d (8.8)	128.96
1b		140.79		138.85
2b	7.87, dd (7.9, 1.4)	128.69	7.86, dd (8.4,1.3)	128.71
3b	7.27, dd (8.2, 6.5)	127.73	7.30 t, (7.6,7.4)	127.9
4b	7.33, dd (8.2, 6.5)	129.94	7.36, t (7.5, 7.5)	130.47
5b	7.27, dd (8.2, 6.5)	127.73	7.30 t, (7.6,7.4)	127.9
6b	7.87, dd (7.9, 1.4)	128.69	7.86, dd (8.4,1.3)	128.71
1’	4.25, d (5.8)	40.07	4.18, d (5.1)	46.26
2’		153.52		134.13
3’	6.29, d (3.2)	107.36	6.89, s	108.08
4’	6.36, dd (3.2, 1.8)	110.76	6.82, m	108.5
5’				146.43
6’				147.68
7’			6.83, m	120.63
8’				5.95, s
10				169.14
Solvent	DMSO-d6		DMSO-d6	

Discussion

The analysis of our *in vitro* activity assays revealed NphB capable of the successful catalytic transfer of several chemically and structurally distinct alkyl-PP onto two different aromatic substrates, 1,6-DHN and sulfabenzamide. Remarkably, these results indicate a clear donor-dependent alkylation reaction and a novel N-prenylation enzymatic functionality resulting in the diversification of the drug compound,

sulfabenzamide. Recently, a donor-dependent acceptor binding mechanism was reported for AtaPT from *A. terreus* NIH2624, wherein a sequential donor and acceptor binding order was determined through isothermal titration calorimetry.[53] The alkyl donor then acceptor binding order was also proposed for NphB, based on the crystal structure complexed with GSPP alone.[54] In the present study, we observed many examples of alkyl donors accepted as substrates by NphB when incubated with 1,6-DHN; however, the same alkyl donors would not result in a product formation using sulfabenzamide. Additionally, by employing structural engineering rationale we generated the single and double mutants M106V and M106V/F123V, and were able to revive the native geranylation capabilities of NphB when incubated with sulfabenzamide.

Alkyl-PP donor specificities were revealed by the enzymatic reaction with 1,6-DHN or sulfabenzamide. As seen in the results, a distinction in chain length preference is made according to the aromatic acceptor substrate. For reactions with 1,6-DHN, a minimal conversion of 8% was seen with DMAPP, which has a linear length of four carbons; whereas, when reacted with sulfabenzamide, a more substantial conversion of 60% was observed. It is our understanding that this is the first occurrence of NphB appreciably accepting DMAPP as a prenyl donor. It became apparent that the enzymatic reactions with sulfabenzamide loss the ability to transfer longer chain and bulkier analogues. GPP and derivatives (**PP29/GPP, PP31, PP32, PP65, PP33** and **PP34**) were solely transferred onto 1,6-DHN to varying product yields.

To explain these results, we offer the following explanations. NphB has been shown to geranlyate 1,6-DHN in three different positions on the naphthalene ring, signifying that 1,6-DHN must adopt three different orientations in the binding pocket that result in product formation.[54] On the bases of complexed crystal structure, 1,6-DHN is stabilized within the active site by a significant contribution from the geranyl tail of GSPP, and without these interactions, such as the case with DMAPP, 1,6-DHN could bind too loosely and therefore be unable to produce any appreciate product. In the case of NphB incubation with sulfabenzamide, the prenylation site resides in the same orientation as it would with 1,6-DHN within the active site, however additional hydrogen bonding potential and the larger size of the substrate is likely to contribute to its increased stability with respect to orientation in the active site in the absence of the geranyl tail of GPP. A fixed conformation could also explain the observation of a single N- alkylation mode for sulfabenzamide derivatives, a similar relationship between larger substrates and a single product have previously been reported for NphB reactions.[54] Because the larger prenyl donors could occupy the same space as the benzamide moiety of sulfabenzamide in the active site, the steric bulk is believed to prevent the binding of sulfabenzamide and therefore the formation of products, as seen in our results. The NphB mutants M106V and M106V/F123V relieved steric restrictions up the prenyl binding pocket, potentially decreasing the steric hindrance between the terminal end of the alkyl donor and benzamide moiety, as the mutants showed higher product conversion with longer chained alkyl-PP (Figure 28).

In conclusion, NphB demonstrated generous capabilities to transfer diverse unnatural and synthetic alkyl donors onto 1,6-DHN as well as the synthetic pharmaceutical drug, sulfabenzamide, ultimately generating novel N-alkylated sulfabenzamide derivatives. Furthermore, through structure-based enzyme engineering NphB was able to broaden it substrate acceptance and generate a geranylated sulfabenzamide derivative. These results implicate the plausibility of prenyltransferases in biotechnologies and expand on their catalytic abilities to feasibly generate novel drug derivatives.

Experimental

Protein Expression and Purification

The recombinant plasmid, pET-28a containing synthetic genes for NphB bearing N-terminal His_6, was transformed into *E. coli* Rosetta cells. After overnight growth, 3 mL of bacterial culture was transferred to 4 L flasks containing 1.2 L Lauria-Berani medium and 50 μg kanamycin ml $^{-1}$ and were grown at 37°C for approximately 4 h at 220 r.p.m. ($O.D_{600}$ =0.6-0.8). Protein expression was induced by the addition of IPTG (0.5 mM final) and continually shaken at 220 r.p.m. for an additional 16-19 h at 20°C. Bacterial cultures were harvested by centrifugation and the resulting cell pellets were resuspended in a lysis buffer (50mM NaH_2PO_4, 200mM NaCl, pH 7.8). Cells were lysed by way of sonication on ice 60 times for 10 s (Fisher Scientific Model FB505; Thermo Fisher Scientific, Waltham, MA). In order to remove unwanted cellular debris and insoluble protein, the lysed cells were spun down at 16000 r.p.m. for 1 h at 10°C. The supernantant, containing the expressed recombinant enzyme with a N-terminal His_6 tag, was purified using Ni Sepharose resin affinity chromatography column (GE

Healthcare, USA). Protein was eluted using 50 mM NaH_2PO_4, 200 mM NaCl, pH 7.8 and 500 mM Imidazole. The purified protein was concentrated and introduced to a new buffer condition (20 mM Tris-HCl, pH 8, 30 mM NaCl) through centrifugal filtration. Purity was evaluated by SDS-PAGE and the resulting protein bands indicate both a high grade of purity and the appropriate molecular weight for NphB. A Bradford assay was conducted to conclude a final enzyme concentration using BSA as a standard.

Site-directed mutagenesis. The plasmids containing the mutated NphB (M106V, M106V/F123V) were constructed by Genescript in a pET-28a vector. Each mutant protein contained an N-terminal His_6 and were expressed and purified identically to the wild type NphB.

***In vitro* Activity Assays**

Analytical Assays. NphB analytical reactions were performed in a final volume of 20ul, consisting of 1.2mM pyrophosphate analogues, 1mM sulfabenzamide (Sigma-Aldrich) or 1,6 Dihydroxy Napthalene and 6uM purified NphB in a reaction buffer (25 mM Tris buffer pH 8.0, 5 mM $MgCl_2$, 50 mM KCl) and incubated at 35 °C for 16 h. Reactions were terminated through cold methanol quenching followed by centrifugation (10,000 g for 30min) to remove precipitated protein. Reaction analysis was completed on RP-HPLC using method A (general method). NphB large scale reactions were conducted in a volume of 1.2ml or 10ml consisting of 4.16mM pyrophosphate analogues, 6mM sulfabenzamide and 0.3mM purified NphB in reaction buffer. Putative products were subsequently isolated by semi-prep HPLC through method B and confirmed by NMR and HRMS with positive (+) and/or negative (-) mode.

HPLC and NMR methods. HPLC was accomplished using Agilent 1220 system equipped with a DAD detector. **Method A (HPLC):** To monitor NphB reactions, analytical reverse-phase (RP) HPLC employed a Gemini-NX, C-18 (5 μm, 4.6 mm × 250 mm) column (Phenomenex, Torrance, California, USA) [gradient of 1% B to 10% B over 10 min, 10% B to 50% B over 5 min, 50% B to 100% B for 12 min, 100% B to 1% B over 1 min, 1% B for 7 min (A = ddH_2O with 0.1% TFA; B = acetonitrile) flow rate = 1 mL min^{-1}; $A_{254/235}$]. The reaction was monitored by the retention time difference between starting material and product. **Method B (HPLC):** Semi-preparative RP HPLC was conducted on a Gemini-NX, C-18 (5 μm, 10 × 250 mm) column (Phenomenex, Torrance, California, USA) to purify the Sulfabenzamide analogues [gradient of 1% B to 10% B over 10 min, 10% B to 50% B over 5 min, 50% B to 100% B for 12 min, 100% B to 1% B over 1 min, 1% B for 7 min (A = ddH_2O with 0.1% TFA; B = acetonitrile) flow rate = 2 mL min^{-1}; A_{254}]. High-resolution mass spectrometric (HRMS) data and liquid chromatography mass spectrometric (LCMS) were obtained on Agilent 6545-QTOF W/1290 HPLC mass spectrometer at the University of Oklahoma, Department of Chemistry and Biochemistry. NMR spectra were obtained on Varian VNMRS 500 MHz instruments at the NMR facility of the Department of Chemistry and Biochemistry of University at the Oklahoma using 99.9% DMSO-d6 with 0.05% v/v TMS. ^{1}H, ^{13}C and ^{31}P chemical shifts were referenced to internal solvent resonances. Multiplicities are indicated by s (singlet), d (doublet), t (triplet), q (quartet), quin (quintet), m (multiplet), and br (broad). Chemical shifts are reported in parts per million (ppm) and coupling constants *J* are given in Hz. All NMR spectra were recorded at ambient temperature and processed using MestReNova software.

*Kinetic characterization sulfabenzamide derivatives for NphB and NphB mutants***.** Specific kinetic measurements involving NphB mutants, sulfabenzamide and GPP were accomplished by monitoring product formation on HPLC (254nm). Reactions took place in 20ul total volume, including 2mM sulfabenzamide, appropriate amount of NphB and various concentrations of GPP (0.05 – 5mM) in a reaction buffer (25 mM Tris buffer pH 8.0, 5 mM $MgCl_2$, 50 mM KCl), The reactions were performed at 35°C and were stopped by the addition of 30ul cold methanol. Each reaction was conducted in triplicate and optimized through enzyme concentration and reaction time to ensure analysis in the linear range. Specific kinetic constants, K_m and k_{cat} were determined by fitting the data to the Michaelis-Menten equations using non-linear regression analysis provided by Prism 5.04 (GraphPad Software, Inc. La Jolla, CA 92037 USA)

Chapter 5. Biocatalytic applications of prenyltransferases in drug diversification: A proof-of-concept study using FDA approved antibiotic, daptomycin

Introduction

Daptomycin is produced in *Streptomyces roseosporus* as a nonribosomally assembled lipopeptide and belonging to the group of calcium-dependent antibiotics. [101-103] Daptomycin was first discovered in 1980 and has been an FDA approved pharmaceutical since 2003 to treat skin infections caused by gram-positive bacteria *S. aureus*, *Streptococcus pyogenes*, *Streptococcus agalactiae*, *Streptococcus dysgalactiae* as well as *E. faecalis* and in 2006 it was approved for non-topical treatment of bacteraemia and endocarditis caused by MSSA and MRSA. [104-110] Additionally, daptomycin has rapid bactericidal activity against many resistant gram-positive organisms including penicillin-, vancomycin-, and methicillin- resistant bacteria making dapyomycin a first-line drug of last resort.[111, 112] Notably, daptomycin cannot be used to treat pneumonia and raspatory infections due to inactivation by the pulmonary surfactant. [113] The structure of daptomycin is made up of 13 amino acids, six of which are non-standard including B-Asn, ornithine (Orn), D-Ala, D-Ser, (2S, 3R)-methylglutamate (MeGlu) and kynurenine (Kyn). The macrocylic core contains 10 amino acids and a ring-closing ester bond between the C-terminal end of Kyn and the side chain of Thr. The exocyclic portion of daptomycin protrudes from the ring and features a distinct acyl chain attached to Trp. (Figure 30). [103] The exact daptomycin-mediated bactericidal mechanism remains poorly understood and highly speculative. To date it has been suggested that the mode of action involves the interaction between

the gram-positive cell membrane and daptomycin, potentially involving insertion into the cell membrane in a Ca^{2+} - dependent action, generating pores and leading to overall membrane depolarization and cell death. It is believed that the pore formation is dependent upon the development of daptomycin aggregates facilitated by free Ca^{2+} . [114-117] However, the studies that reported these conclusions were all performed at concentrations much greater than the reported MIC values. It can therefore be speculated that these events could not perceivably take place *in vivo.* Additionally, it has been proposed that daptomycin inhibits peptidoglycan and/or lipoteichoic acid synthesis within the cell although the mechanism is also not understood. Although bacterial resistance remains uncommon, resistance in *S. aureus, E. faecium* and *E. faecalis* are appearing during treatment with increasing frequency. [118-120] The exact mechanism of resistance remains unresolved; however, it has been proposed that daptomycin resistance in *S. aureus* could be mediated by increasing the overall positive charge of the surface of the cell instigating an electrostatic repulsion of the daptomycin-Ca^{2+} complex. The rise in cases of resistant strains prompts interest in developing new daptomycin derivatives to further investigate the mechanism of action as well developing new drug analogues with increased antibiotic activity. Many strategies have been implemented to developed daptomycin analogues including total chemical synthesis, chemoenzymatic synthesis and solid phase approaches, focusing on the alteration of amino acids, acyl chain length and ornithine derivatives. [101, 121-132] In order to generate daptomycin derivatives and maintain the overall potent scaffold of the molecule, we propose to employ a decorator enzyme to perform late-stage modification the natural product. In this study we will use the aromatic prenyltransferase CdpNPT

from *Aspergill fumigatus* to generate alkyl diversified Trp of daptomycin and evaluate the antibacterial properties.

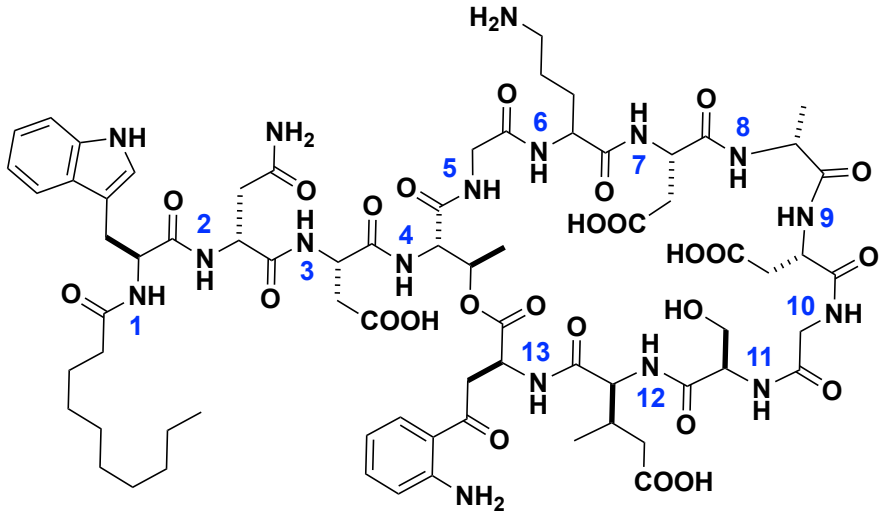


Figure 30. Daptomycin structure
The structure of daptomycin comprised of 13 (numbered in blue) amino acids.

Research Objectives

In this study we sought to test the capability of producing daptomycin derivatives using chemoenzymatic methodology. Specifically, we utilized indole prenyltransferase CdpNPT, known to accept daptomycin as a substrate, to generate daptomycin analogues substituted with diverse alkyl moieties[40]. CdpNPT was found to catalytically transfer alkyl groups onto the N1, C2, C5 or C6 position of the tryptophan residue of daptomycin. The structural analysis and subsequent *in vitro* biological activity assays revealed a SAR in daptomycin susceptible and resistant strains yielding high improvements in the MIC values for some of daptomycin derivatives.

Contributions

Syntheses of alkyl pyrophosphates were carried out by Dr. Chandrasekhar Bandari, Tejaswi Bavineni, Johanna Masterson, Rachel Tran, and Eric Gardner. Large-scale

enzymatic reaction and purification of daptomycin analogs were carried out in part by Dr. Singh, Dr. Bandari and me. NMR data collection of daptomycin analogs was done at NMRFAM (Madison, WI) by Dr. Marco Tonelli, NMR data analysis and structural characterization was performed by Dr. Singh, and reconfirmation of NMR assignments was performed by Eric Gardner. Cytotoxicity assay was carried out by Dr. JianLan You. I carried out the expression, purification of CdpNPT, RP-HPLC based assessment, antibacterial activity assays, and calculation of LogP values. Most of the contents in this chapter including text, tables and figures will be directly used for the publication in a peer-reviewed journal.

Results and discussion

Assaying the alkyl pyrophosphate substrate tolerance of CdpNPT to construct daptomycin analogues.

To explore the ability of CdpNPT to catalyze the differential alkylation of daptomycin, we synthesized a 71-member alkyl pyrophosphate donor library (Figure 31). Specifically, the alkyl pyrophosphate library includes various carbon chain length (C_3-C_{15}), benzylic analogues, heterocylic analogues, as well as pyrophosphate analogues with chemoselective components such as azides and alkynes. For the assay, recombinant CdpNPT was expressed and soluble in *E. coli* containing a N-terminal His_6 tag and cultured in a total of 4L and purified by Ni-NTA affinity chromatography resulting in a yield of 48.5 mg mL^{-1}. Assaying CdpNPT mediated daptomycin alkylation revealed the successful transfer of 37 pyrophosphate analogues, including the previously determined DMAPP, onto daptomycin (Figure 29).[40] Remarkably, the conversion to alkylated daptomycin was >20% for 33 alkyl analogues and >50% for 13

alkyl analogues. Overall, we were able to enzymatically produce daptomycin derivatives featuring DMAPP analogues (**S3-S9, S13-S15, S17-21**), cinnamyl analogues (**S25-S27**), GPP analogues (**S32, S34, S38**), benzyl analogues (**S40-S42, S44-S46, S50**), heterocycle analogue (**S53, S54, S57, S58, S60**), and chemoselective analogues with azido (**S62**) and akyne groups (**S67, S70**). Several reactions indicated the formation of multiple product isomers, corresponding to different retention times upon HPLC analysis, with some reactions displaying as many 4 distinct product peaks (Figure 32). In all cases, product formation of daptomycin derivatives was verified through HPLC and high-resolution LC-MS (Table 8).

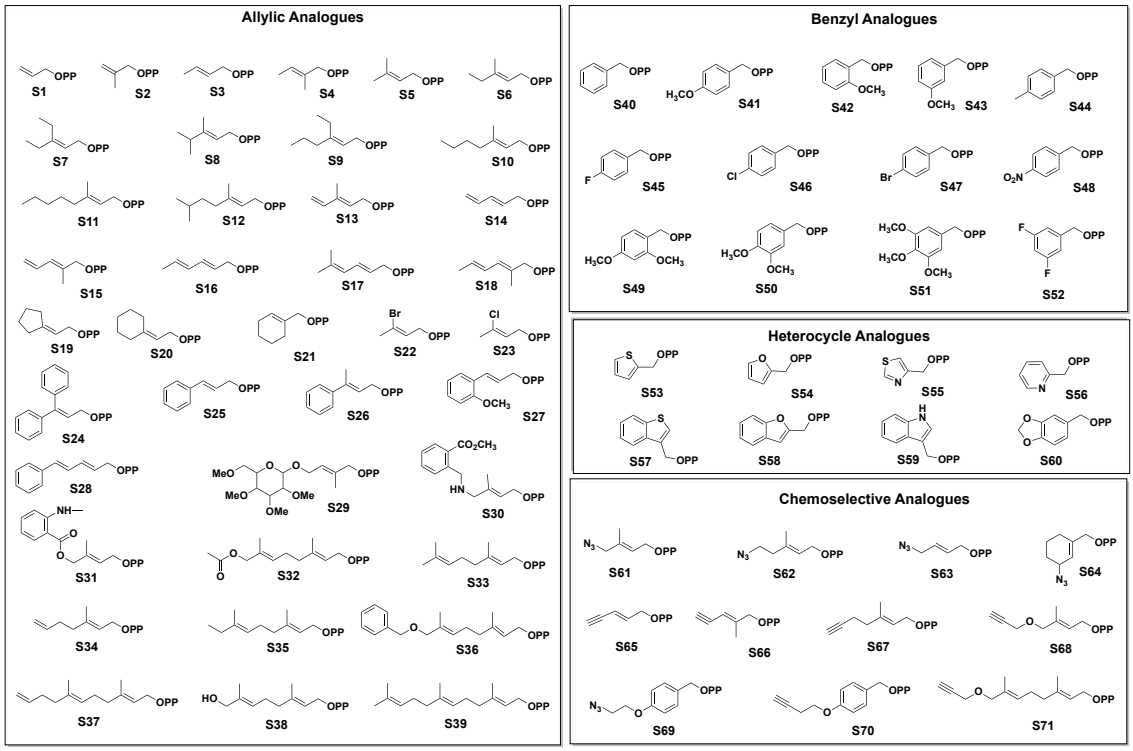


Figure 31. Synthetic alkyl pyrophosphate library

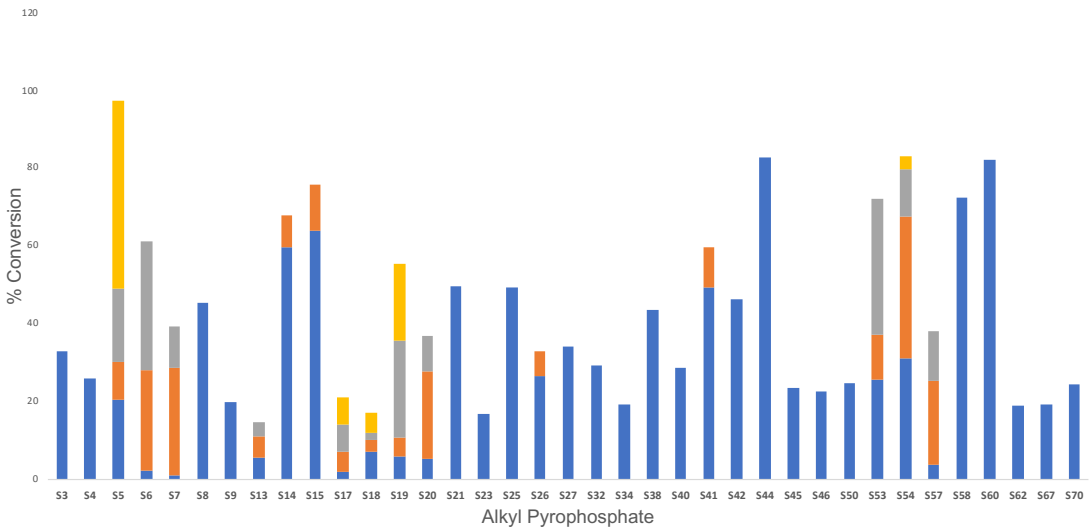
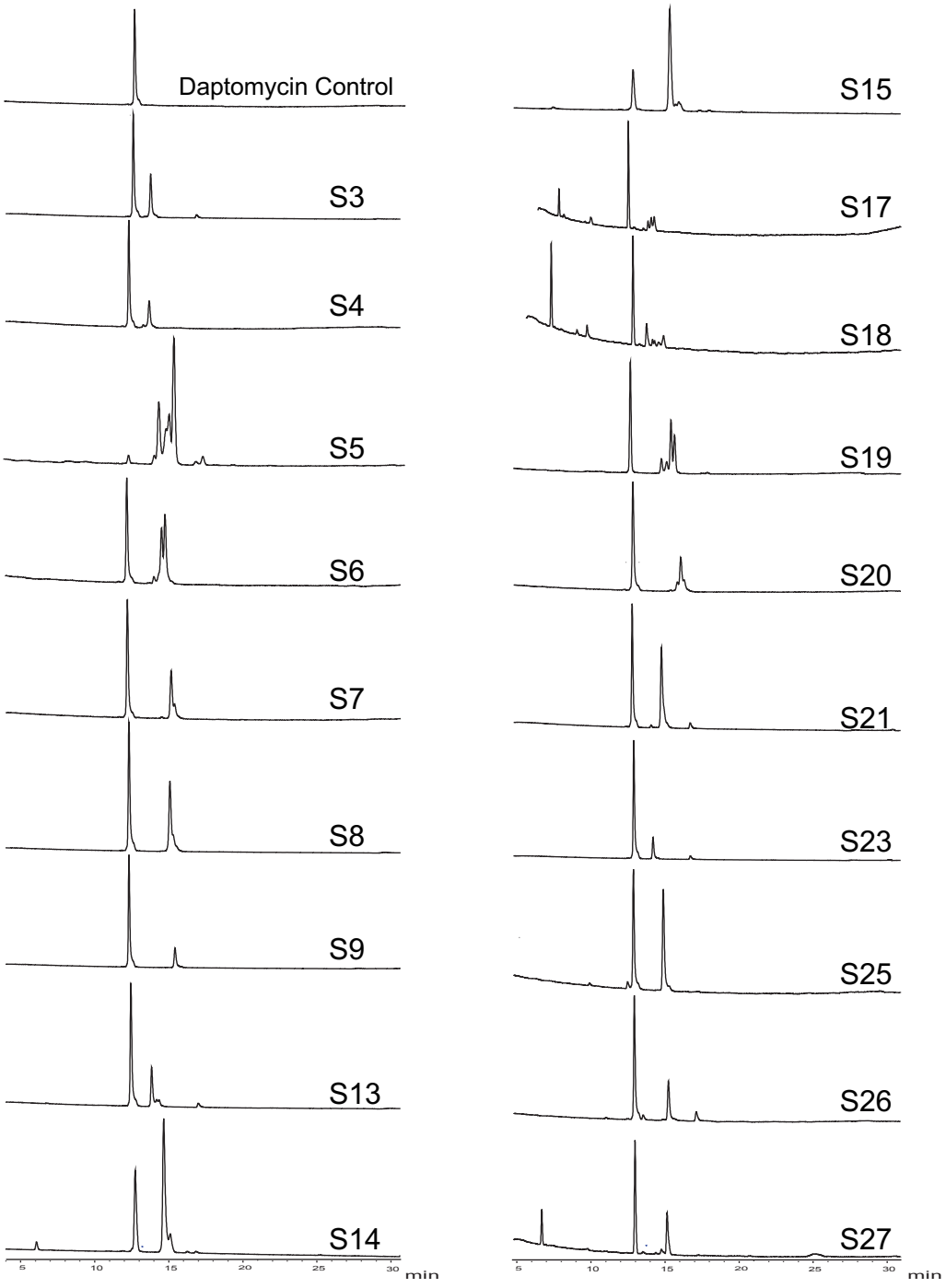


Figure 32. Percent Conversion Daptomycin analogues using CdpNPT
The percent conversion of alkyl-pyrophosphate analogues with daptomycin catalyzed by CdpNPT under standard conditions based upon RP-HPLC. The blue, orange, grey and yellow colors correspond to different product peaks as seen on the RP-HPLC chromatogram, Reactions were performed with 1.2 mM alkyl-pyrophosphate analogue, 1 mM daptomycin, CdpNPT, 25 mM Tris, 5 mM $CaCl_2$, 50 mM KCl, pH 7.5, 16 h at 35 °C. No product formation was observed in the absence of CdpNPT or alkyl-pyrophosphate analogue.


Daptomycin Control
S3
S4
S5
S6
S7
S8
S9
S13
S14
S15
S17
S18
S19
S20
S21
S23
S25
S26
S27
5
10
15
20
25
30
min

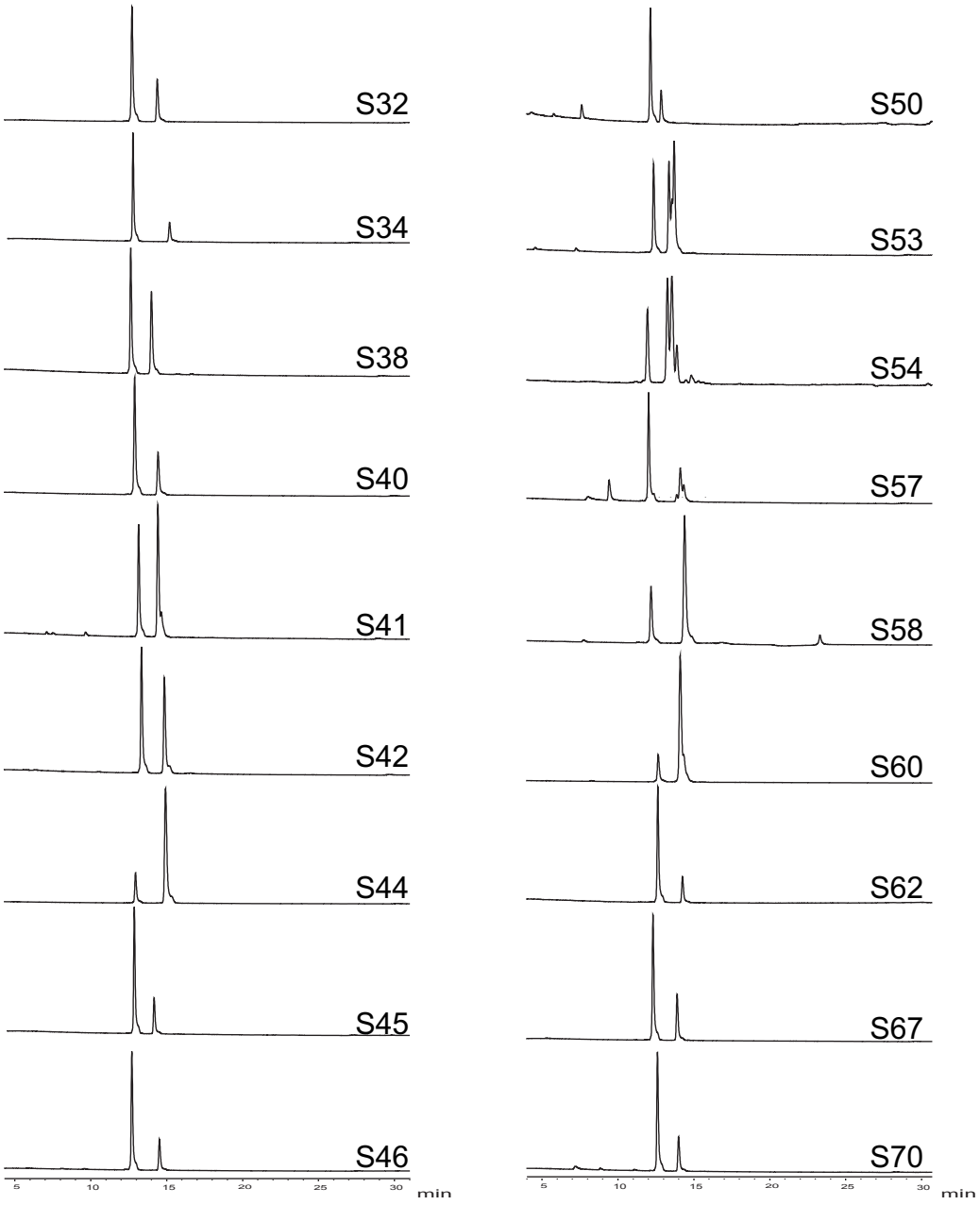


Figure 33. HPLC chromatograms
HPLC chromatograms of the CdpNPT catalyzed reaction using synthetic alkyl pyrophosphate library with daptomycin. Reactions were analyzed after incubation understand conditions for 16hrs at 35℃

Table 8 HRMS analytical scale daptomycin analogues

Enzyme Product	Chemical Formula $[M+H]^+$	Calculated Mass	Observed Mass	Retention Time (mins)
S3-DAP	$C_{76}H_{108}N_{17}O_{26}$	1674.7646	1674.7670*	4.499
S4-DAP	$C_{77}H_{109}N_{17}O_{26}$	1687.7724	1688.7753*	4.610
S5-DAP	$C_{77}H_{110}N_{17}O_{26}$	1688.7802	1688.7813a*	4.424
	$C_{77}H_{110}N_{17}O_{26}$	1688.7802	1688.7824b*	4.49
	$C_{77}H_{110}N_{17}O_{26}$	1688.7802	1688.7818c*	4.722
	$C_{82}H_{118}N_{17}O_{26}$	1756.8428	1756.8416d#	4.722
S6-DAP	$C_{78}H_{112}N_{17}O_{26}$	1702.7959	1702.7978a*	4.641
	$C_{78}H_{112}N_{17}O_{26}$	1702.7959	1702.7973b*	4.79
S7-DAP	$C_{79}H_{114}N_{17}O_{26}$	1716.8115	1716.8121*	4.852
S8-DAP	$C_{79}H_{113}N_{17}O_{26}$	1716.8115	1716.8091*	4.783
S9-DAP	$C_{80}H_{115}N_{17}O_{26}$	1730.8272	1730.8261*	4.780
S13-DAP	$C_{78}H_{109}N_{17}O_{26}$	1699.7724	1700.7802	4.508
S14-DAP	$C_{77}H_{108}N_{17}O_{26}$	1686.7646	1686.7638a*	4.564
	$C_{82}H_{114}N_{17}O_{26}$	1752.8115	1752.8094b#	4.713
S15-DAP	$C_{78}H_{110}N_{17}O_{26}$	1700.7802	1700.7830a*	4.431
	$C_{78}H_{110}N_{17}O_{26}$	1700.7802	1700.7823b*	4.762
S17-DAP	$C_{79}H_{113}N_{17}O_{26}$ $[M+2H]^{2+}$	857.9016	857.9004*	4.688
S18-DAP	$C_{79}H_{112}N_{17}O_{26}$	1714.7959	1714.7982a*	4.578
	$C_{79}H_{112}N_{17}O_{26}$	1714.7959	1714.7984b*	4.752
S19-DAP	$C_{79}H_{112}N_{17}O_{26}$	1714.7959	1714.7935	4.750
S20-DAP	$C_{80}H_{114}N_{17}O_{26}$	1728.8115	1728.8111*	4.835
S21-DAP	$C_{79}H_{112}N_{17}O_{26}$	1714.7959	1714.7970a*	4.538
	$C_{79}H_{112}N_{17}O_{26}$	1714.7959	1714.7995b*	4.669
	$C_{79}H_{112}N_{17}O_{26}$	1714.7959	1714.7986c*	4.794
S25-DAP	$C_{81}H_{110}N_{17}O_{26}$	1736.7802	1736.7806*	4.706
S26-DAP	$C_{82}H_{112}N_{17}O_{26}$	1750.7959	1750.7978*	4.734
S27-DAP	$C_{82}H_{112}N_{17}O_{27}$	1766.7908	1766.7914*	4.366
S34-DAP	$C_{80}H_{113}N_{17}O_{26}$	1728.8115	1728.8067*	4.756
S38-DAP	$C_{82}H_{118}N_{17}O_{27}$	1773.8456	1773.8328	4.521
S40-DAP	$C_{79}H_{107}N_{17}O_{26}$	1710.7646	1710.7569*	4.536
S41-DAP	$C_{80}H_{110}N_{17}O_{27}$	1740.7752	1740.7767a*	4.41
	$C_{80}H_{110}N_{17}O_{27}$	1740.7752	1740.7749b*	4.617
S42-DAP	$C_{80}H_{110}N_{17}O_{27}$	1740.7752	1740.7669*	4.565
S44-DAP	$C_{80}H_{110}N_{17}O_{26}$	1724.7802	1724.7731*	4.687
S45-DAP	$C_{79}H_{106}FN_{17}O_{26}$	1728.7552	1728.7498*	4.517
S50-DAP	$C_{81}H_{111}N_{17}O_{28}$	1770.7857	1770.7799*	4.230
S54-DAP	$C_{77}H_{105}N_{17}O_{27}$	1700.7439	1700.7363	4.414
S57-DAP	$C_{81}H_{107}N_{17}O_{26}S$	1766.7367	1766.7290*	4.730

S58-DAP	$C_{81}H_{107}N_{17}O_{27}$	1750.7595	1750.7522*	4.708
S60-DAP	$C_{80}H_{107}N_{17}O_{28}$	1754.7544	1754.7481*	4.459
S62-DAP	$C_{78}H_{111}N_{20}O_{26}$	1743.7973	1743.7892*	4.621

Derivatization and determination of bioactivity of daptomycin.

The analytical reactions described above suggest CdpNPT is a permissive and effective alkylation catalyst towards daptomycin, which lead us into the investigation of antibacterial potency of the daptomycin analogues. Therefore, to explore the significance of the derivatization of daptomycin we carried out semi preparative-scale reactions involving 10 alkyl pyrophosphates (**S5, S6, S7, S14, S15, S18, S20, S21, S25, S41**). The reactions were purified using reverse phase HPLC where each product peak was separated based on retention times. The resulting purified products were subjected to ESI-HMRS and NMR analysis for structure elucidation (Table 8; Figure 35). NMR analysis confirmed N and C alkylation was performed solely on the tryptophan residue of daptomycin, as previously reported.[40] Additionally, several regio- and structural isomers were identified amongst the purified compounds, some of which were inseparable isomeric mixtures. Ultimately, the semi-preparative purification resulted in 16 distinct daptomycin analogues (**DAP1-DAP16**) involving N1, C2, C5, C6 alkylation of the indole ring (Figure 34 and 37).

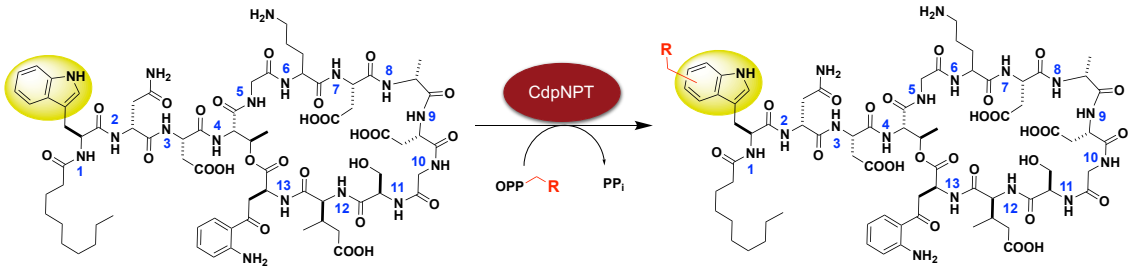


Figure 34. CdpNPT catalyzed reaction producing daptomycin derivatives
CdpNPT catalyzes the alkylation of daptomycin by diversifying the tryptophan (colored yellow) found on the exocycle portion of the compound

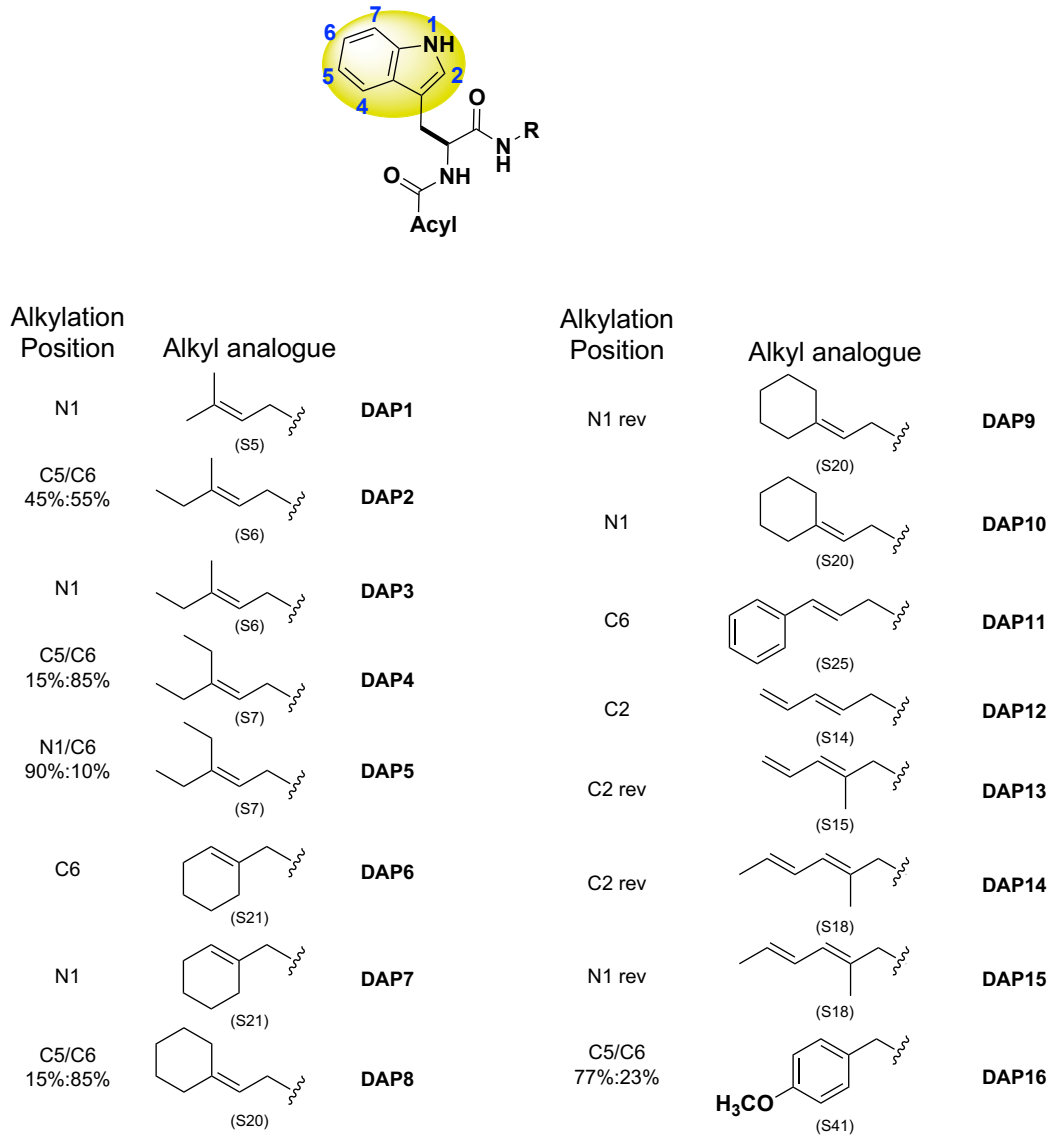


Figure 35. Daptomycin derivatives and placement on the indole ring.
Shown are the 16 different structurally elucidated daptomycin derivatives. Placement on the tryptophan was determined through H^1 and 2D NMR analysis. In some cases, an inseparable mixture of isomers was found.

Table 9. HRMS data of purified alkyl daptomycin analogues

Enzyme Product	Chemical Formula	Calculated Mass	Observed Mass
***N*1-S5-DAP**	$C_{77}H_{108}N_{17}O_{26}$ $[M-H]^-$	1686.7651	1686.7659
***N*1-S6-DAP**	$C_{78}H_{110}N_{17}O_{26}$ $[M-H]^-$	1700.7808	1700.7818
***C*5-S6-DAP: *C*6-S6-DAP**	$C_{78}H_{110}N_{17}O_{26}$ $[M-H]^-$	1700.7808	1700.7816*
***N*1-S7-DAP: *C*6-S7-DAP**	$C_{79}H_{112}N_{17}O_{26}$ $[M-H]^-$	1714.7964	1714.7978*
***C*5-S7-DAP: *C*6-S7-DAP**	$C_{79}H_{112}N_{17}O_{26}$ $[M-H]^-$	1714.7964	1714.7979*
***N*1-S21-DAP**	$C_{79}H_{112}N_{17}O_{26}$ $[M+H]^+$	1714.7964	1714.7970
***C*6-S21-DAP**	$C_{79}H_{112}N_{17}O_{26}$ $[M+H]^+$	1714.7964	1714.7995
***N*1^R-S20-DAP**	$C_{80}H_{112}N_{17}O_{26}$ $[M-H]^-$	1726.7964	1726.7957
***N*1-S20-DAP**	$C_{80}H_{112}N_{17}O_{26}$ $[M-H]^-$	1726.7964	1726.7956
***C*5-S20-DAP:*C*6-S20-DAP**	$C_{80}H_{114}N_{17}O_{26}$ $[M+H]^+$	1728.8121	1728.8111*
***C*6-S25-DAP**	$C_{81}H_{108}N_{17}O_{26}$ $[M-H]^-$	1734.7651	1734.7659
***C*2-S14-DAP**	$C_{77}H_{108}N_{17}O_{26}$ $[M+H]^+$	1686.7651	1686.7638
***C*2^R-S15-DAP**	$C_{78}H_{108}N_{17}O_{26}$ $[M-H]^-$	1698.7651	1698.7605
***N*1^R-S18-DAP**	$C_{79}H_{110}N_{17}O_{26}$ $[M-H]^-$	1712.7808	1712.7814
***C*2^R-S18-DAP**	$C_{79}H_{110}N_{17}O_{26}$ $[M-H]^-$	1712.7808	1712.7800
***C*5-S41-DAP: *C*6-S41-DAP**	$C_{80}H_{108}N_{17}O_{27}$ $[M-H]^-$	1738.7601	1738.7578*
DAP	$C_{72}H_{102}N_{17}O_{26}$ $[M+H]^+$	1620.7182	1620.7177

*Inseparable mixture of isomers.

DAP1-DA16 were evaluated for antibacterial activity against 4 bacterial species, *Staphylococcus aureus, Bacillus subtillis*, *Enterococcus faecalis* and *Staphylococcus epidermidis,* including 12 clinical isolates using the micro dilution method (see experimental methods) (Table 10). To assess the possibility of improved antibiotic susceptibility using daptomycin derivatives, three daptomycin resistant strains were also tested, two transposon mutants, *S. aureus* (SAUSA300 1713 NE573, SAUSA300 1715 NE1656) as well as hospital acquired *E. faecalis* S712. *S. aureus* ATCC 25923 was used as a quality control strain and tested with daptomycin to ensure proper techniques and analysis. The MIC value for the parent compound was 0.6 μg ml^{-1} as recommended by the CLSI and FDA (0.12-1.0 μg mL^{-1}). [133, 134] In order to gauge the relative

antibiotic activity, daptomycin was also evaluated against all strains used in this study and compared against MICs for derivatives (Figure 36). Daptomycin showed an MIC range of 0.3-16.2μg mL^{-1} against the clinical isolates, not including daptomycin resistant strains. For the daptomycin resistant strains, the parent compound displayed an MIC range 16.2->32.4μg mL^{-1}, consistent with the noted high resistance. C-2 substituted compounds, such as **DAP12**, **DAP13** and **DAP14** display the lowest antibacterial activity with MICs ranging from 4.2 - >33.7μg mL^{-1} , 4.2 – >34.0μg mL^{-1} and 2.1 - > 34.3 μg mL^{-1}, respectively. Amongst the compounds with highest antibacterial activity are C5 and C6 substituted, including **DAP2**, **DAP4**, **DAP5**, **DAP6**, and **DAP8** with MICs ranging from 0.1-8.5μg mL^{-1}, 0.5-2.7μg mL^{-1}, 0.3-4.3μg mL^{-1}, 0.1- 6.2μg mL^{-1}, and 0.2-2.2μg mL^{-1}, respectively (Table 10). Interestingly, **DAP6** and **DAP7** are both substituted with alkyl analogue S21 at different positions on the indole ring. **DAP6**, a C6 substituted compound, displayed up to an 80-fold MIC improvement compared to N1 substituted **DAP7**. To assess the effect of the lipophilicity of each derivative towards the antibacterial activity, logP values of daptomycin and **DAP1-DAP16** were plotted against their corresponding MIC relative to daptomycin MIC[135] (Figure 37). As anticipated, the addition of the alkyl group increases the logP value from -0.47 (daptomycin) to 0.25 (**DAP11**). A correlation between increasing logP values of the daptomycin derivatives and overall MIC improvement is most strongly seen with *E. faecalis* S613 and daptomycin resistant strains. **DAP2**, **DAP4**, **DAP6** and **DAP8** display an impressive 15 – 80-fold improvement over the parent compound. As seen in the LogP correlation plots, LogP values are a characteristic of both the alkyl group as well as the position on the indole ring (Figure 37). C-2 substituted analogues

exhibit the lowest logP values (-0.2 – -0.1) while C-5 and C-6 gave rise to the highest logP values (-0.17 – 0.25). A comparison of MIC and logP for compounds with high logP values (0.0 – 0.25), such as **DAP11**, **DAP8**, **DAP16**, and **DAP4,** did not show any direct correlation. However, when tested with the resistant strains **DAP16** and **DAP11** had lower improvement despite being C-5/C-6 substituted with logP values similar to the most effective analogues. Overall, the properties of the alkyl group and the alkylation position on the indole ring influences the antibacterial activity of the daptomycin derivatives. These results imply the aromatic moiety could potentially be contributing to the bioactivity of these compounds. Notably, the bacterial strains respond differently to the DAP analogues either indicating a different mechanism of action or a different cellular environment.

Table 10. In-vitro MIC (μg mL^{-1}) values for Daptomycin and daptomycin derivatives.

MIC (μg mL^{-1}) values for Daptomycin and Daptomycin derivatives	**DAP**	**DAP1 Trp-N1-S5**	**DAP2 Trp-C5/C6-S6 (45%:55%)**	**DAP3 Trp-N1-S6**	**DAP4 Trp-C5/C6-S7 (15%:85%)**	**DAP5 Trp-N1/C6-S7 (90%:10%)**	**DAP6 Trp-C6-S21**	**DAP7 Trp-N1-S21**	**DAP8 Trp-C5/C6 (15%:85%)**
S. aureus (ATCC 25923)	0.6	0.5	0.2	0.7	1.1	0.5	0.1	1.1	0.2
S. aureus (MRSA, ATCC 700787)	0.6	0.7	2.1	1.2	2.7	1.4	2.1	2.7	2.2
S. epidermidis (ATCC 12228)	0.3	0.5	0.5	1.2	0.5	0.5	0.5	1.1	0.5
E. faecalis (hVRE, ATCC 700802)	1.5	2.1	0.1	0.2	0.5	1.1	0.3	1.1	0.5
B. subtilis (ATCC 6051)	2.0	8.4	2.1	2.1	1.1	2.7	2.1	2.1	2.2
S. aureus (hVISA, SR220)	4.0	0.5	0.5	0.5	1.1	0.5	0.5	2.1	0.6
S. aureus (SR1129)	2.0	0.3	0.5	0.3	0.7	0.3	0.3	1.4	0.3
S. aureus (SR2609)	4.0	2.1	0.3	0.3	1.1	0.3	0.3	2.1	0.6
S. aureus (SR2852)	2.0	2.1	0.5	2.1	0.7	0.5	0.2	1.4	0.6
S. aureus (hVISA, SR3777)	2.0	2.1	0.5	2.1	1.1	0.5	0.2	1.4	1.1
S. aureus (hVISA, SR4035)	8.1	4.2	1.4	4.3	2.1	2.1	1.1	8.6	2.2
E. faecalis (S613)	16.2	4.2	1.1	1.1	0.5	0.5	0.4	17.1	0.3
E. faecalis (**DapR**, S712)	>32.4	33.7	8.5	17.0	2.1	4.3	6.2	>17.1	2.2
S. aureus (**DapR**, SAUSA300_1713 NE573)	16.2	4.2	0.5	2.1	0.5	2.1	0.4	17.1	0.5
S. aureus (**DapR**, SAUSA300_1715 NE1656)	16.2	4.2	0.5	2.1	0.5	0.5	0.2	17.1	0.5

MIC (μg mL^{-1}) values for Daptomycin and Daptomycin derivatives	**DAP9 Trp-N1rev-S20**	**DAP10 Trp-N1-S20**	**DAP11 Trp-C6-S25**	**DAP12 Trp-C2-S14**	**DAP13 Trp-C2rev-S15**	**DAP14 Trp-C2rev-S18**	**DAP15 Trp-N1rev-S18**	**DAP16 Trp-C5/C6-S41 (77%:23%)**
S. aureus (ATCC 25923)	0.5	0.5	2.8	16.9	8.5	>34.3	17.1	0.3
S. aureus (MRSA, ATCC 700787)	2.8	2.8	2.4	>33.7	>34.0	>34.3	4.3	0.3
S. epidermidis (ATCC 12228)	1.1	0.7	1.1	16.9	8.5	34.3	1.1	0.4
E. faecalis (hVRE, ATCC 700802)	0.5	0.3	0.5	33.7	8.5	34.3	0.5	1.4
B. subtilis (ATCC 6051)	2.8	2.2	2.8	4.2	4.2	8.6	2.1	2.2
S. aureus (hVISA, SR220)	1.1	1.1	1.1	33.7	17.0	>34.3	1.1	0.6
S. aureus (SR1129)	0.6	0.6	1.1	16.9	8.5	34.3	1.4	0.6
S. aureus (SR2609)	0.6	0.6	1.1	16.9	8.5	34.3	1.1	0.6
S. aureus (SR2852)	1.1	1.1	0.7	16.9	8.5	34.3	2.1	1.1
S. aureus (hVISA, SR3777)	1.1	0.6	1.1	16.9	8.5	34.3	1.1	2.2
S. aureus (hVISA, SR4035)	2.2	1.4	2.8	>33.7	8.5	2.1	2.7	4.2
E. faecalis (S613)	1.1	1.3	1.1	>8.4	>34.0	>34.3	2.1	1.1
E. faecalis (**DapR**, S712)	17.3	5.2	8.7	>8.4	>34.0	>34.3	17.1	>34.3
S. aureus (**DapR**, SAUSA300_1713 NE573)	2.2	1.3	1.1	>8.4	>34.0	>34.3	2.1	1.1
S. aureus (**DapR**, SAUSA300_1715 NE1656)	2.2	2.6	1.1	>8.4	>34.0	>34.3	2.1	1.1

*All strains were acquired from BPEI Resources

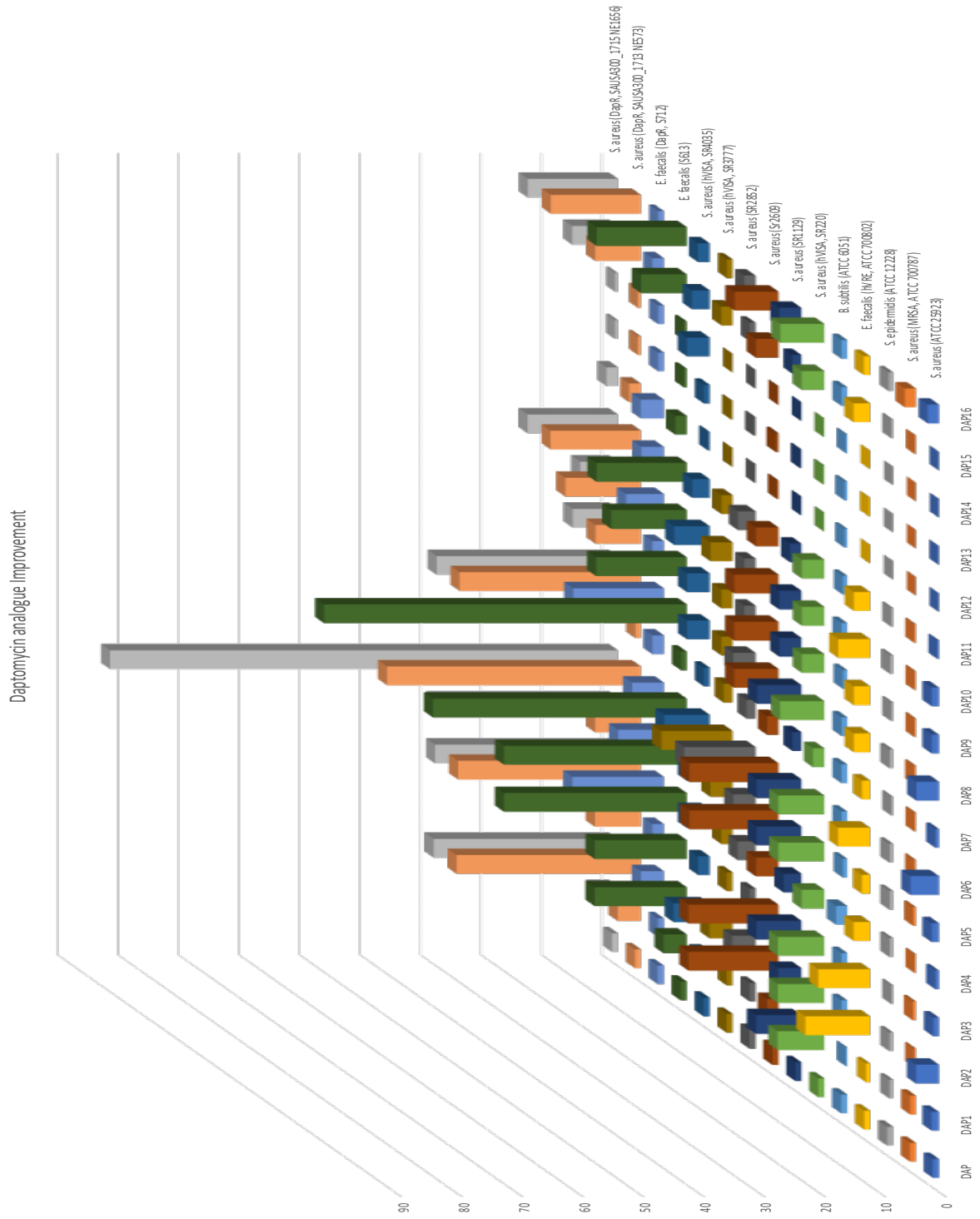
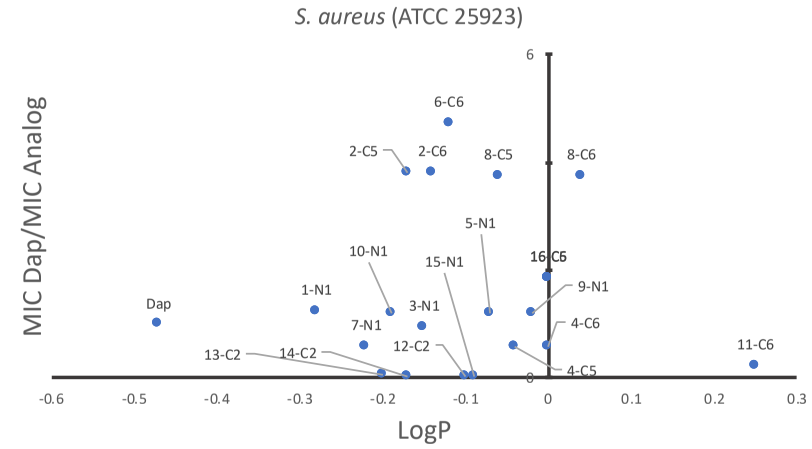
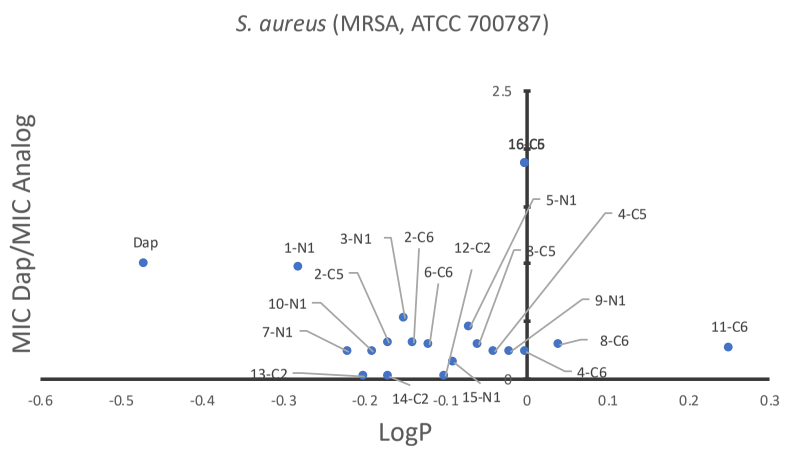


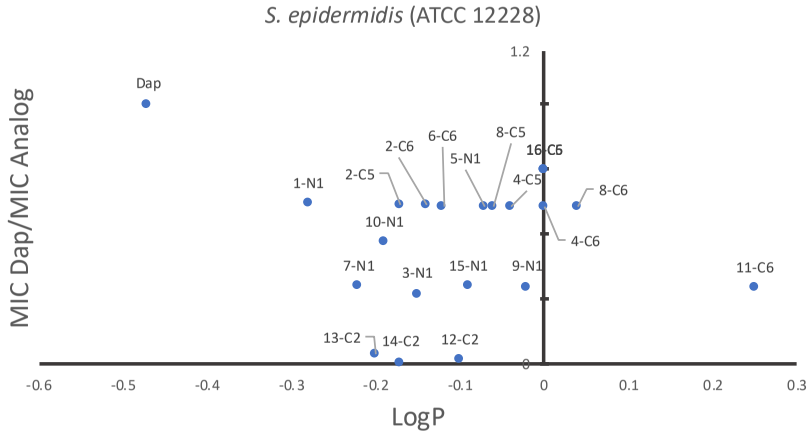
Figure 36. MIC improvement of Daptomycin analogues compared to daptomycin.

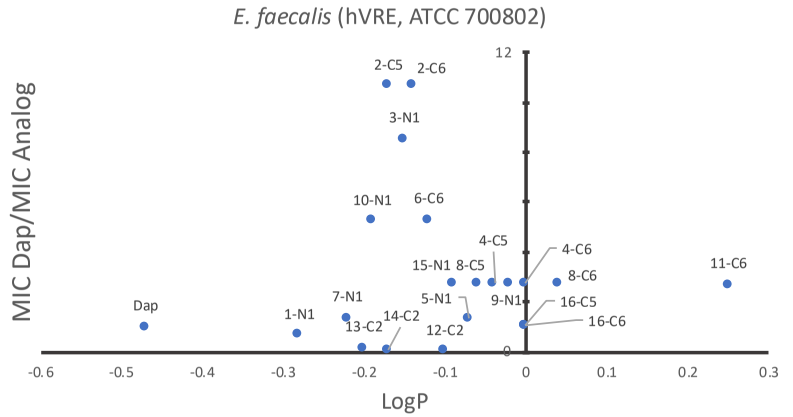
MIC values from daptomycin derivatives were compared to daptomycin for each

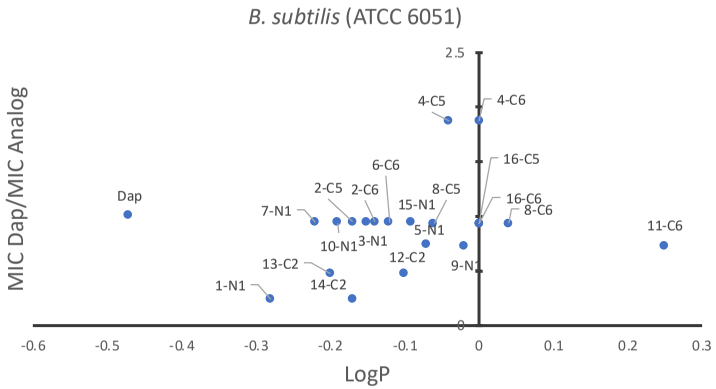
bacterial strain. Fold improvement was found by the ratio of MIC daptomycin/ MIC daptomycin derivatives; MIC values found in ***Table 10.***

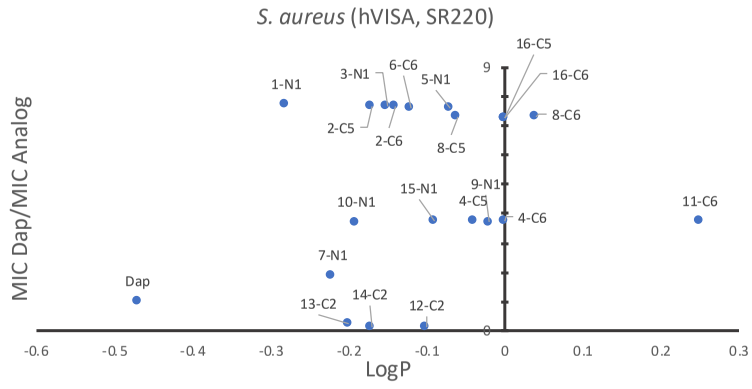

S. aureus (ATCC 25923)
MIC Dap/MIC Analog
LogP
Dap
1-N1
2-C5
2-C6
6-C6
8-C5
8-C6
5-N1
10-N1
15-N1
16-C5
9-N1
3-N1
7-N1
4-C6
12-C2
13-C2
14-C2
4-C5
11-C6

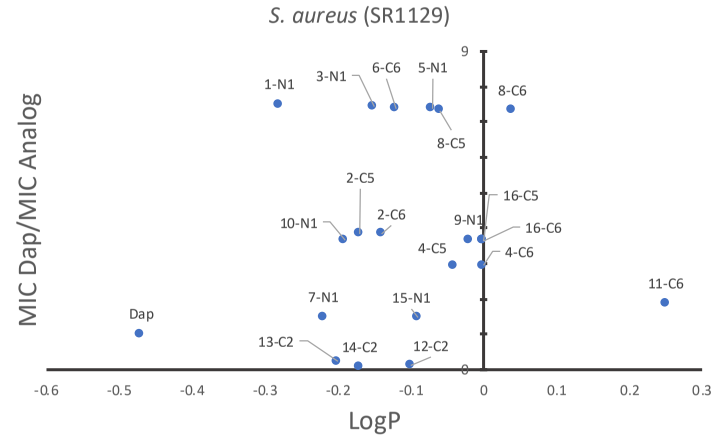

S. aureus (MRSA, ATCC 700787)
MIC Dap/MIC Analog
LogP
Dap
1-N1
2-C5
3-N1
2-C6
6-C6
12-C2
16-C5
5-N1
4-C5
8-C5
10-N1
9-N1
7-N1
8-C6
11-C6
13-C2
14-C2
15-N1
4-C6

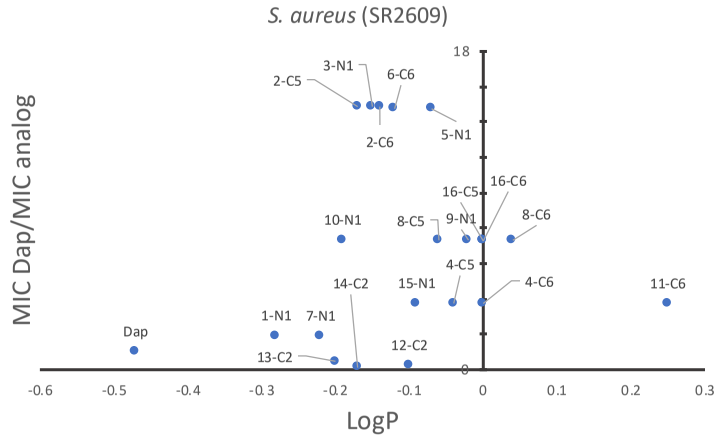

S. epidermidis (ATCC 12228)
MIC Dap/MIC Analog
LogP
Dap
1-N1
2-C5
2-C6
6-C6
8-C5
16-C5
5-N1
4-C5
8-C6
10-N1
4-C6
7-N1
3-N1
15-N1
9-N1
11-C6
13-C2
14-C2
12-C2

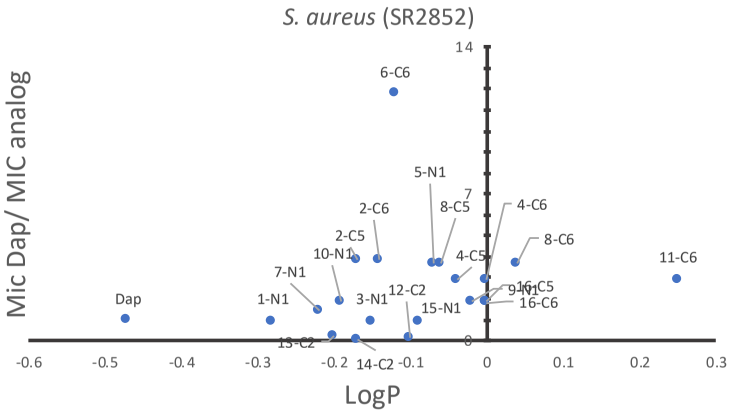

E. faecalis (hVRE, ATCC 700802)
MIC Dap/MIC Analog
LogP
Dap
2-C5
2-C6
3-N1
10-N1
6-C6
4-C5
4-C6
15-N1
8-C5
8-C6
11-C6
7-N1
5-N1
9-N1
16-C5
1-N1
13-C2
14-C2
16-C6
12-C2

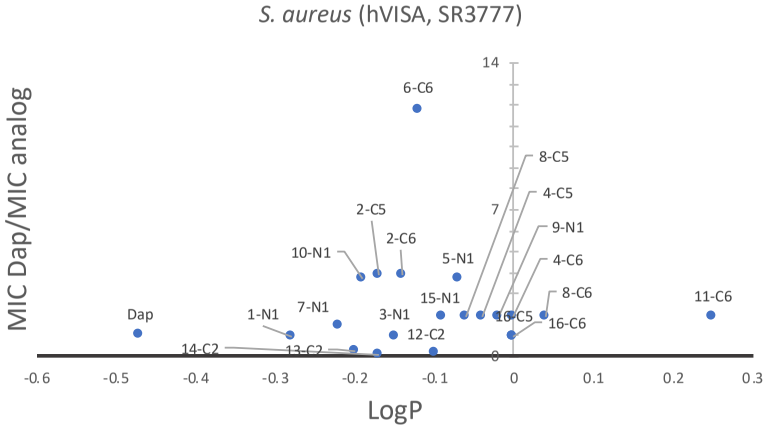

B. subtilis (ATCC 6051)
MIC Dap/MIC Analog
LogP
Dap
4-C5
4-C6
16-C5
6-C6
2-C5
2-C6
8-C5
16-C6
7-N1
15-N1
8-C6
5-N1
11-C6
10-N1
3-N1
12-C2
9-N1
13-C2
1-N1
14-C2

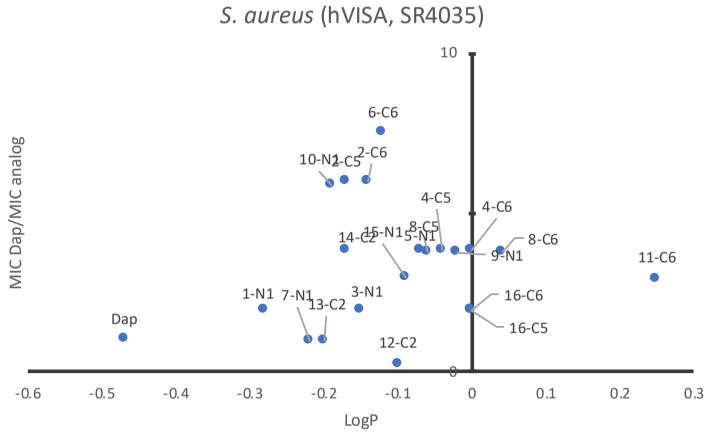

S. aureus (hVISA, SR220)
MIC Dap/MIC Analog
LogP
16-C5
1-N1
3-N1
6-C6
16-C6
5-N1
2-C5
8-C6
2-C6
8-C5
9-N1
15-N1
10-N1
4-C5
11-C6
4-C6
7-N1
Dap
13-C2
14-C2
12-C2


S. aureus (SR1129)
MIC Dap/MIC Analog
LogP
1-N1
3-N1
6-C6
5-N1
8-C6
8-C5
2-C5
16-C5
10-N1
2-C6
9-N1
16-C6
4-C5
4-C6
11-C6
7-N1
15-N1
Dap
13-C2
14-C2
12-C2


S. aureus (SR2609)
MIC Dap/MIC analog
LogP
3-N1
2-C5
6-C6
2-C6
5-N1
16-C5
16-C6
10-N1
8-C5
9-N1
8-C6
4-C5
14-C2
15-N1
4-C6
11-C6
1-N1
7-N1
Dap
13-C2
12-C2


S. aureus (SR2852)
Mic Dap/ MIC analog
LogP
14
10
7
0
-0.6
-0.5
-0.4
-0.3
-0.2
-0.1
0
0.1
0.2
0.3
6-C6
5-N1
8-C5
4-C6
2-C6
2-C5
8-C6
10-N1
4-C5
11-C6
7-N1
16-C5
9-N1
Dap
1-N1
3-N1
12-C2
16-C6
15-N1
13-C2
14-C2


S. aureus (hVISA, SR3777)
MIC Dap/MIC analog
LogP
14
7
0
-0.6
-0.5
-0.4
-0.3
-0.2
-0.1
0
0.1
0.2
0.3
6-C6
8-C5
4-C5
2-C5
9-N1
2-C6
10-N1
5-N1
4-C6
8-C6
11-C6
15-N1
16-C5
16-C6
Dap
1-N1
7-N1
3-N1
12-C2
14-C2
13-C2


S. aureus (hVISA, SR4035)
MIC Dap/MIC analog
LogP
10
0
-0.6
-0.5
-0.4
-0.3
-0.2
-0.1
0
0.1
0.2
0.3
6-C6
10-N1
2-C6
2-C5
4-C5
4-C6
15-N1
8-C5
14-C2
5-N1
8-C6
9-N1
11-C6
1-N1
7-N1
3-N1
16-C6
13-C2
Dap
16-C5
12-C2

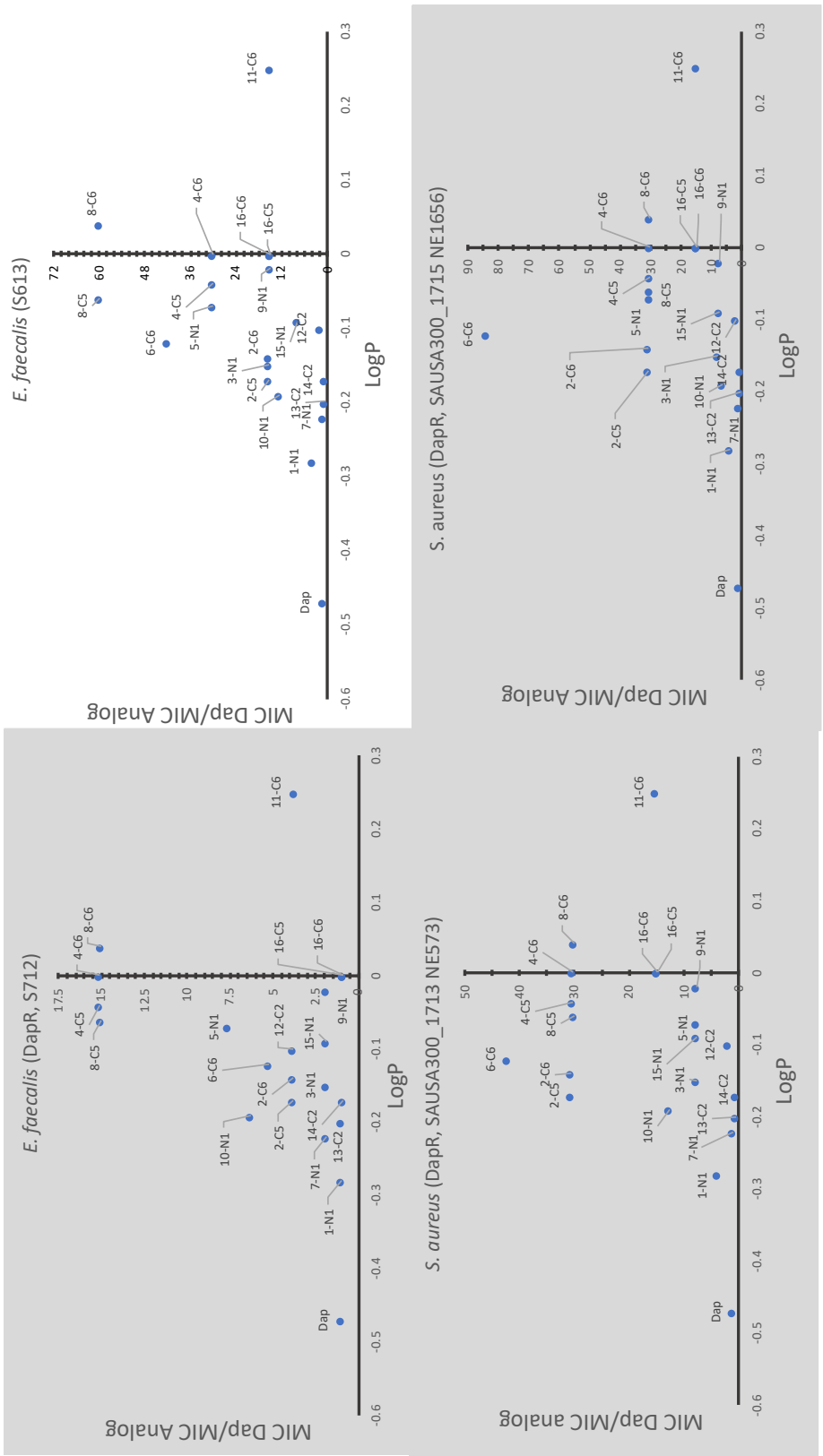


Figure 37. LogP vs MIC improvement plots for daptomycin and daptomycin analogues.

LogP values for daptomycin and daptomycin derivatives were correlated to their MIC improvement as compared to daptomycin for each bacterial strain. Gray plots represent the daptomycin resistant strains. LogP values were calculated using ALOGPS.[135]

Nonribosomal peptides represent a highly promising chemical space with great potential for pharmaceutical relevance and medical advancement. Among these compounds, daptomycin, a clinically approved antibiotic, represents a unique class of macrolactone antibiotics. Due to the fact that daptomycin is a highly complex molecule to approach synthetically, the chemoenzymatic strategy that we describe is a successful methodology to generate tryptophan substituted daptomycin derivatives.

Our chemoenzymatic strategy involves the utilization of the highly permissive prenyltransferase CdpNPT which uniformly transfers an alkyl group onto the indole moiety of daptomycin. Through this strategy we have revealed the transfer of a large variety of alkyl groups onto the C5, C6, C2 and N1 position of the indole ring. As reported in Table 8, the position of the substitution has a crucial influence on the antibacterial behavior of the derivatized compounds. The C-2 substituted variants display a significant increase of MIC values (up to 80-fold) compared to the N1, C-5 and C-6 substituted compounds. Based on the results of the logP values, the alkylation position as well as the substituent affects the overall lipophilicity of the compound.

In conclusion, through our chemoenzymatic strategy we were able to specifically modify the tryptophan of the highly chemically complex natural product daptomycin. These daptomycin derivatives show great improvement of MIC values over the parent

compound towards clinically isolated strains including highly relevant daptomycin resistant strains. Many issues that have arisen with daptomycin could potentially be addressed by further synthesis and evaluation of daptomycin analogues such as the ones generated here.

Experimental

General methods. HPLC analysis was accomplished using Agilent Technologies 1220 Infinity LC system equipped with a diode array detector. *Method A (HPLC):* Monitoring CdpNPT catalyzed reaction was completed using an analytical reverse-phase (RP) HPLC Gemini-NX, C-18 (5 μm, 4.6 mm × 250 mm) column (Phenomenex, Torrance, California, USA) employing a gradient of 10% B to 55% B over 10 min, 55% B to 100%B for 15 min, 10%B for 5 min (A=H_2O with 0.1% TFA; B= acetonitrile), flow rate = 1mL min^{-1} ; $A_{280.}$ Reaction progression was monitored by the different retention times between product and starting material. *Method B (HPLC):* Semi-preparative RP HPLC was conducted using a Gemini-NX, C-18 (5 μm, 10 × 250 mm) column (Phenomenex, Torrance, California, USA), peak separation and product purification was completed using a shallow gradient of 35% B to 55% B in 20 min, 55% B to 100% B in 3 min, 35%B for 7 min. (A=H_2O with 0.05% formic acid; B= acetonitrile) flow rate = 2 mL min^{-1}; A_{280}. High-resolution mass spectrometric (HRMS) data and liquid chromatography mass spectrometric (LCMS) were obtained on Agilent 6545-QTOF W/1290 HPLC mass spectrometer at the University of Oklahoma, Department of Chemistry and Biochemistry. All logP values were calculated using ALOGPS software found in virtual computational chemistry laboratory[135]

Prenyltransferase CdpNPT expression and purification. The synthetic gene for CpdNPT, bearing an N-terminal His_6 tag, was inserted into vector pET-28a and transformed into E. coli Rosetta cells. After overnight growth, 3 mL of bacterial culture was used to inoculated 1.2 L Lauria-Berani medium containing 50 μg kanamycin mL^{-1}. Cultures were grown at 37°C for approximately 4 h at 220 r.p.m. (O. D_{600} =0.6-0.8). Protein expression was induced by the addition of isopropyl β-D-1-thiogalactopyranoside (IPTG) (0.5 mM final) and continually shaken at 220 r.p.m. for an additional 16-19 h at 20°C. Bacterial cultures were harvested by centrifugation and the resulting cell pellets were resuspended in a lysis buffer (50mM NaH_2PO_4, 200mM NaCl, pH 7.8) and stored at -80°C until use. Resuspended cells were thawed then lysed by way of sonication on ice 60 times for 10 s. In order separate insoluble and undesirable cellular components, lysed cells were centrifuged for 1 h at 10°C at 16000 r.p.m. The supernatant, containing the expressed recombinant CdpNPT with an N-terminal His_6 tag, was purified using nickel sepharose resin affinity chromatography column (GE Healthcare, USA). Protein was eluted using an imidazole gradient from 10mM to 500mM in elusion buffer (50 mM NaH_2PO_4, 200 mM NaCl, pH 7.8). The purified protein was concentrated and introduced to a new buffer condition (25 mM Tris-HCl, pH 8, 50 mM KCl) using a desalting column (PD-10 desalting column, GE healthcare). Eluents were evaluated by SDS-PAGE for purity, concentration was determined using NanoDrop One (Thermo Scientific, USA) and the purified protein was stored flash frozen in 20μL aliquots at -80°C.

***In-vitro* CpdNPT assay with daptomycin.** *In vitro* CdpNPT analytical reactions with daptomycin were performed in a final volume of 20μL, consisting of 1.2mM

pyrophosphate analogues, 1mM daptomycin (TCI, TCI America) and 8μM purified CdpNPT in reaction buffer (Tris-HCl pH 7.8, 5 mM $CaCl_2$, 50mM KCl) and incubated at 35 °C for 16 h. Reactions were terminated by addition of 60μL cold methanol followed by centrifugation (10,000 g for 30 min) in order to remove precipitated enzyme. Analysis of the reactions was completed on RP-HPLC using method A (general method). For each reaction the percent conversion was calculated by the integration of the product peak at 280nm divided by the overall sum of the integrated product peak and starting material at 280nm. All enzymatic products were confirmed by using ESI-HRMS. Large scale reactions of daptomycin analogues were performed on a 10 mL scale consisting of 1mM daptomycin, 1.25mM pyrophosphate analogue, and 100μM purified CdpNPT in reaction buffer. Putative products were subsequently isolated by semi-prep HPLC using method B (general method, above) and confirmed by NMR and ESI-HRMS.

Antibacterial assays. All daptomycin analogue stocks were calibrated by absorbance (Calibration curve at λ= 280nm, ε_{366} = 4,000 L mol^{-1} cm^{-1})[101] and all bioactivity assays were conducted in triplicate. The strains for which MICs were determined included, thirteen daptomycin sensitive (**Dap**S) and three daptomycin resistant (**Dap**R) strains. The **Dap**S strains are: *S. aureus* (ATCC 25923), methicillin-resistant *S. aureus* ATCC 700787, *S. epidermidis* ATCC 12228, vancomycin-resistant *Enterococcus. faecalis* ATCC 700802, *Bacillus subtilis* (ATCC 6051), hetero-vancomycin intermediate *S. aureus* SR220 (BEI product NR-50512), *S. aureus*, Strain SR1129 (NR-50506), *S. aureus*, Strain SR2609 (NR-50507), *S. aureus*, Strain SR2852 (NR-50508),

hetero-vancomycin intermediate *S. aureus* SR3777 (BEI product NR-50509), hetero-vancomycin intermediate *S. aureus*, SR4035 (BEI product NR-50510), and *Enterococcus faecalis* S613 (HM-334). The **Dap**R strains are *S. aureus*, Strain JE2, Transposon Mutant NE573 (NR-47116), *S. aureus* JE2, Transposon Mutant NE1656 (BEI product NR-48198), and *Enterococcus faecalis* R712 (HM-335). Enterococcus Faecalis Strains S613 and R712 were isolated from the blood of a 64- year old hemodialysis patient with fatal bactermia. Strain S613 was isolated from the patient before treatment with daptomycin and is reported to be susceptible to daptomycin. Strain R712 was isolated from blood drawn after treatment of daptomycin. (Minimum inhibitory concentration (MIC) testing against all strains was performed in Mueller-Hinton Broth (MHB) or Brain Heart Infusion (BHI) broth, for DapS and DapR strains respectively, supplemented with 50 mg L^{-1} of calcium [136, 137] following the CLSI guidelines for broth microdilution methods using inoculum of $1 \times 10^5 - 5 \times 10^5$ CFU/mL.[138] All Dap analogue stocks were made in DMSO. Serial two-fold dilutions of the compounds ranged from 20 to 0.16 μM, 5 to 0.039 μM and 1.6 to 0.0125 μM. Briefly, the overnight cultures were grown at 35 °C in MHB. Daptomycin and daptomycin analogues were serially diluted in MHB followed by inoculation of serially diluted media with 10,000 counts of bacteria from the overnight culture. The culture plates were incubated with shaking at 35 °C for 20–24 h. Growth was evaluated using the absorbance at 600 nm. The lowest concentration causing 80% inhibition microbial growth was defined as the MIC. Growth and sterility controls were included in each experiment. In addition, two representative gram-negative bacteria *E. coli* (ATCC 11775) and *P. aeruginosa* (ATCC 10145) were included in the activity assays. The

cancer cell-line cytotoxicity assays as a measure of general eukaryotic cell toxicity employed the human hepatocyte carcinoma cell line HepG2. The cytotoxicity of daptomycin and its analogues were tested against HepG2 cell line at 20 μM by using MTT assay.[139]

Appendix

Copy-right permission

RightsLink Printable License 6/20/19, 8*40 PM

JOHN WILEY AND SONS LICENSE TERMS AND CONDITIONS

Jun 20, 2019

This Agreement between university of oklahoma -- Erin scull ("You") and John Wiley and Sons ("John Wiley and Sons") consists of your license details and the terms and conditions provided by John Wiley and Sons and Copyright Clearance Center.

License Number
License date
Licensed Content Publisher Licensed Content Publication Licensed Content Title

Licensed Content Author Licensed Content Date Licensed Content Volume Licensed Content Issue Licensed Content Pages Type of use

Requestor type

Format

Portion

Will you be translating?

Title of your thesis / dissertation

Expected completion date

Expected size (number of pages)

Requestor Location

Publisher Tax ID
Total
Terms and Conditions

4612621505740

Jun 19, 2019

John Wiley and Sons

ChemBioChem

Determination of Alkyl-Donor Promiscuity of Tyrosine-O-Prenyltransferase SirD from Leptosphaeria maculans

Chandrasekhar Bandari, Erin M. Scull, Johanna M. Masterson, et al Oct 27, 2017
18
23

5
Dissertation/Thesis
Author of this Wiley article
Electronic
Full article
No
Understanding the alkyl donor specificity of aromatic penyltransferases Jun 2019
140

university of oklahoma 321 east apache

NORMAN, OK 73069 United States
Attn: university of oklahoma

EU826007151 0.00 USD

TERMS AND CONDITIONS

This copyrighted material is owned by or exclusively licensed to John Wiley & Sons, Inc. or one of its group companies (each a"Wiley Company") or handled on behalf of a society with

which a Wiley Company has exclusive publishing rights in relation to a particular work (collectively "WILEY"). By clicking "accept" in connection with completing this licensing transaction, you agree that the following terms and conditions apply to this transaction (along with the billing and payment terms and conditions established by the Copyright Clearance Center Inc., ("CCC's Billing and Payment terms and conditions"), at the time that you opened your RightsLink account (these are available at any time at http://myaccount.copyright.com).

Terms and Conditions

The materials you have requested permission to reproduce or reuse (the "Wiley Materials") are protected by copyright.

You are hereby granted a personal, non-exclusive, non-sub licensable (on a stand- alone basis), non-transferable, worldwide, limited license to reproduce the Wiley Materials for the purpose specified in the licensing process. This license, **and any CONTENT (PDF or image file) purchased as part of your order,** is for a one-time use only and limited to any maximum distribution number specified in the license. The first instance of republication or reuse granted by this license must be completed within two years of the date of the grant of this license (although copies prepared before the end date may be distributed thereafter). The Wiley Materials shall not be used in any other manner or for any other purpose, beyond what is granted in the license. Permission is granted subject to an appropriate acknowledgement given to the author, title of the material/book/journal and the publisher. You shall also duplicate the copyright notice that appears in the Wiley publication in your use of the Wiley Material. Permission is also granted on the understanding that nowhere in the text is a previously published source acknowledged for all or part of this Wiley Material. Any third party content is expressly excluded from this permission.

With respect to the Wiley Materials, all rights are reserved. Except as expressly granted by the terms of the license, no part of the Wiley Materials may be copied, modified, adapted (except for minor reformatting required by the new Publication), translated, reproduced, transferred or distributed, in any form or by any means, and no derivative works may be made based on the Wiley Materials without the prior permission of the respective copyright owner.**For STM Signatory Publishers clearing permission under the terms of the STM Permissions Guidelines only, the terms of the license are extended to include subsequent editions and for editions in other languages, provided such editions are for the work as a whole in situ and does not involve the separate exploitation of the permitted figures or extracts,** You may not alter, remove or suppress in any manner any copyright, trademark or other notices displayed by the Wiley Materials. You may not license, rent, sell, loan, lease, pledge, offer as security, transfer or assign the Wiley Materials on a stand-alone basis, or any of the rights granted to you hereunder to any other person.

The Wiley Materials and all of the intellectual property rights therein shall at all times remain the exclusive property of John Wiley & Sons Inc, the Wiley Companies, or their respective licensors, and your interest therein is only that of having possession of

and the right to reproduce the Wiley Materials pursuant to Section 2 herein during the continuance of this Agreement. You agree that you own no right, title or interest in or to the Wiley Materials or any of the intellectual property rights therein. You shall have no rights hereunder other than the license as provided for above in Section 2. No right, license or interest to any trademark, trade name, service mark or other branding ("Marks") of WILEY or its licensors is granted hereunder, and you agree that you shall not assert any such right, license or interest with respect thereto

NEITHER WILEY NOR ITS LICENSORS MAKES ANY WARRANTY OR REPRESENTATION OF ANY KIND TO YOU OR ANY THIRD PARTY, EXPRESS, IMPLIED OR STATUTORY, WITH RESPECT TO THE MATERIALS OR THE ACCURACY OF ANY INFORMATION CONTAINED IN THE MATERIALS, INCLUDING, WITHOUT LIMITATION, ANY IMPLIED WARRANTY OF MERCHANTABILITY, ACCURACY, SATISFACTORY QUALITY, FITNESS FOR A PARTICULAR PURPOSE, USABILITY, INTEGRATION OR NON-INFRINGEMENT AND ALL SUCH WARRANTIES ARE HEREBY EXCLUDED BY WILEY AND ITS LICENSORS AND WAIVED BY YOU.

WILEY shall have the right to terminate this Agreement immediately upon breach of this Agreement by you.

You shall indemnify, defend and hold harmless WILEY, its Licensors and their respective directors, officers, agents and employees, from and against any actual or threatened claims, demands, causes of action or proceedings arising from any breach of this Agreement by you.

IN NO EVENT SHALL WILEY OR ITS LICENSORS BE LIABLE TO YOU OR ANY OTHER PARTY OR ANY OTHER PERSON OR ENTITY FOR ANY SPECIAL, CONSEQUENTIAL, INCIDENTAL, INDIRECT, EXEMPLARY OR PUNITIVE DAMAGES, HOWEVER CAUSED, ARISING OUT OF OR IN CONNECTION WITH THE DOWNLOADING, PROVISIONING, VIEWING OR USE OF THE MATERIALS REGARDLESS OF THE FORM OF ACTION, WHETHER FOR BREACH OF CONTRACT, BREACH OF WARRANTY, TORT, NEGLIGENCE, INFRINGEMENT OR OTHERWISE (INCLUDING, WITHOUT LIMITATION, DAMAGES BASED ON LOSS OF PROFITS, DATA, FILES, USE, BUSINESS OPPORTUNITY OR CLAIMS OF THIRD PARTIES), AND WHETHER OR NOT THE PARTY HAS BEEN ADVISED OF THE POSSIBILITY OF SUCH DAMAGES. THIS

LIMITATION SHALL APPLY NOTWITHSTANDING ANY FAILURE OF ESSENTIAL PURPOSE OF ANY LIMITED REMEDY PROVIDED HEREIN.

Should any provision of this Agreement be held by a court of competent jurisdiction to be illegal, invalid, or unenforceable, that provision shall be deemed amended to achieve as nearly as possible the same economic effect as the original provision, and the legality, validity and enforceability of the remaining provisions of this Agreement shall not be affected or impaired thereby.

The failure of either party to enforce any term or condition of this Agreement shall not constitute a waiver of either party's right to enforce each and every term and condition of this Agreement. No breach under this agreement shall be deemed waived or excused by either party unless such waiver or consent is in writing signed by the party granting such waiver or consent. The waiver by or consent of a party to a breach of any provision of this Agreement shall not operate or be construed as a waiver of or consent to any other or subsequent breach by such other party.

This Agreement may not be assigned (including by operation of law or otherwise) by you without WILEY's prior written consent.

Any fee required for this permission shall be non-refundable after thirty (30) days from receipt by the CCC.

These terms and conditions together with CCC's Billing and Payment terms and conditions (which are incorporated herein) form the entire agreement between you and WILEY concerning this licensing transaction and (in the absence of fraud) supersedes all prior agreements and representations of the parties, oral or written. This Agreement may not be amended except in writing signed by both parties. This Agreement shall be binding upon and inure to the benefit of the parties' successors, legal representatives, and authorized assigns.

In the event of any conflict between your obligations established by these terms and conditions and those established by CCC's Billing and Payment terms and conditions, these terms and conditions shall prevail.

WILEY expressly reserves all rights not specifically granted in the combination of (i) the license details provided by you and accepted in the course of this

licensing transaction, (ii) these terms and conditions and (iii) CCC's Billing and Payment terms and conditions.

This Agreement will be void if the Type of Use, Format, Circulation, or Requestor Type was misrepresented during the licensing process.

This Agreement shall be governed by and construed in accordance with the laws of the State of New York, USA, without regards to such state's conflict of law rules. Any legal action, suit or proceeding arising out of or relating to these Terms and Conditions or the breach thereof shall be instituted in a court of competent jurisdiction in New York County in the State of New York in the United States of America and each party hereby consents and submits to the personal jurisdiction of such court, waives any objection to venue in such court and consents to service of process by registered or certified mail, return receipt requested, at the last known address of such party.

WILEY OPEN ACCESS TERMS AND CONDITIONS

Wiley Publishes Open Access Articles in fully Open Access Journals and in Subscription

journals offering Online Open. Although most of the fully Open Access journals publish open access articles under the terms of the Creative Commons Attribution (CC BY) License only, the subscription journals and a few of the Open Access Journals offer a choice of Creative Commons Licenses. The license type is clearly identified on the article.

The Creative Commons Attribution License

The Creative Commons Attribution License (CC-BY) allows users to copy, distribute and transmit an article, adapt the article and make commercial use of the article. The CC-BY license permits commercial and non-

Creative Commons Attribution Non-Commercial License

The Creative Commons Attribution Non-Commercial (CC-BY-NC)License permits use, distribution and reproduction in any medium, provided the original work is properly cited and is not used for commercial purposes.(see below)

Creative Commons Attribution-Non-Commercial-NoDerivs License

The Creative Commons Attribution Non-Commercial-NoDerivs License (CC-BY-NC-ND) permits use, distribution and reproduction in any medium, provided the original work is properly cited, is not used for commercial purposes and no modifications or adaptations are made. (see below)

Use by commercial "for-profit" organizations

Use of Wiley Open Access articles for commercial, promotional, or marketing purposes requires further explicit permission from Wiley and will be subject to a fee.
Further details can be found on Wiley Online Library
http://olabout.wiley.com/WileyCDA/Section/id-410895.html

Other Terms and Conditions:

v1.10 Last updated September 2015

Questions? customercare@copyright.com or +1-855-239-3415 (toll free in the US) or +1-978-646-2777.



From: RSC1 (shared) RSC1@rsc.org **Subject:** RE: request for copy right permission

Date: June 20, 2019 at 8:33 AM **To:** erinscull@ou.edu

Dear Erin Scull

Thank you for your email. Permission is granted to reproduce your article in your thesis as long as it is fully acknowledged and includes a link back to the article on our website. Please ensure that all authors are aware that it is being included.

If you have any further questions, please let me know. Kind regards
Kate

Kate McCallum
Publishing Assistant, Customer Services Royal Society of Chemistry

T: +44 (0) 1223 432176 I www.rsc.org

References

1. Schardl, C.L., D.G. Panaccione, and P. Tudzynski, *Ergot alkaloids--biology and molecular biology.* Alkaloids Chem Biol, 2006. **63**: p. 45-86.
2. Williams, R.M., E.M. Stocking, and J.F. Sanz-Cervera, *Biosynthesis of prenylated alkaloids derived from tryptophan*, in *Biosynthesis*. 2000, Springer. p. 97-173.
3. Jain, H.D., et al., *Synthesis and structure–activity relationship studies on tryprostatin A, an inhibitor of breast cancer resistance protein.* Bioorganic & Medicinal Chemistry, 2008. **16**(8): p. 4626-4651.
4. Raju, R., et al., *Nocardioazines: A Novel Bridged Diketopiperazine Scaffold from a Marine-Derived Bacterium Inhibits P-Glycoprotein.* Organic Letters, 2011. **13**(10): p. 2770-2773.
5. Ma, Y.M., et al., *Structural Diversity and Biological Activities of Indole Diketopiperazine Alkaloids from Fungi.* J Agric Food Chem, 2016. **64**(35): p. 6659-71.
6. Viola Wohlgemuth, F.K., Xiulan Xie, Bin-Gui Wang, and Shu-Ming Li, *Two Prenyltransferases Govern a Consecutive Prenylation Cascade in the Biosynthesis of Echinulin and Neoechinulin.* Organic Letters, 2017. **19**(21): p. 5928-5931.
7. Schultz, A.W., et al., *Functional Characterization of the Cyclomarin/Cyclomarazine Prenyltransferase CymD Directs the Biosynthesis of Unnatural Cyclic Peptides.* Journal of Natural Products, 2010. **73**(3): p. 373-377.
8. Kunze, B., G. Hofle, and H. Reichenbach, *The aurachins, new quinoline antibiotics from myxobacteria: production, physico-chemical and biological properties.* J Antibiot (Tokyo), 1987. **40**(3): p. 258-65.
9. Yamamoto, K., et al., *Napyradiomycin A1, an inhibitor of mitochondrial complexes I and II.* The Journal Of Antibiotics, 2012. **65**: p. 211.
10. Zhang, M., et al., *Aurachin SS, a new antibiotic from Streptomyces sp. NA04227.* The Journal Of Antibiotics, 2017. **70**: p. 853.
11. Gourdeau, H., et al., *Identification, characterization and potent antitumor activity of ECO-4601, a novel peripheral benzodiazepine receptor ligand.* Cancer Chemother Pharmacol, 2008. **61**(6): p. 911-21.
12. Bonitz, T., et al., *Unusual N-prenylation in diazepinomicin biosynthesis: the farnesylation of a benzodiazepine substrate is catalyzed by a new member of the ABBA prenyltransferase superfamily.* PLoS One, 2013. **8**(12): p. e85707.
13. Mason, W.P., et al., *A phase II study of the Ras-MAPK signaling pathway inhibitor TLN-4601 in patients with glioblastoma at first progression.* J Neurooncol, 2012. **107**(2): p. 343-9.
14. Lee, H.-J., et al., *Growth Inhibition and Apoptosis-Inducing Effects of Cudraflavone B in Human Oral Cancer Cells via MAPK, NF-κB, and SIRT1 Signaling Pathway.* Planta Med, 2013. **79**(14): p. 1298-1306.
15. Lee, D.S., et al., *Cudarflavone B provides neuroprotection against glutamate-induced mouse hippocampal HT22 cell damage through the Nrf2 and PI3K/Akt signaling pathways.* Molecules, 2014. **19**(8): p. 10818-31.

16. Liang, P.H., T.P. Ko, and A.H.J. Wang, *Structure, mechanism and function of prenyltransferases.* European Journal of Biochemistry, 2002. **269**(14): p. 3339-3354.
17. Boronat, A. and M. Rodriguez-Concepcion, *Terpenoid biosynthesis in prokaryotes.* Adv Biochem Eng Biotechnol, 2015. **148**: p. 3-18.
18. Kellogg, B.A. and C.D. Poulter, *Chain elongation in the isoprenoid biosynthetic pathway.* Curr Opin Chem Biol, 1997. **1**(4): p. 570-8.
19. Hao, Y., et al., *Molecular basis for the broad substrate selectivity of a peptide prenyltransferase.* Proc Natl Acad Sci U S A, 2016. **113**(49): p. 14037-14042.
20. Palsuledesai, C.C. and M.D. Distefano, *Protein Prenylation: Enzymes, Therapeutics, and Biotechnology Applications.* ACS Chemical Biology, 2015. **10**(1): p. 51-62.
21. Dumelin, C.E., et al., *Discovery and biological characterization of geranylated RNA in bacteria.* Nat Chem Biol, 2012. **8**(11): p. 913-9.
22. Xie, W., C. Zhou, and R.H. Huang, *Structure of tRNA dimethylallyltransferase: RNA modification through a channel.* Journal of molecular biology, 2007. **367**(3): p. 872-881.
23. Heide, L., *Prenyl transfer to aromatic substrates: genetics and enzymology.* Curr Opin Chem Biol, 2009. **13**(2): p. 171-9.
24. Li, S.M., *Evolution of aromatic prenyltransferases in the biosynthesis of indole derivatives.* Phytochemistry, 2009. **70**(15-16): p. 1746-57.
25. Yazaki, K., K. Sasaki, and Y. Tsurumaru, *Prenylation of aromatic compounds, a key diversification of plant secondary metabolites.* Phytochemistry, 2009. **70**(15-16): p. 1739-45.
26. Ding, Y., et al., *Genome-based characterization of two prenylation steps in the assembly of the stephacidin and notoamide anticancer agents in a marine-derived Aspergillus sp.* J Am Chem Soc, 2010. **132**(36): p. 12733-40.
27. Bladt, T.T., et al., *Anticancer and antifungal compounds from Aspergillus, Penicillium and other filamentous fungi.* Molecules, 2013. **18**(9): p. 11338-76.
28. Fan, A., J. Winkelblech, and S.M. Li, *Impacts and perspectives of prenyltransferases of the DMATS superfamily for use in biotechnology.* Appl Microbiol Biotechnol, 2015. **99**(18): p. 7399-415.
29. Rudolf, J.D. and C.D. Poulter, *Tyrosine O-Prenyltransferase SirD Catalyzes S-, C-, and N-Prenylations on Tyrosine and Tryptophan Derivatives.* ACS Chemical Biology, 2013. **8**(12): p. 2707-2714.
30. Zou, H.X., et al., *The tyrosine O-prenyltransferase SirD catalyzes O-, N-, and C-prenylations.* Appl Microbiol Biotechnol, 2011. **89**(5): p. 1443-51.
31. Winkelblech, J., et al., *Tryptophan C5-, C6- and C7-Prenylating Enzymes Displaying a Preference for C-6 of the Indole Ring in the Presence of Unnatural Dimethylallyl Diphosphate Analogues.* Advanced Synthesis & Catalysis, 2015. **357**(5): p. 975-986.
32. Yu, H., et al., *Tyrosine O-prenyltransferases TyrPT and SirD displaying similar behavior toward unnatural alkyl or benzyl diphosphate as their natural prenyl donor dimethylallyl diphosphate.* Applied Microbiology and Biotechnology, 2015. **99**(17): p. 7115-7124.

33. Heide, L., *Prenyl transfer to aromatic substrates: genetics and enzymology.* Current Opinion in Chemical Biology, 2009. **13**(2): p. 171-179.
34. Tello, M., et al., *The ABBA family of aromatic prenyltransferases: broadening natural product diversity.* Cell Mol Life Sci, 2008. **65**(10): p. 1459-63.
35. Metzger, U., et al., *The structure of dimethylallyl tryptophan synthase reveals a common architecture of aromatic prenyltransferases in fungi and bacteria.* Proceedings of the National Academy of Sciences, 2009. **106**(34): p. 14309-14314.
36. Kuzuyama, T., J.P. Noel, and S.B. Richard, *Structural basis for the promiscuous biosynthetic prenylation of aromatic natural products.* Nature, 2005. **435**(7044): p. 983-7.
37. Metzger, U., et al., *Structure and mechanism of the magnesium-independent aromatic prenyltransferase CloQ from the clorobiocin biosynthetic pathway.* J Mol Biol, 2010. **404**(4): p. 611-26.
38. Wang, J., et al., *Structural insight into a novel indole prenyltransferase in hapalindole-type alkaloid biosynthesis.* Biochem Biophys Res Commun, 2018. **495**(2): p. 1782-1788.
39. Wong, C.P., et al., *Two Distinct Substrate Binding Modes for the Normal and Reverse Prenylation of Hapalindoles by the Prenyltransferase AmbP3.* Angew Chem Int Ed Engl, 2018. **57**(2): p. 560-563.
40. Elshahawi, S.I., et al., *Structure and specificity of a permissive bacterial C-prenyltransferase.* Nat Chem Biol, 2017. **13**(4): p. 366-368.
41. Jost, M., et al., *Structure-function analysis of an enzymatic prenyl transfer reaction identifies a reaction chamber with modifiable specificity.* J Am Chem Soc, 2010. **132**(50): p. 17849-58.
42. Pojer, F., et al., *CloQ, a prenyltransferase involved in clorobiocin biosynthesis.* Proc Natl Acad Sci U S A, 2003. **100**(5): p. 2316-21.
43. Steffensky, M., et al., *Identification of the Novobiocin Biosynthetic Gene Cluster of Streptomyces spheroides NCIB 11891.* Antimicrobial Agents and Chemotherapy, 2000. **44**(5): p. 1214-1222.
44. Winkelblech, J., A. Fan, and S.M. Li, *Prenyltransferases as key enzymes in primary and secondary metabolism.* Appl Microbiol Biotechnol, 2015. **99**(18): p. 7379-97.
45. Winkelblech, J., A. Fan, and S.-M. Li, *Prenyltransferases as key enzymes in primary and secondary metabolism.* Applied Microbiology and Biotechnology, 2015. **99**(18): p. 7379-7397.
46. Zocher, G., et al., *Structure-based engineering increased the catalytic turnover rate of a novel phenazine prenyltransferase.* PLoS One, 2012. **7**(10): p. e48427.
47. Chen, R., et al., *Molecular insights into the enzyme promiscuity of an aromatic prenyltransferase.* Nat Chem Biol, 2017. **13**(2): p. 226-234.
48. Awakawa, T., et al., *Molecular Insight into the Mg(2+) -Dependent Allosteric Control of Indole Prenylation by Aromatic Prenyltransferase AmbP1.* Angew Chem Int Ed Engl, 2018. **57**(23): p. 6810-6813.
49. Schuller, J.M., et al., *Structure and catalytic mechanism of a cyclic dipeptide prenyltransferase with broad substrate promiscuity.* J Mol Biol, 2012. **422**(1): p. 87-99.

50. Wierenga, R.K., *The TIM-barrel fold: a versatile framework for efficient enzymes.* FEBS Letters, 2001. **492**(3): p. 193-198.
51. Metzger, U., et al., *The structure of dimethylallyl tryptophan synthase reveals a common architecture of aromatic prenyltransferases in fungi and bacteria.* Proc Natl Acad Sci U S A, 2009. **106**(34): p. 14309-14.
52. Bayse, C.A. and K.M. Merz, *Mechanistic insights into Mg2+-independent prenylation by CloQ from classical molecular mechanics and hybrid quantum mechanics/molecular mechanics molecular dynamics simulations.* Biochemistry, 2014. **53**(30): p. 5034-41.
53. Mori, T., et al., *Manipulation of prenylation reactions by structure-based engineering of bacterial indolactam prenyltransferases.* Nature communications, 2016. **7**: p. 10849-10849.
54. Kumano, T., et al., *Chemoenzymatic syntheses of prenylated aromatic small molecules using Streptomyces prenyltransferases with relaxed substrate specificities.* Bioorg Med Chem, 2008. **16**(17): p. 8117-26.
55. Koehl, P., *Relaxed specificity in aromatic prenyltransferases.* Nat Chem Biol, 2005. **1**(2): p. 71-2.
56. Tanner, M.E., *Mechanistic studies on the indole prenyltransferases.* Nat Prod Rep, 2015. **32**(1): p. 88-101.
57. Zheng, L., et al., *Switching a regular tryptophan C4-prenyltransferase to a reverse tryptophan-containing cyclic dipeptide C3-prenyltransferase by sequential site-directed mutagenesis.* Organic & Biomolecular Chemistry, 2018. **16**(36): p. 6688-6694.
58. Luk, L.Y.P. and M.E. Tanner, *Mechanism of Dimethylallyltryptophan Synthase: Evidence for a Dimethylallyl Cation Intermediate in an Aromatic Prenyltransferase Reaction.* Journal of the American Chemical Society, 2009. **131**(39): p. 13932-13933.
59. Yang, Y., et al., *Catalytic mechanism of aromatic prenylation by NphB.* Biochemistry, 2012. **51**(12): p. 2606-18.
60. Liebhold, M., X. Xie, and S.M. Li, *Expansion of enzymatic Friedel-Crafts alkylation on indoles: acceptance of unnatural beta-unsaturated allyl diphospates by dimethylallyl-tryptophan synthases.* Org Lett, 2012. **14**(18): p. 4882-5.
61. Welch, T.R. and R.M. Williams, *Epidithiodioxopiperazines. occurrence, synthesis and biogenesis.* Nat Prod Rep, 2014. **31**(10): p. 1376-404.
62. Gardiner, D.M., P. Waring, and B.J. Howlett, *The epipolythiodioxopiperazine (ETP) class of fungal toxins: distribution, mode of action, functions and biosynthesis.* Microbiology, 2005. **151**(Pt 4): p. 1021-32.
63. Fox, E.M. and B.J. Howlett, *Biosynthetic gene clusters for epipolythiodioxopiperazines in filamentous fungi.* Mycol Res, 2008. **112**(Pt 2): p. 162-9.
64. Gardiner, D.M., et al., *The sirodesmin biosynthetic gene cluster of the plant pathogenic fungus Leptosphaeria maculans.* Mol Microbiol, 2004. **53**(5): p. 1307-18.

65. Kremer, A. and S.M. Li, *A tyrosine O-prenyltransferase catalyses the first pathway-specific step in the biosynthesis of sirodesmin PL.* Microbiology, 2010. **156**(Pt 1): p. 278-86.
66. Rudolf, J.D. and C.D. Poulter, *Tyrosine O-prenyltransferase SirD catalyzes S-, C-, and N-prenylations on tyrosine and tryptophan derivatives.* ACS Chem Biol, 2013. **8**(12): p. 2707-14.
67. Fan, A. and S.-M. Li, *Prenylation of tyrosine and derivatives by a tryptophan C7-prenyltransferase.* Tetrahedron Letters, 2014. **55**(37): p. 5199-5202.
68. Liebhold, M. and S.M. Li, *Regiospecific benzylation of tryptophan and derivatives catalyzed by a fungal dimethylallyl transferase.* Org Lett, 2013. **15**(22): p. 5834-7.
69. Liebhold, M., X. Xie, and S.M. Li, *Breaking cyclic dipeptide prenyltransferase regioselectivity by unnatural alkyl donors.* Org Lett, 2013. **15**(12): p. 3062-5.
70. Yu, H., et al., *Tyrosine O-prenyltransferases TyrPT and SirD displaying similar behavior toward unnatural alkyl or benzyl diphosphate as their natural prenyl donor dimethylallyl diphosphate.* Appl Microbiol Biotechnol, 2015. **99**(17): p. 7115-24.
71. Bandari, C., et al., *Determination of Alkyl-Donor Promiscuity of Tyrosine-O-Prenyltransferase SirD from Leptosphaeria maculans.* ChemBioChem, 2017. **18**(23): p. 2323-2327.
72. Lossing, F.P. and J.L. Holmes, *Stabilization energy and ion size in carbocations in the gas phase.* Journal of the American Chemical Society, 1984. **106**(23): p. 6917-6920.
73. Kim, J.D., et al., *Study of the stability of carbocations by chlorosulfonyl isocyanate reaction with ethers.* Tetrahedron, 2002. **58**(22): p. 4395-4402.
74. Biasini, M., et al., *SWISS-MODEL: modelling protein tertiary and quaternary structure using evolutionary information.* Nucleic Acids Res, 2014. **42**(Web Server issue): p. W252-8.
75. Newman, D.J. and G.M. Cragg, *Natural products as sources of new drugs over the 30 years from 1981 to 2010.* J Nat Prod, 2012. **75**(3): p. 311-35.
76. Cress, W.A., L.T. Chayet, and H.C. Rilling, *Crystallization and partial characterization of dimethylallyl pyrophosphate: L-tryptophan dimethylallyltransferase from Claviceps sp. SD58.* J Biol Chem, 1981. **256**(21): p. 10917-23.
77. Unsold, I.A. and S.M. Li, *Overproduction, purification and characterization of FgaPT2, a dimethylallyltryptophan synthase from Aspergillus fumigatus.* Microbiology, 2005. **151**(Pt 5): p. 1499-505.
78. Fan, A., X. Xie, and S.M. Li, *Tryptophan prenyltransferases showing higher catalytic activities for Friedel-Crafts alkylation of o- and m-tyrosines than tyrosine prenyltransferases.* Org Biomol Chem, 2015. **13**(27): p. 7551-7.
79. Fan, A., J. Winkelblech, and S.M. Li, *Impacts and perspectives of prenyltransferases of the DMATS superfamily for use in biotechnology.* Applied Microbiology and Biotechnology, 2015. **99**(18): p. 7399-415.
80. Kranen, E., et al., *Development of a Whole Cell Biocatalyst for the Efficient Prenylation of Indole Derivatives by Autodisplay of the Aromatic Prenyltransferase FgaPT2.* ChemCatChem, 2011. **3**(7): p. 1200-1207.

81. Fan, A. and S.-M. Li, *One Substrate - Seven Products with Different Prenylation Positions in One-Step Reactions: Prenyltransferases Make it Possible.* Advanced Synthesis & Catalysis, 2013. **355**(13): p. 2659-2666.
82. Yu, X., X. Xie, and S.-M. Li, *Substrate promiscuity of secondary metabolite enzymes: prenylation of hydroxynaphthalenes by fungal indole prenyltransferases.* Applied Microbiology & Biotechnology, 2011. **92**(4): p. 737-748.
83. Elshahawi, S.I., et al., *Structure and specificity of a permissive bacterial C-prenyltransferase.* Nature Chemical Biology, 2017. **13**: p. 366.
84. Liao, G., et al., *Complete Decoration of the Indolyl Residue in cyclo-l-Trp-l-Trp with Geranyl Moieties by Using Engineered Dimethylallyl Transferases.* Org Lett, 2018. **20**(22): p. 7201-7205.
85. Mai, P., et al., *Structure-based protein engineering enables prenyl donor switching of a fungal aromatic prenyltransferase.* Org Biomol Chem, 2018. **16**(40): p. 7461-7469.
86. Fan, A. and S.-M. Li, *Saturation mutagenesis on Arg244 of the tryptophan C4-prenyltransferase FgaPT2 leads to enhanced catalytic ability and different preferences for tryptophan-containing cyclic dipeptides.* Applied Microbiology & Biotechnology, 2016. **100**(12): p. 5389-5399.
87. Zheng, L., et al., *Switching a regular tryptophan C4-prenyltransferase to a reverse tryptophan-containing cyclic dipeptide C3-prenyltransferase by sequential site-directed mutagenesis.* Org Biomol Chem, 2018. **16**(36): p. 6688-6694.
88. Stec, E., et al., *Two lysine residues are responsible for the enzymatic activities of indole prenyltransferases from fungi.* Chembiochem, 2008. **9**(13): p. 2055-8.
89. Steffan, N., I.A. Unsold, and S.M. Li, *Chemoenzymatic synthesis of prenylated indole derivatives by using a 4-dimethylallyltryptophan synthase from Aspergillus fumigatus.* Chembiochem, 2007. **8**(11): p. 1298-307.
90. Steffan, N. and S.M. Li, Arch. Microbiol., 2009. **191**: p. 461.
91. Yu, X., X. Xie, and S.M. Li, *Substrate promiscuity of secondary metabolite enzymes: prenylation of hydroxynaphthalenes by fungal indole prenyltransferases.* Appl Microbiol Biotechnol, 2011. **92**(4): p. 737-48.
92. Yu, X., et al., *Friedel–Crafts alkylation on indolocarbazoles catalyzed by two dimethylallyltryptophan synthases from Aspergillus.* Tetrahedron Letters, 2012. **53**(50): p. 6861-6864.
93. Mai, P., et al., *Actions of Tryptophan Prenyltransferases Toward Fumiquinazolines and their Potential Application for the Generation of Prenylated Derivatives by Combining Chemical and Chemoenzymatic Syntheses.* Advanced Synthesis & Catalysis, 2016. **358**(10): p. 1639-1653.
94. Rudolf, J.D., H. Wang, and C.D. Poulter, *Multisite prenylation of 4-substituted tryptophans by dimethylallyltryptophan synthase.* J Am Chem Soc, 2013. **135**(5): p. 1895-902.
95. Bandari, C., et al., *Determination of Alkyl-Donor Promiscuity of Tyrosine-O-Prenyltransferase SirD from Leptosphaeria maculans.* Chembiochem, 2017. **18**(23): p. 2323-2327.

96. Mohammadpour, R., et al., *Sulfabenzamide promotes autophagic cell death in T-47D breast cancer cells through p53/DRAM pathway.* Journal of Cell & Molecular Biology, 2012. **10**(1).
97. Shin-ya, K., et al., *Isolation and structural elucidation of an antioxidative agent, naphterpin.* J Antibiot (Tokyo), 1990. **43**(4): p. 444-7.
98. Xiao, Y., et al., *Prenyltransferase substrate binding pocket flexibility and its application in isoprenoid profiling.* Mol Biosyst, 2009. **5**(9): p. 913-7.
99. Xiao, Y., et al., *Prenyltransferase substrate binding pocket flexibility and its application in isoprenoid profiling.* Molecular BioSystems, 2009. **5**(9): p. 913-917.
100. Estrada, P., et al., *A Single Amino Acid Switch Alters the Isoprene Donor Specificity in Ribosomally Synthesized and Post-Translationally Modified Peptide Prenyltransferases.* J Am Chem Soc, 2018. **140**(26): p. 8124-8127.
101. Debono, M., et al., *Enzymatic and chemical modifications of lipopeptide antibiotic A21978C: the synthesis and evaluation of daptomycin (LY146032).* J Antibiot (Tokyo), 1988. **41**(8): p. 1093-105.
102. Debono, M., et al., *A21978C, a complex of new acidic peptide antibiotics: isolation, chemistry, and mass spectral structure elucidation.* J Antibiot (Tokyo), 1987. **40**(6): p. 761-77.
103. Miao, V., et al., *Daptomycin biosynthesis in Streptomyces roseosporus: cloning and analysis of the gene cluster and revision of peptide stereochemistry.* Microbiology, 2005. **151**(Pt 5): p. 1507-23.
104. Tally, F.P. and M.F. DeBruin, *Development of daptomycin for Gram-positive infections.* Journal of Antimicrobial Chemotherapy, 2000. **46**(4): p. 523-526.
105. Steenbergen, J.N., et al., *Daptomycin: a lipopeptide antibiotic for the treatment of serious Gram-positive infections.* J Antimicrob Chemother, 2005. **55**(3): p. 283-8.
106. Sakoulas, G., *Clinical outcomes with daptomycin: a post-marketing, real-world evaluation.* Clin Microbiol Infect, 2009. **15 Suppl 6**: p. 11-6.
107. Arbeit, R.D., et al., *The safety and efficacy of daptomycin for the treatment of complicated skin and skin-structure infections.* Clin Infect Dis, 2004. **38**(12): p. 1673-81.
108. Eisenstein, B.I., J.F.B. Oleson, and R.H. Baltz, *Daptomycin: From the Mountain to the Clinic, with Essential Help from Francis Tally, MD.* Clinical Infectious Diseases, 2010. **50**(Supplement_1): p. S10-S15.
109. Fowler, V.G., Jr., et al., *Daptomycin versus standard therapy for bacteremia and endocarditis caused by Staphylococcus aureus.* N Engl J Med, 2006. **355**(7): p. 653-65.
110. Chan Tompkins, N.H. and S.J. Harnicar, *Prescribing trends with daptomycin (cubicin) for the treatment of gram-positive infections.* P & T : a peer-reviewed journal for formulary management, 2008. **33**(5): p. 282-288.
111. Pader, V. and A.M. Edwards, *Daptomycin: new insights into an antibiotic of last resort.* Future Microbiol, 2017. **12**: p. 461-464.
112. Sader, H.S., et al., *Antimicrobial susceptibility of daptomycin and comparator agents tested against methicillin-resistant Staphylococcus aureus and*

vancomycin-resistant enterococci: trend analysis of a 6-year period in US medical centers (2005-2010). Diagn Microbiol Infect Dis, 2011. **70**(3): p. 412-6.
113. Silverman, J.A., et al., *Inhibition of daptomycin by pulmonary surfactant: in vitro modeling and clinical impact.* J Infect Dis, 2005. **191**(12): p. 2149-52.
114. Taylor, R., et al., *Daptomycin Pore Formation Is Restricted by Lipid Acyl Chain Composition.* ACS Infect Dis, 2017. **3**(11): p. 797-801.
115. Taylor, S.D. and M. Palmer, *The action mechanism of daptomycin.* Bioorg Med Chem, 2016. **24**(24): p. 6253-6268.
116. Zhang, T., et al., *Cardiolipin prevents membrane translocation and permeabilization by daptomycin.* J Biol Chem, 2014. **289**(17): p. 11584-91.
117. Silverman, J.A., N.G. Perlmutter, and H.M. Shapiro, *Correlation of daptomycin bactericidal activity and membrane depolarization in Staphylococcus aureus.* Antimicrob Agents Chemother, 2003. **47**(8): p. 2538-44.
118. Boudjemaa, R., et al., *Failure of daptomycin to kill Staphylococcus aureus: impact of bacterial membrane fatty acid composition.* Antimicrob Agents Chemother, 2018.
119. Gomez Casanova, N., M. Siller Ruiz, and J.L. Munoz Bellido, *Mechanisms of resistance to daptomycin in Staphylococcus aureus.* Rev Esp Quimioter, 2017. **30**(6): p. 391-396.
120. Vilhena, C. and A. Bettencourt, *Daptomycin: a review of properties, clinical use, drug delivery and resistance.* Mini Rev Med Chem, 2012. **12**(3): p. 202-9.
121. Lohani, C.R., et al., *Solid-phase synthesis and in vitro biological activity of a Thr4-->Ser4 analog of daptomycin.* Bioorg Med Chem Lett, 2015. **25**(23): p. 5490-4.
122. Lohani, C.R., et al., *Solid-phase total synthesis of daptomycin and analogs.* Org Lett, 2015. **17**(3): p. 748-51.
123. Barnawi, G., et al., *An entirely fmoc solid phase approach to the synthesis of daptomycin analogs.* Biopolymers, 2018.
124. Lin, D., et al., *Structure-activity relationship of daptomycin analogues with substitution at (2S, 3R) 3-methyl glutamic acid position.* Bioorg Med Chem Lett, 2017. **27**(3): p. 456-459.
125. Lam, H.Y., et al., *Total Synthesis of Daptomycin by Cyclization via a Chemoselective Serine Ligation.* Journal of the American Chemical Society, 2013. **135**(16): p. 6272-6279.
126. Siedlecki, J., et al., *Array synthesis of novel lipodepsipeptide.* Bioorg Med Chem Lett, 2003. **13**(23): p. 4245-9.
127. Hill, J., et al., *Synthesis and biological activity of N-Acylated ornithine analogues of daptomycin.* Bioorg Med Chem Lett, 2003. **13**(23): p. 4187-91.
128. t Hart, P., et al., *A combined solid- and solution-phase approach provides convenient access to analogues of the calcium-dependent lipopeptide antibiotics.* Org Biomol Chem, 2014. **12**(6): p. 913-8.
129. Yoganathan, S., et al., *An efficient chemical synthesis of carboxylate-isostere analogs of daptomycin.* Org Biomol Chem, 2013. **11**(28): p. 4680-5.
130. He, Y., et al., *Reduced pulmonary surfactant interaction of daptomycin analogs via tryptophan replacement with alternative amino acids.* Bioorg Med Chem Lett, 2012. **22**(19): p. 6248-51.

131. Kopp, F., et al., *Chemoenzymatic Design of Acidic Lipopeptide Hybrids: New Insights into the Structure−Activity Relationship of Daptomycin and A54145.* Biochemistry, 2006. **45**(35): p. 10474-10481.
132. Grünewald, J., et al., *Synthesis and Derivatization of Daptomycin: A Chemoenzymatic Route to Acidic Lipopeptide Antibiotics.* Journal of the American Chemical Society, 2004. **126**(51): p. 17025-17031.
133. Tedesco, K.L. and M.J. Rybak, *Daptomycin.* Pharmacotherapy: The Journal of Human Pharmacology and Drug Therapy, 2004. **24**(1): p. 41-57.
134. Streit, J.M., R.N. Jones, and H.S. Sader, *Daptomycin activity and spectrum: a worldwide sample of 6737 clinical Gram-positive organisms.* Journal of Antimicrobial Chemotherapy, 2004. **53**(4): p. 669-674.
135. Tetko, I.V., et al., *Virtual computational chemistry laboratory--design and description.* J Comput Aided Mol Des, 2005. **19**(6): p. 453-63.
136. Silverman, J.A., et al., *Resistance studies with daptomycin.* Antimicrob Agents Chemother, 2001. **45**(6): p. 1799-802.
137. Barry, A.L., P.C. Fuchs, and R.N. Jones, *Statistical criteria for selecting quality control limits for broth microdilution susceptibility tests with 39 different antimicrobial agents. Collaborative Antimicrobial Susceptibility Testing Group.* Diagn Microbiol Infect Dis, 1989. **12**(5): p. 413-20.
138. CLSI., *Methods for Dilution Antimicrobial Susceptibility Tests f or Bacteria That Grow Aerobically; Approved St Clinical and Laboratory Standards Institute.* CLSI document 2015. **M07-A10**.
139. You, J., et al., *Trichoderone, a novel cytotoxic cyclopentenone and cholesta-7, 22-diene-3 beta, 5 alpha, 6 beta-triol, with new activities from the marine-derived fungus Trichoderma sp.* J Ind Microbiol Biotechnol, 2010. **37**(3): p. 245-52.